HYBRID SOL-GEL COATINGS WITH BARRIER AND SELF-HEALING PROPERTIES FOR CORROSION PROTECTION OF ALUMINUM ALLOYS

Urša Tiringer

Doctoral Dissertation
Jožef Stefan International Postgraduate School
Ljubljana, Slovenia

Supervisor: Prof. Dr. Ingrid Milošev, Jožef Stefan Institute, Ljubljana, Slovenia

Evaluation Board:
Asst. Prof. Janez Kovač, Chair, Jožef Stefan Institute, Ljubljana, Slovenia
Prof. Dr. Barbara Malič, Member, Jožef Stefan Institute, Ljubljana, Slovenia
Prof. Dr. Marjan Veber, Member, Faculty of Chemistry and Chemical Technology, Ljubljana, Slovenia
Prof. Dr. Stojan Stavber, Member, Jožef Stefan Institute, Ljubljana, Slovenia

MEDNARODNA PODIPLOMSKA ŠOLA JOŽEFA STEFANA
JOŽEF STEFAN INTERNATIONAL POSTGRADUATE SCHOOL



Urša Tiringer

HYBRID SOL-GEL COATINGS WITH BARRIER AND SELF-HEALING PROPERTIES FOR CORROSION PROTECTION OF ALUMINUM ALLOYS

Doctoral Dissertation

HIBRIDNE BARIERNE SOL-GEL PREVLEKE Z LASTNOSTJO SAMOCELJENJA ZA PROTIKOROZIJSKO ZAŠČITO ALUMINIJEVIH

Doktorska disertacija

Supervisor: Prof. Dr. Ingrid Milošev

Ljubljana, Slovenia, April 2018

. . .To my dearest parents Andreja and Tomo . . .

Acknowledgments

There is a number of people that helped me along my doctoral study. First and foremost, my infinitive gratitude goes to my dearest supervisor Prof. Dr. Ingrid Milošev. Without her nothing of this would be possible. Her humanity, patience, care and guidance have made my study easier, successful and wormer. It was a big pleasure to work with her and to have her in my life.

Additionally, I wish to thank my evaluation board, Prof. Dr. Barbara Malič, Prof. Dr. Marjan Veber, Prof. Dr. Stojan Stavber and Asst. Prof. Janez Kovač, for their comments and observations on my thesis. A big thank you also goes to Asst. Prof. Janez Kovač for his support and helpful discussion in the experimental part of my thesis. Special thanks goes to Prof. Dr. Alicia Durán, who welcomed me to the Institute of Ceramics and Glass, at the Department of Glasses (CSIC) in Madrid, for four months, and shared her extensive knowledge with me about the sol-gel methodology.

Furthermore, I would like to thank my dear colleagues from the Department of Physical and Organic Chemistry, Dunja, Dolores, Barbara, Klara, Tina, Monika, Matic, Peter, etc. who helped me during my study and made my working days nicer. Special thanks goes to my dear colleague and roommate Gavrilo, who shared his ideas and thoughts with me, as well as many laughs and jokes which made even the worsts days brighter. At the same time, I would like to thank Dr. Antonija Lesar, Asst. Prof. Anton Kokalj, Dr. Peter Panjan and Dr. Matjaž Panjan for their contributions to the positive environment at work.

Moreover, a special thank you goes to Dr. Yolanda Castro from the Institute of Ceramics and Glass, from the Department of Glasses, Madrid, for all her help, advice, comments and technical support. At this point I would like to thank also the entire Department of Glasses from the Institute of Ceramics and Glass, Madrid, for their kindness and acceptance, especially to Desiree and Aritz, without whom my stay in Madrid would not be as nice as it was.

I would like to thank my dearest friend Dr. Sheila Omar from Argentina, who helped me with her advice about work during my stay in Madrid, made my days in Madrid unforgettable and showed me that real friendship is possible no matter how far away we live.

I would also like to thank my Master Supervisor Asst. Prof. Črtomir Podlipnik, who believed in me, advised and helped me continue my study as a young researcher at the Jožef Stefan Institute.

Most importantly, none of this would have been possible without the continuous support, patience and big love of my parents Andreja and Tomo, who are most responsible

for my success. My infinitive thanks goes also to my boyfriend Aljaž for his patience and support and to my grandmother Babi for her big care and love during my study.

A big thank you goes also to my friends from my hometown, Nina, Danjela, Marko, etc. who believed in me and helped me disconnect from work when it was necessary.

At the end I would like to acknowledge the financial support from the Slovenian Research Agency (research core funding No. P2-0393 and the project "Lightweight alloys based on aluminum as materials with increasing potential in the transportation industry", ID J1-6734) and the Ad Futura scholarship Fund (11012-56/2015) for financing my stay at the CSIC.

Abstract

The emphasis of this doctoral dissertation is on the corrosion protection of aluminum alloys. As a first step in the investigation, the effect of different pre-treatments of aluminum alloys 7075-T6 and 2024-T3 on their surface properties was studied. Mechanical pre-treatments, water-based grinding and non-water based polishing were studied, while the chemical cleaning consisted of a non-commercial cleaner NaOH and of a commercial cleaner SurTec, both followed by nitric acid desmutting. It was found out that the mechanical pre-treatments have a higher effect on aluminum alloy 7075-T6 than on the 2024-T3. Both chemical treatments decrease the corrosion resistance of these aluminum alloys and their surface became hydrophilic.

After pre-treatment, aluminum alloy's surface is protected against corrosion using different procedures. Traditionally, chromate conversion or phosphate coatings have been used for this purpose; as chromate coatings are nowadays recognized as toxic, alternative procedures are being sought to replace them. In this doctoral dissertation hybrid sol-gel coatings were regarded as a potentially suitable replacement for chromate coatings. Hybrid coatings were based on (3-glycidyloxypropyl) trimethoxysilane (GPTMS) and tetraethoxysilane (TEOS) and applied on aluminum alloy 7075-T6. SiO_2 nanoparticles were added to the precursors′s solution to achieve barrier property of coating, while $Ce(NO_3)_3$ was added to obtain an active corrosion protection. Optimization of sol synthesis was based on ATR-FTIR spectroscopy and UV-vis-NIR spectroscopy and the opening of the epoxy rings and completion of hydrolysis and condensation reactions were confirmed, based on ATR-FTIR results. A high degree of cross-linking between GPTMS and TEOS was achieved, *in situ*, during the synthesis and the effect of the curing process on coating′s properties was confirmed. A double-layer system was applied on aluminum alloy 7075-T6, where the first layer was doped with $Ce(NO_3)_3$ and the second was un-doped. It was found out that cerium has a role in the self-healing only if it is "locked" within the first layer of multi-layer coating. Coating characterization was carried out by the immersion test and electrochemical potentiodynamic measurements and electrochemical impedance spectroscopy. The self-healing effect was confirmed by immersion of un-scribed and scribed coated AA7075-T6 in electrolyte NaCl by using the immersion test, electrochemical impedance spectroscopy, X-ray photoelectron spectroscopy and scanning electron spectroscopy equipped with energy dispersive X-ray spectroscopy.

A systematic study of mechanical and chemical pre-treatment of aluminum alloys 7075-T6 and 2024-T3 was performed followed by the development of hybrid sol-gel coating which achieved an efficient corrosion protection of aluminum alloy 7075-T6 in chloride containing electrolyte and represents a potential replacement for chromate coatings.

Povzetek

Poudarek moje doktorske disertacije je na protikorozijski zaščiti aluminijevih zlitin. Prvi del raziskave je posvečen študiji vpliva različnih pred-priprav površine aluminijevih zlitin 7075-T6 in 2024-T3 na njihove površinske lastnosti. Testirala sem dve mehanski pred-pripravi, brušenje na vodni osnovi in poliranje na ne-vodni osnovi, ter kemijski čiščenji na osnovi nekomercialnega čistila NaOH in na osnovi komercialnega čistila SurTec. Obema kemijskima čiščenjema je sledilo dodatno čiščenje z dušikovo kislino. Ugotovila sem, da ima mehanska pred-priprava večji vpliv na aluminijevo zlitino 7075-T6 kot na zlitino 2024-T3, ter da obe kemijski čiščenji zmanjšata korozijo aluminijevih zlitin in naredita njuno površino hidrofilno.

Nadalje, predpripravi površine aluminijevih zlitin sledi nanos protikorozijske prevleke, ki bi v čim večji meri dosegala lastnosti prepovedanih kromatnih konverzijskih prevlek. V moji doktorski nalogi so bile pripravljene hibridne sol-gel prevleke na osnovi (3-glicidiloksipropil) trimetoksisilana (GPTMS) in tetraetoksisilana (TEOS) ter kot protikorozijska zaščita nanešene na aluminijevo zlitino 7075-T6. Za dosego bariernih lastnosti prevleke sem prekurzorjema dodala SiO_2 nanodelce, za dosego aktivne korozijske zaščite pa korozijski inhibitor $Ce(NO_3)_3$. Optimizacijo sinteze solov sem določila na podlagi ATR-FTIR in UV-vis-NIR rezultatov. Potrdila sem tudi odprtje epoksi obročev v GPTMS ter dokončani hidrolizo in kondenzacijo. Ugotovila sem visoko stopnjo mreženja med prekurzorjema GPTMS in TEOS, *in situ*, med samo sintezo. Potrdila sem tudi vpliv načina toplotne obdelave prevleke na njihove lastnosti.

Na aluminijevo zlitino 7075-T6 sem nanesla dvoplastno prevleko, kjer je prva plast vsebovala $Ce(NO_3)_3$, druga ne. Ugotovila sem, da ima dodatek Ce aktivno vlogo pri samoceljenju prevleke, le če je vgrajen v prvo plast dvoplastne prevleke. Lastnosti prevleke sem določila s potopitvenim testom ter z elektrokemijskimi meritvami. Učinek samoceljenja prevleke sem potrdila tako, da sem nepoškodovane ter poškodovane vzorce potopila v elektrolit NaCl ter s potopitvenim testom, elektrokemijsko impedančno spektroskopijo, rentgensko fotoelektronsko spektroskopijo ter vrstično elektronsko mikroskopijo s kemično analizo opazovala razvoj oziroma zaviranje korozije po površini raze.

V moji doktorski nalogi je bila narejena sistematična študija vpliva mehanske in kemične predobdelave aluminijevih zlitin 7075-T6 in 2024-T3, čemur je sledil razvoj hibridne sol-gel prevleke, ki izkazuje učinkovito protikorozijsko zaščito aluminijeve zlitine 7075-T6 v kloridnem mediju in tako predstavlja dobro osnovo kot možno nadomestilo kromatnim prevlekam.

Contents

List of Figures **xv**

List of Tables **xvii**

Abbreviations **xix**

1 Introduction **1**
1.1 Definition of the Problem ... 1
1.2 Aluminum and Aluminum Alloys ... 1
1.2.1 Aluminum alloys AA7075 and AA2024 ... 5
1.3 Pre-Treatment of Aluminum Alloys ... 5
1.4 Corrosion Protection ... 6
1.4.1 Hybrid sol-gel coatings ... 7
Corrosion protection of aluminum alloys ... 10
1.5 Purpose of the Dissertation ... 11
1.6 Objectives of the Dissertation ... 12
1.7 Hypothesis of the Dissertation ... 12
1.8 Scientific Contribution ... 13
1.9 Methodology ... 14
1.10 Structure of the Dissertation ... 15

2 Effect of Mechanical and Chemical Pre-treatments on the Morphology and Composition on Surfaces of Aluminum Alloys 7075-T6 and 2024-T3 **17**

3 Hybrid Sol-Gel Coatings Based on GPTMS/TEOS Containing Colloidal SiO_2 and Cerium Nitrate for Increasing Corrosion Protection of Aluminum Alloy 7075-T6 **33**

4 Self-Healing Effect of Hybrid Sol-Gel Coatings Based on GPTMS, TEOS, SiO_2 Nanoparticles and $Ce(NO_3)_3$ Applied on Aluminum Alloy 7075-T6 **47**

5 Conclusions and Future Outlook **63**

References **69**

Bibliography **77**

Biography **79**

List of Figures

Figure 1.1: Pourbaix diagram of aluminum [8]. 2

Figure 1.2: SEM images of aluminum (left) [9] and aluminum alloy AA7075-T6 (right). ..3

Figure 1.3: Steps of the synthesis of sol-gel coating [5]. 8

Figure 1.4: The main reactions proceeding during sol-gel synthesis; a) hydrolysis, b) polycondensation [38]. M represents a metallic substrate, R is an alkyl group and R^* is a carbon chain containing a functional group. 9

Figure 1.5: Alkoxide precursors used in hybrid sol-gel coatings [5]. 9

Figure 1.6: Interactions between hybrid sol-gel coating and substrate aluminum alloy. ..10

Figure 1.7: Schemes of different possibilities to open the epoxy ring [64]. 11

Figure 1.8: Graphical abstract of Chapter 2. 18

Figure 1.9: Graphical abstract of chapter 3. 34

Figure 10: Graphical abstract of Chapter 4. 48

Figure 1.11: Potentiodynamic polarization curves recorded in 0.1 M NaCl, after 1 hour of stabilization for uncoated AA7075-T6 and coated by GTS, GTS-Ce and GTS-Ce+GTS and by green chromate primer-CCC. 66

List of Tables

Table 1.1: Designation of wrought aluminum alloys. 3

Table 1.2: Designation of cast aluminum alloys. 4

Table 1.3: Temper designation system of alloys. 4

Table 1.4: The composition of AA7075-T6 and AA2024-T3 5

Abbreviations

AA	...	aluminum alloy
IMPs	...	intermetallic particles
CCCs	...	chromate conversion coatings
TEOS	...	Tetraethoxysilane
GPTMS	...	(3-glycidyloxypropyl) trimethoxysilane
UV-vis	...	ultraviolet visible spectroscopy
ATR-FTIR	...	attenuated total reflectance Fourier transform infrared spectroscopy
XPS	...	X-ray photoelectron spectroscopy
SEM	...	scanning electron microscopy
EDS	...	energy dispersive X-ray spectroscopy
EIS	...	electrochemical impedance spectroscopy
PD	...	potentiodynamic
w_g	...	ground under water
d_p	...	diamond polished
at	...	atomic
j_{corr}	...	corrosion current density
E_{corr}	...	corrosion potential
t	...	time
^{1}H NMR	...	proton nuclear magnetic resonance spectroscopy
^{13}C NMR	...	carbon-13 nuclear magnetic resonance spectroscopy
^{29}Si NMR	...	silicon-29 nuclear magnetic resonance spectroscopy

Chapter 1

Introduction

1.1 Definition of the Problem

Reduction of CO_2 emission is an important goal set by the directives of the European Union [1]. Aluminum and aluminum alloys belong to the group of light metals and are most commonly used in the transportation industry, such as aircraft industry, automotive industry, train industry and marine industry.

Despite the fact that pure aluminum resists corrosion well, its alloys may not be corrosion resistant in various environments, especially those containing chlorides. Chromate conversion coatings (CCCs) have provided an effective corrosion protection of aluminum alloys for many years. Their use is however, becoming limited because of their toxicity [2].

Many studies have been focused on the development of technologies alternative to CCCs, such as anodizing, conversion coatings, electro polymerization, sol-gel coatings, etc. Sol-gel coatings are one of the most promising and environmentally friendly replacements for CCCs and are the basis of the present doctoral dissertation [3]–[5].

1.2 Aluminum and Aluminum Alloys

The properties of aluminum that contribute to their usage in many applications are the following: lightness, thermal and electrical conductivity, strength-to-weight ratio and corrosion resistance.

Corrosion of aluminum occurs by the electrochemical reaction, affecting a metal and aqueous phase. The basic reactions which summarized the corrosion of aluminum are the following: [6], [7]

- oxidation of aluminum in water:

$$Al \rightarrow Al^{3+} + 3e^{-} \quad (1)$$

- reduction of H^+ protons, which are derived by the dissociation of water:

$$3H^{+} + 3e^{-} \rightarrow \frac{3}{2} H_2 \quad (2)$$

- reduction of oxygen which is dissolved in water:

if media is alkaline or neutral:

$$O_2 + 2H_2O + 4e^- \rightarrow 4OH^- \quad (3)$$

if media is acidic:

$$O_2 + 4H^+ + 4e^- \rightarrow 2H_2O \quad (4)$$

According to diagrams of electrochemical potential vs. pH (so called Pourbaix diagrams [8]), E_H vs. pH) of aluminum in aqueous solution, aluminum can be attacked by corrosion in both, acidic and alkaline media (Figure 1.1). In acidic medium, Al^{3+} ions are formed, while in alkaline media AlO_2^- ions are formed. Between pH 4 and 9 is a range of passivation, where natural oxide film Al_2O_3 is formed on the surface of aluminum, which protects it against corrosion. Moreover, there is also a range of pH, at lower potentials, where aluminum is immune to corrosion [8].

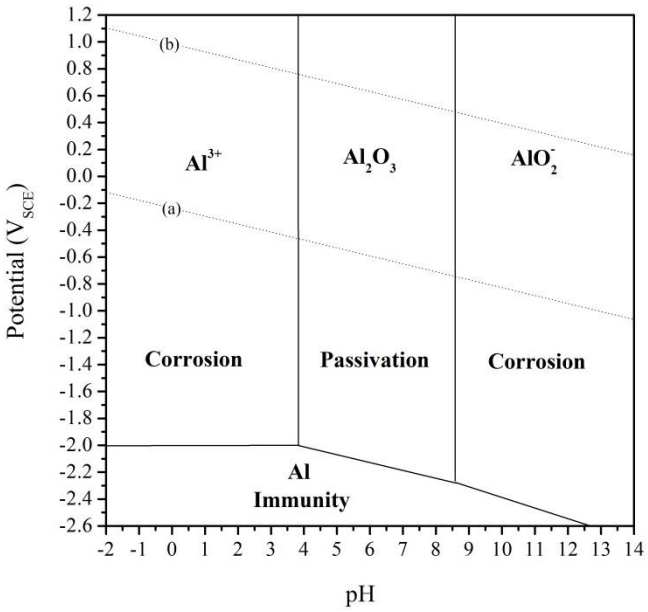


Figure 1.1: Pourbaix diagram of aluminum [8].

However, aluminum has some disadvantages, such as its softness and weak mechanical properties. Thus, aluminum alloys were developed to greatly surpass these disadvantages. In aluminum alloys, selected alloying elements (called intermetallic particles, IMPs), e. g. copper, manganese, silicon, magnesium, zinc, are added to pure aluminum [6], [7]. Figure 1.2 presents scanning electron microscope images of pure aluminum (left) and of aluminum alloy AA2024-T3 (right).

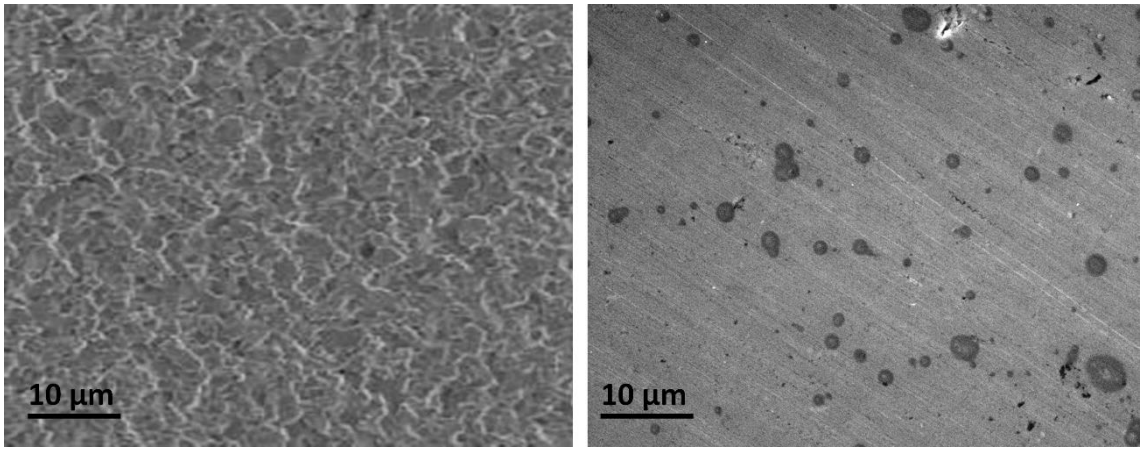


Figure 1.2: SEM images of aluminum (left) [9] and aluminum alloy AA7075-T6 (right).

Aluminum alloys are classified in two classes: wrought alloys and cast alloys. They are listed and described in Tables 1.1 and 1.2 [6], [7].

Table 1.1: Designation of wrought aluminum alloys.

Designation of wrought alloy	**Description**
1xxx	Unalloyed composition that consists mainly of pure aluminum, mostly used in chemical and electrical industries.
2xxx	Alloys based on alloying element copper, also magnesium can be found, mostly used in aircraft industry.
3xxx	Alloys based on alloying element manganese, mostly used in architectural industry.
4xxx	Alloys based on alloying element silicon, mostly used in welding rods.
5xxx	Alloys based on alloying element magnesium, mostly used in marine industry.
6xxx	Alloys based on alloying elements magnesium and silicon, mostly used for architectural extrusion.
7xxx	Alloys based on alloying element zinc, mostly used in aircraft structural components.
8xxx	Alloys based on lithium, iron or tin.
9xxx	Alloys reserved for the future.

Table 1.2: Designation of cast aluminum alloys.

Designation of cast alloy	Description
1xx.x	Unalloyed composition that consists mainly of pure aluminum, mostly used for rotor manufacture.
2xx.x	Alloys based on alloying element copper.
3xx.x	Alloys based on alloying element silicon, also copper and magnesium can be observed.
4xx.x	Alloys based on alloying element silicon.
5xx.x	Alloys based on alloying element magnesium.
6xx.x	Unused alloys.
7xx.x	Alloys based on alloying element zinc.
8xx.x	Alloys based on alloying element tin.
9xx.x	Un-used alloys.

The temper designation system is used for wrought and cast alloys. It is based on mechanical or thermal treatment and includes four letters, H, T, O or F. Their properties are explained in Table 1.3 [6], [7], [10].

Table 1.3: Temper designation system of alloys.

Designation	Description
H	Hardened and strengthened alloys by any deformation at room temperature.
T	Hardened and strengthened alloys by an aging heat treatment.
O	Annealed alloys to achieve its softest condition.
F	Not treated alloys (as-fabricated).

Despite the fact that pure aluminum resists corrosion well, aluminum alloys may not be corrosion resistant in various environments, as a result of IMPs presence. In near-neutral bulk solution, corrosion of aluminum alloys is influenced by IMPs which have different characteristics and electrochemical potential than the matrix. They may be either anodic or cathodic relative to Al-matrix, thus leading to local difference in electrochemical activity and initiation of galvanic corrosion [7].

1.2.1 Aluminum alloys AA7075 and AA2024

In this doctoral dissertation aluminum alloys AA7075-T6 and AA2024-T3 were studied. Due to its high strength and excellent strength-to-weight ratio, AA7075-T6 is used in transportation industry, e.g. marine, automotive and aircraft industry, while AA2024-T3 is due to its high strength and excellent fatigue resistance widely used in aircraft industry, especially in wings construction [11]. The composition of AA7075-T6 and of AA2024-T3 is listed in Table 1.4. Thus, AA7075-T6 is based on Mg and Zn, while AA2024-T3 is based on Cu.

Table 1.4: The composition of AA7075-T6 and AA2024-T3.

AA	Zn (wt%)	Mg (wt%)	Cu (wt%)	Fe (wt%)	Si (wt%)	Mn (wt%)	Ti (wt%)	Cr (wt%)	Al (wt%)
7075-T6	5.1–6.1	2.1–2.9	1.2–2.0	0.5	0.4	0.3	0.2	0.2–0.3	rest
2024-T3	0.3	1.2–1.8	3.8–4.9	0.5	0.5	0.3–0.9	0.2	0.1	rest

IMPs present in AA7075-T6 and AA2024-T3 can be divided into the following categories [12]–[15]:

- Small (up to μm);

e.g. $MgZn_2$, Mg_2Al_3, Al_2Cu, formed by nucleation and growth from supersaturated solution during natural or artificial aging,

- Larger (1-10 μm);

e.g. Al_3Fe, Al_7Cu_2Fe, Al_2CuMg (S-phase), irregularly shaped and formed during alloy solidification,

- Very small (< 1 μm);

e.g. Al_3Ti, Al_6Mg, dispersions, insoluble in Al.

The potential of IMPs differs. Some of IMPs have high electrochemical activity and the ability to sustain a large cathodic current (Al_2Cu, Al_7Cu_2Fe), while some of them have high dissolution rate and can sustain an anodic current ($MgZn_2$). Moreover, some IMPs include a noble element component (S-phase Al_2CuMg), where Mg from S-phase is dissolved and the potential of IM is changed from cathodic to anodic. Thus, IMPs are the sites of the initiation of local corrosion as a result of high potential difference between them (galvanic couple) and also between each IMP and Al matrix (galvanic corrosion) [12]–[15].

There are several ways how to improve the corrosion resistance of aluminum alloys [3], [6], [10], [16], as it will be described in Section 1.4.

1.3 Pre-Treatment of Aluminum Alloys

However, before performing any kind of protection treatment, it is necessary to properly pre-treat or clean the surface which will be protected. The most common types of surface pre-treatment for aluminum alloys are degreasing, mechanical pre-treatment, chemical

cleaning, chemical brightening, anodizing, powder coating and wet coating. In this doctoral dissertation, the effect of mechanical pre-treatment and chemical cleaning on properties of aluminum alloys AA7075-T6 and AA2024-T3 was studied. The goal of either mechanical pre-treatment or chemical cleaning is to remove inorganic and organic residues from the surface before painting or applying coatings [6], [7], [10], [16]–[18].

Grinding and polishing are the most commonly used mechanical pre-treatments. The former is usually based on SiC grinding papers and produces a macro-rough surface [17], [19]. A diamond paste is used in polishing pre-treatment. The effects of grinding and polishing on localized breakdown of AA7075-T6 and of AA2024-T3 surfaces have been studied [20]–[24]. Mechanical grinding and polishing under water can promote aggressive corrosion, but even in non-aqueous conditions such pre-treatment was found to affect the microstructure and corrosion properties [20]–[23].

Chemical cleaning is carried out after, or in place of mechanical pre-treatment for removing surface contamination originating from mechanical pre-treatment and for removing oxides present at the metal surface [18], [19]. It includes processes such as vapor degreasing, solvent cleaning, acid cleaning, alkaline cleaning, milling, etching, chromating/phosphating, electrochemically plating with copper, tin, nickel or silver, etc. Chemical cleaners are divided into two groups, water-based and organic solvent cleaners. Acidic or alkaline cleaners are most commonly used water-based cleaners. They can act as pickling agents, etching agents, detergents, degreasing agents or corrosion inhibitors [25]. Commercial cleaners are usually alkaline cleaners for liquid degreasing and contain mainly phosphate, sodium-based carbonates or silicate, surfactants and additives including corrosion inhibitors [6], [19]. Chemical cleaning is often followed by acid treatment, pickling or desmutting, with the aim of removing residues arising from prior alkaline cleaning and of increasing surface roughness in order to facilitate the adhesion of organic coatings to the surface [26]. The most commonly used desmutters are nitric acid and fluoric acid. Copper enrichment after chemical cleaning has been commonly observed on AA7075 and AA2024 surfaces [4], [27]–[30], which affects the subsequent treatment of the surface using conversion coatings based on cerium [31].

In this doctoral dissertation the effect of two mechanical pre-treatments, grinding under water and polishing under non-aqueous liquid on properties of AA7075-T6 and AA2024-T3 was studied. Moreover, the effect of two chemical cleanings, non-commercial cleaning, based on NaOH and commercial cleaning, based on SurTec cleaner, both followed by desmutting in nitric acid, on properties of AA7075-T6 and AA2024-T3, was studied.

1.4 Corrosion Protection

After pre-treatment, treatment of alloy's surface is carried out to protect it against the corrosion. Different ways of protection exist and can be summarized as follows: [7]

- **Modification of the surface**; anodization and chemical conversion coatings,
- **Modification of the medium**; the addition of inhibitors into the medium,

- **Applying continuous coating on the surface**; painting and sol-gel coatings.

One of the most cost-efficient and effective surface treatments are chromate conversion coatings, which have provided effective corrosion protection of aluminum alloys for more than 100 years, as pre-treatment or as final surface finish [3], [6], [16], [32]. They consist of a backbone of chromium oxide/hydroxide with Cr^{3+} oxidation state and also compounds with Cr^{6+} oxidation state. The Cr^{6+} provides the characteristic of self-healing, which is the ability to reform a protective coating after it has been breached by mechanical or chemical process. The self-healing is achieved by the reduction of the remained Cr^{6+} into an insoluble Cr^{3+} compound [3]. Thus, CCCs can act as a barrier and as an active corrosion protection, leading to the self-healing effect. In addition, CCCs improve adhesion of primers and top coatings [16]. However, the main compound of CCCs Cr^{6+} is highly toxic, therefore their use was restricted in European Union, by the Restriction of Hazardous Substances (RoHS) Directive 2002/95/EC, in 2006 [2]. Sunset date for CCCs in EU was September 2017, since when their use is allowed only in special industries, such as defense and aerospace industries [2].

Many surface treatments have been proposed to replace CCCs, but only zirconium and titanium conversion coatings are commercialized and have been used in industries. However, they still do not meet the performance levels of CCCs [3].

1.4.1 Hybrid sol-gel coatings

Sol-gel process is one of the most promising and environmentally friendly replacements for CCCs [4], [30], [32]–[35]. It offers important advantages, such as cost effectiveness and simple application procedures, easily adaptable in the industry [36].

According to the latest definition, sol-gel process is every process which starts from the precursor's solution and goes through the stage of *sol* and *gel* [37].

The first step of sol-gel synthesis is to select the chemical compounds, known as precursors, and dissolve them in the solvent, leading to the *sol* formation, which is a stable suspension of colloidal particles within a liquid [38]. As *sol* is a fluid, it can be applied to a metal surface using various techniques, e.g. spraying, dipping, spinning. After chemical transformations in *sol*, a rigid and interconnected network is formed, called *gel*, which is limited by the walls of the container. The last step includes drying, which results in concentrated gelled network [4], [5]. The volume of dry *gel* is from five to ten times smaller compared to the initial wet *gel* [4]. In many cases, a dry *gel* needs further thermal treatment-curing to be densified [5]. The main steps of the synthesis of sol-gel coating are presented in Figure 1.3.

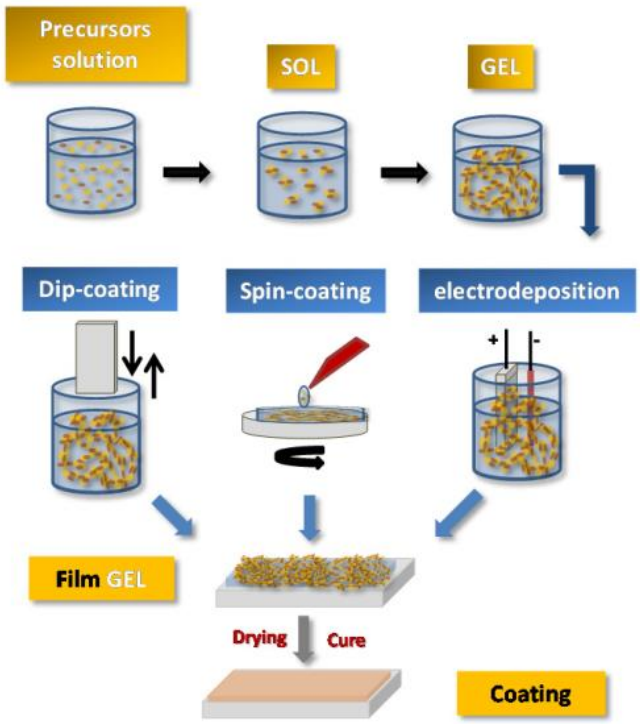


Figure 1.3: Steps of the synthesis of sol-gel coating [5].

The first sol-gel coatings were based on inorganic silane precursors which offer good mechanical properties and promote a good adhesion between the metal substrate and organic coatings, leading to low oxygen diffusion [34]. However, these inorganic coatings contain micropores and microcracks and, furthermore, high temperatures are required to obtain dense coatings [4]. In the early 80's the first hybrid sol-gel coatings were made from alkoxysilanes [4]. They are usually prepared with a combination of inorganic and organic polymerization and improve the overall performance of the coating; the inorganic component offers good mechanical properties, while the organic component increases the flexibility and ductility of coating, with decreased treatment temperature [4], [35], [39]–[41].

Hybrid sol-gel coatings are divided into three general classes: class I, II and III. In class I the organic and inorganic components are connected by hydrogen bonds, Van der Waals forces or ionic bonds, in class II they are connected by covalent bonds and in class III by both types of interactions, assigned in classes I and II. Due to the chemical and physical properties, hybrid sol-gel coatings from class II are suitable for corrosion protection of metals and their alloys and are the basis of this doctoral dissertation. Their synthesis involves polycondensation reaction between metal inorganic alkoxides $M(OR)_4$ and metal organic alkoxide $(R\text{-}O)_{4\text{-}n}MR_n^*$, where M represents a network-forming element, such as Si, Ti, Zr, Al, etc., R is an alkyl group (C_xH_{2x+1}), and R^* is carbon chain containing functional group, e.g. amino, epoxy, etc.

The synthesis of hybrid sol-gel coatings consists of two main reactions, **hydrolysis** of metal alkoxides (nucleophilic attack) (Figure 1.4a), where (–OR) groups are replaced by (–OH) groups, in the presence of water and catalyst (acid or basic), and **polycondensation** of hydroxyl groups (Figure 1.4b), leading to a network/*gel* [4], [5], [38]. The conversion of the precursors into hybrid sol-gel coatings proceeds through the formation of M–O–M bonds.

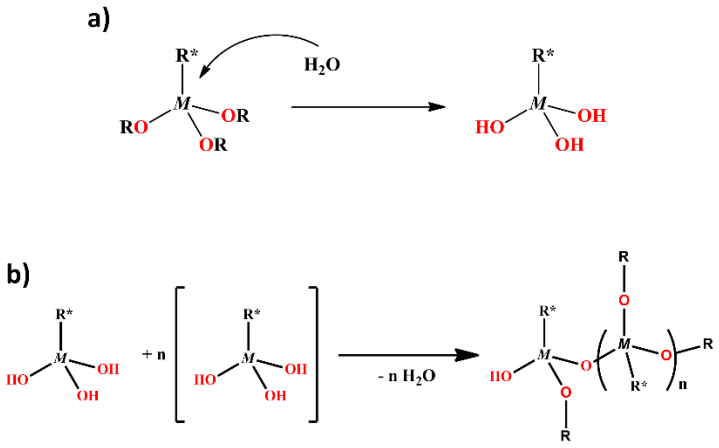


Figure 1.4: The main reactions proceeding during sol-gel synthesis; a) hydrolysis, b) polycondensation [38]. M represents a metallic substrate, R is an alkyl group and R* is a carbon chain containing a functional group.

There are several precursors which are used in the synthesis of hybrid sol-gel coatings [4], [5]. Some of examples are shown in Figure 1.5, where, e.g. TEOS is an inorganic alkoxisilane, while GPTMS belongs to the organic alkoxisilane.

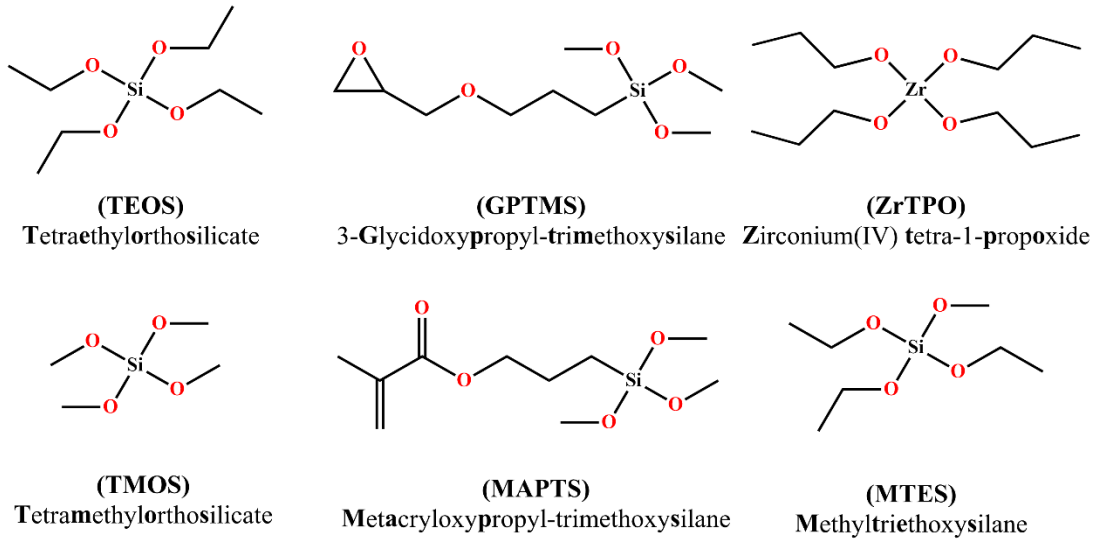


Figure 1.5: Alkoxide precursors used in hybrid sol-gel coatings [5].

Based on their low chemical reactivity, the silicon alkoxides, named alkoxysilanes, are the most commonly used precursors in hybrid sol-gel coatings [5].

Corrosion protection of aluminum alloys

Hybrid sol-gel coatings from class II have been confirmed as a promising alternative for CCCs for corrosion protection of aluminum alloys [5], [33], [36], [42]–[45]. They are based on organo-alkoxysilane, which is further polymerized with inorganic-alkoxysilane to increase the barrier properties of coating [5]. Moreover, these materials can provide a stable Si–O–Al bonding between hybrid sol-gel coatings and aluminum oxide Al_2O_3, which is naturally formed on the surface of aluminum alloys (Figure 1.6) [46].

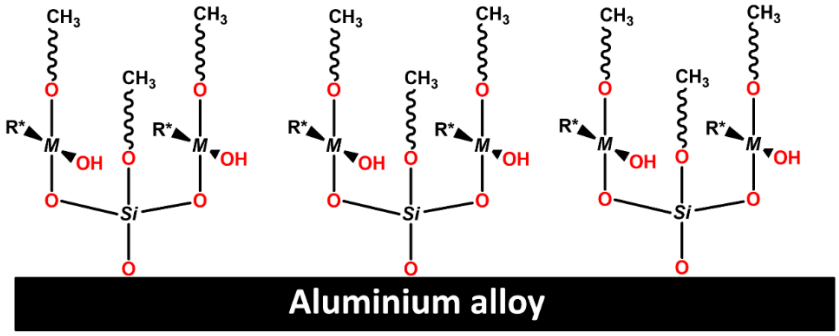


Figure 1.6: Interactions between hybrid sol-gel coating and substrate aluminum alloy.

According to the previous studies, hybrid sol-gel coatings, which contain an epoxy functional group in organic-alkoxysilane, offer an efficient corrosion protection of aluminum alloy AA7075-T6, which was the basis of this doctoral dissertation [39], [41], [43], [46], [46]–[53]. (3-glycidyloxypropyl)trimethoxysilane (GPTMS) is one of the most used epoxy-based organo-alkoxysilanes for hybrid sol-gel coating. It is used as a binder in paints or as a filler in inorganic and composite materials [54]. The epoxy group of GPTMS can crosslink with an inorganic-alkoxisilane, such as tetraethyl orthosilicate (TEOS), resulting in better mechanical properties, corrosion resistance and flexibility of coatings [51], [55]–[60]. Cross-linking between these two networks can be achieved by direct reaction of silanols with epoxy rings or by the condensation of silanols with the hydroxyl of the opened epoxy rings [61]. In many cases the opening of epoxy ring is thermally catalysed [62], but it can also be opened at room temperature by the addition of amine curing agents (DETA), each hydrogen of the amine being capable of opening and linking to one epoxy group [61]. In accordance with the literature the epoxy rings of GPTMS can be opened by the following reactions [52], [62], [63]: the ring can be opened by methanol produced by the hydrolysis of the silicon alkoxide, leading to the formation of methylether (Figure 1.7A), water can convert the epoxy group in acidic condition to form diol (Figure 1.7B) and the oxirane can react with another epoxy ring, resulting in oligo or poly(ethylene) oxide derivate (Figure 1.7C).

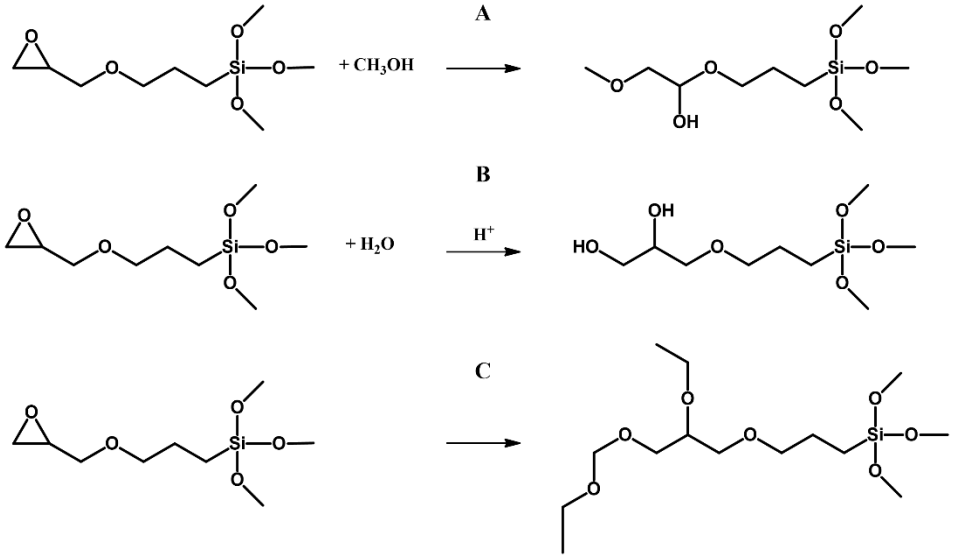


Figure 1.7: Schemes of different possibilities to open the epoxy ring [64].

In order to improve the densification of hybrid silica coatings, silica (SiO_2) nanoparticles could be incorporated into the sol-gel solution [65]. Their addition increases the barrier property of coating by increasing the coating thickness, density and reinforcement [66]–[72]. However, their addition does not provide an active corrosion protection of aluminum alloys.

Thus, corrosion inhibitors, such as Ce^{3+} ions, could be incorporated into the hybrid sol-gel coating to attain an active corrosion protection of alloy [73], [74]. When corrosion occurs, reduction of oxygen takes place at the cathodic sites of aluminum alloy, OH ions are formed and pH increases. Under these conditions, $Ce(OH)_3$ precipitates at the cathodic sites and can be further oxidized into the $Ce(OH)_4$ and insoluble CeO_2 , which act as a protective barrier to oxygen and lower the cathodic activity by hindering the transfer of electrons from the anodic cathodic sites [75]–[79]. Moreover, the addition of Ce^{3+} into the hybrid sol-gel coating has also provided self-healing [57], [72], [78], [80]–[83]. Thus, when the coating is mechanically damaged or local defects are present, the inhibitor is released and acts in such a way to repair the damage or retard the corrosion process.

In this doctoral dissertation developed hybrid sol-gel coatings were based on GPTMS and TEOS, with the addition of SiO_2 nanoparticles and corrosion inhibitor $Ce(NO_3)_3$.

1.5 Purpose of the Dissertation

Although the effects of pre-treatments have been reported as summarized above, a systematic approach involving both mechanical and chemical treatments is still lacking. Thus, the first purpose of the dissertation is a detailed study and understanding of the effect of various mechanical and chemical pre-treatments on surface properties of aluminum alloys AA2024-T3 and AA7075-T6. We planned to optimize two mechanical pre-treatments, grinding under water and polishing under non aqueous liquid, and two chemical pre-treatments, alkaline cleaning using either non-commercial NaOH solution or commercial SurTec cleaner. Both chemical cleanings were followed by desmutting in nitric

acid. The purpose was also to show the importance of the choice of pre-treatment of alloys before any further treatment.

The second purpose was aimed at finding the replacement for CCCs for corrosion protection of AA7075-T6, which would meet the current environmental requirements. For that purpose, we planned to develop a hybrid sol-gel coating which would combine a barrier and active corrosion protection of AA7075-T6, resulting also in a self-healing effect. The developed hybrid sol-gel coating was based on (3-glycidyloxypropyl)trimethoxysilane (GPTMS) and tetraethyl orthosilicate (TEOS) and doped with SiO_2 nanoparticles to gain a barrier property of coating and with $Ce(NO_3)_3$ to gain an active corrosion protection and self-healing of coating.

1.6 Objectives of the Dissertation

The objectives of this doctoral dissertation are the following:

1) To gain a systematic understanding of mechanical and chemical pre-treatment of aluminum alloys AA7075-T6 and AA2024-T3.

2) To gain a barrier and active corrosion protection of hybrid sol-gel coating based on GPTMS and TEOS.

3) To induce the in situ polymerization of the sol and to optimize the synthesis and curing of hybrid sol-gel coatings.

4) To obtain a self-healing effect on scribed coating.

5) To develop hybrid sol-gel coating as a potential replacement for chromate conversion coatings.

1.7 Hypothesis of the Dissertation

This doctoral dissertation builds on the following hypotheses:

- Different mechanical and chemical pre-treatments have a different effect on surface properties of AA2024-T3 and AA7075-T6.
- The polymerization of the sol is carried out *in situ*, during the synthesis.
- Hybrid sol-gel coatings based on GPTMS, TEOS and SiO_2 nanoparticles have a barrier corrosion protection.
- The incorporation of $Ce(NO_3)_3$ into the hybrid sol-gel coating leads to an active corrosion protection and self-healing of coating.
- Developed hybrid sol-gel coatings are a potential replacement for CCCs.

1.8 Scientific Contribution

The results and findings of the research work presented within this doctoral dissertation contribute to the field of pre-treatment of aluminum alloys and corrosion protection of aluminum alloys. The original scientific contributions are as follows.

The effect of pre-treatment of aluminum alloys on their surface properties

Published in: U. Tiringer, J. Kovač, I. Milošev, "Effect of mechanical and chemical pre-treatments on the morphology and composition of surfaces of aluminium alloys 7075-T6 and 2024-T3. *Corros. Sci.*, vol. 119, pp. 46–59, 2017

The systematic approach involving both mechanical and chemical pre-treatments is presented in this paper. The effect of different pre-treatments on aluminum alloys was studied in previous studies, but the novelty of this paper is the systematic comparison between the effect of mechanical and chemical pre-treatment of AA7075-T6 and AA2024-T3 on their microstructure and corrosion properties. Moreover, the comparison between non-commercial and commercial chemical pre-treatment was studied in this paper. Thus, the main scientific contribution is the importance of the choice of the type of pre-treatment of AA7075-T6 and AA2024-T3 for their further treatment. Moreover, this paper also contributes to the field of industry, where choosing of a proper pre-treatment is often doubtful.

Synthesis of hybrid sol gel coatings offering a barrier and active corrosion protection of AA7075-T6

Published in: U. Tiringer, I. Milošev, A. Durán, Y. Castro, " Hybrid sol–gel coatings based on GPTMS/TEOS containing colloidal SiO_2 and cerium nitrate for increasing corrosion protection of aluminium alloy 7075-T6. *J. Sol-Gel Sci. Technol.* Vol. 85, pp. 546–557, 2017

One of the novelties of this paper is the improved cross-linking degree of silica matrix through the organic and inorganic polymerization, *in situ* during the synthesis of the sol. It was found out that the addition of concentrated HNO_3 into the sol-gel solution sufficiently heated the sol-gel solution that the epoxy rings of GPTMS opened, leading to a better cross-linking between GPTMS and TEOS. The effect of curing ramp in the densification of the coating was studied and how it affected the corrosion resistance. This represents a novel contribution to the coating production.

The incorporation of silica nanoparticles into the sol-gel solution increases the densification of the coating provoking a high barrier effect, whilst cerium is added to achieve active protection. The present paper reported the synthesis of coatings

that would be able to protect a highly active substrate like aluminum alloy 7075-T6 in chloride containing electrolyte.

The detailed study of the mechanism of the self-healing based on $Ce(NO_3)_3$ in scribed hybrid sol-gel coatings applied on AA7075-T6

Published in: U. Tiringer, Y. Castro, A Durán, I. Milošev, "Self-healing effect of $Ce(NO_3)_3$ in hybrid sol-gel coatings based on GPTMS, TEOS and SiO_2 nanoparticles applied on aluminium alloy 7075-T6." *J. Electrochem. Soc.,* Vol. 165, pp. C213–C225, 2018

In this paper the synthesized hybrid sol-gel coating was bi-layer, meaning that the first coating, deposited on AA7075-T6, was doped with cerium, while the second was undoped. "Locking" cerium under the second layer retarded its leaching from the coating. This active inhibitor component enabled the self-healing ability which was proved by several different experiments on scribed coatings, i.e. on artificially made corrosion defect. The use of different characterization methods (EIS, EDS, XPS, UV/vis) contributed to the detailed study of self-healing mechanism. The novelty of the present paper was also the proof of the self-healing effect on the scribed coating by the increase in impedance at low frequency after several days of immersion in chloride solution. Self-healing was based on the progressive deposition of Ce-based compounds at the damaged sites.

1.9 Methodology

Chemicals used for synthesis procedures in this doctoral dissertation were commercially available and of known suppliers (Sigma-Aldrich, Merck, etc.).

During the doctoral dissertation several methods were used which are the following:

- **Methods for sol characterization**: Fourier transform infrared spectroscopy (FTIR), Ultraviolet-visible-near infrared spectroscopy (UV-vis-NIR), viscosimeter.

- **Methods for surface/coating analysis:** X-ray photoelectron spectroscopy (XPS), Scanning electron spectroscopy (SEM) equipped with energy dispersive X-ray spectroscopy (EDS).

- **Methods for coating characterization:** 3D profilometry, adhesion test, elipsometer.

- **Methods for electrochemical measurements:** potentiodynamic measurements (PD), electrochemical impedance spectroscopy (EIS).

- Other methods: immersion test.

1.10 Structure of the Dissertation

The doctoral dissertation is organized as follows. Chapter 2 describes the effect of mechanical and chemical pre-treatments on the morphology and corrosion property of aluminum alloys AA7075-T6 and AA2024-T3. Chapter 3 describes the synthesis, characterization and corrosion behavior of hybrid sol–gel coatings based on GPTMS/TEOS containing colloidal SiO_2 and cerium nitrate applied on aluminum alloy AA7075-T6. Finally, Chapter 4 describes the self-healing effect of $Ce(NO_3)_3$ in scribed hybrid sol-gel coatings based on GPTMS, TEOS and SiO_2 nanoparticles and applied on aluminum alloy AA7075-T6.

Chapter 2

Effect of Mechanical and Chemical Pre-treatments on the Morphology and Composition on Surfaces of Aluminum Alloys 7075-T6 and 2024-T3

This chapter presents the overview of the effect of mechanical and chemical pre-treatments of aluminum alloys 7075-T6 and 2024-T3 on their properties. The effect of these two pre-treatments on morphology, composition, wettability of the surface and on corrosion properties in sodium chloride solution was studied and discussed in detail. The mechanical treatment included grinding under water and polishing under non-aqueous liquid, while the chemical treatment included non-commercial chemical cleaning, based on sodium hydroxide and commercial cleaning, based on SurTec cleaner, both followed by desmutting in nitric acid. This chapter gives a clear overview of the topic and current state-of-the-art.

In Figure 1.8 a Graphical abstract of Chapter 2 is present.

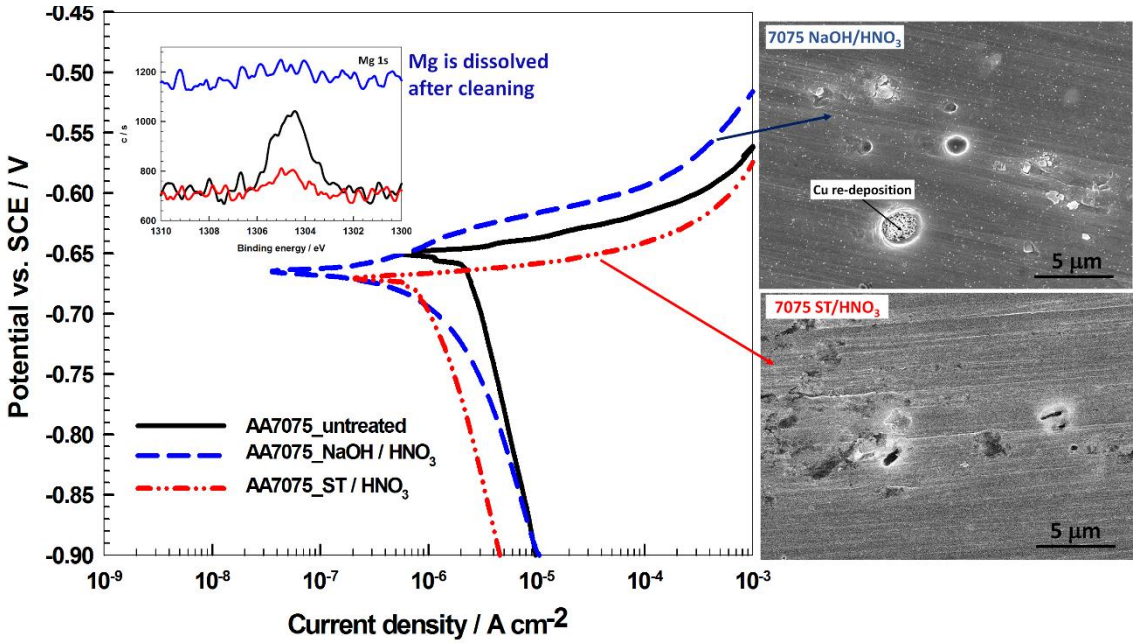


Figure 1.8: Graphical abstract of Chapter 2.

This chapter addresses thesis Objective 1) from Chapter 1.6.

Regarding my contribution: I made a literature overview of the topic, co-formulated the basic idea for the object of the investigation, co-planned, co-designed and performed the experiments and jointly prepared the manuscript with co-authors.

Corrosion Science 119 (2017) 46–59

Contents lists available at ScienceDirect

Corrosion Science

journal homepage: www.elsevier.com/locate/corsci

Effects of mechanical and chemical pre-treatments on the morphology and composition of surfaces of aluminium alloys 7075-T6 and 2024-T3

Urša Tiringer[a,b], Janez Kovač[b,c], Ingrid Milošev[a,*]

[a] Jožef Stefan Institute, Department of Physical and Organic Chemistry, Jamova c. 39, SI-1000 Ljubljana, Slovenia
[b] Jožef Stefan International Postgraduate School, Jamova c. 39, SI-1000 Ljubljana, Slovenia
[c] Jožef Stefan Institute, Department of Surface Engineering and Optoelectronics, Jamova c. 39, SI-1000 Ljubljana, Slovenia

ARTICLE INFO

Article history:
Received 26 November 2016
Received in revised form 8 February 2017
Accepted 9 February 2017
Available online 13 February 2017

Keywords:
(A) Aluminium alloy
AA7075-T6
AA2024-T3
(B) Polarization
(B) SEM
(B) XPS
(C) Alkaline cleaning
(C) Grinding

ABSTRACT

The effects of mechanical and chemical pre-treatments of AA7075-T6 and AA2024-T3 aluminium alloys were studied in terms of changes of morphology, composition and wettability of the surface, and of the related corrosion properties in sodium chloride solution. The mechanical treatments tested include grinding under water and polishing under non-aqueous liquid. The latter preserved the content of Mg at the AA7075-T6 surface. The effect of mechanical treatment was less pronounced on AA2024-T3. The chemical treatments included etching with sodium hydroxide and with a commercial cleaner and desmutting in nitric acid. The sample pre-treatment affects the polarization curves in sodium chloride.

© 2017 Elsevier Ltd. All rights reserved.

1. Introduction

Aluminium and aluminium alloys are commonly used light metals in the transportation industry [1–3]. Before applying any kind of coating against corrosion on aluminium alloys, however, it is necessary to pre-treat or clean appropriately the surface of the metal to be coated. The goal of either pre-treatment or cleaning is to remove organic and inorganic residues from the surface before treating it with paints or coatings [1–6]. The most common types of surface treatment for aluminium alloys are degreasing, mechanical treatment, chemical treatment, chemical brightening, anodising, powder coating and wet coating. The type of pre-treatment depends on the type of environment, such as automotive, aerospace industry, etc. [7].

Grinding and polishing are the most common mechanical pre-treatments. The former is usually based on SiC grinding papers and produces a macro-rough surface [6]. A diamond paste is used in polishing pre-treatment. The effects of grinding and polishing on localized breakdown of AA7075-T6 and of AA2024-T3 surfaces have been studied [8–12]. Mechanical grinding and polishing under water can promote aggressive corrosion, but even in non-aqueous conditions such pre-treatment was found to affect the microstructure and corrosion properties [7–10]. The near-surface region of an alloy was subjected to severe strain by the treatment and a nanograined deformed surface layer devoid of the $MgZn_2$ of AA7075-T6 hardening particles developed [9]. Moreover, the Zn and Mg alloying elements were found to segregate at the nanograin boundaries, creating bands of enhanced susceptibility that allowed surface layer dissolution at low potentials. One of the mechanical pre-treatments are also cold and hot rolling of alloys, which induce the formation of thin layer of metal in the surface with different properties and microstructural characteristics compared to the underlying bulk. The micro-structural difference between surface and bulk may lead to increased susceptibility to filiform corrosion after high temperature annealing. Polishing after rolling resulted in a high filiform corrosion resistance irrespective of prior heat treatment [13,14]. Using *in situ* X-ray microtomography a high localized susceptibility to intergranular corrosion of surface-deformed layers was evidenced [15]. As corrosion propagates, however, they are not

* Corresponding author.
E-mail address: ingrid.milosev@ijs.si (I. Milošev).

http://dx.doi.org/10.1016/j.corsci.2017.02.018
0010-938X/© 2017 Elsevier Ltd. All rights reserved.

uniformly corroded further, even though the matrix underneath dissolves completely [15].

Chemical pre-treatment is carried out after, or in place of, mechanical pre-treatment for removing surface contamination originating from mechanical pre-treatment and for removing oxides present at the metal surface [7]. It includes processes such as vapour degreasing, solvent cleaning, acid cleaning, alkaline cleaning, milling, etching, chromating/phosphating and electrochemically plating with copper, tin, nickel or silver. Chemical cleaners are divided into two groups, water-based and organic solvent cleaners. Acidic or alkaline cleaners are commonly used water-based cleaners. They can act as pickling agents, etching agents, detergents, degreasing agents or corrosion inhibitors [16]. Commercial cleaners are usually alkaline cleaners for liquid degreasing, and contain mainly phosphate, sodium-based carbonates or silicate, surfactants and additives including corrosion inhibitors [2]. The exact composition of commercial cleaners is usually held as a trade secret. Cleaning is often followed by acid treatment, pickling or desmutting, with the aim of removing residues arising from prior alkaline cleaning and of increasing surface roughness in order to facilitate the adhesion of organic coatings to the surface [17]. The most commonly used desmutters are nitric acid and fluoric acid.

Different surface cleaning agents and pre-treatments have been studied in relation to various conversion coatings [18–35]. The results differ considerably and depend on the type of substrate and the type of cleaning and desmutting agent [32]. One of the most commonly used pre-treatments of aluminium alloys is zincating. It was observed that with immersion in a zincate solution, aluminium is possible to be electroplated successfully. The adhesion od such surface is not always very good but may be improved with the addition of different ions [33]. To improve zinc-alloy film chemically deposited prior to nickel electroplating, a new pre-treatment, including double-step nitric hydrofluoric acid solution immersion with NaOH immersion between these two acid steps, was designed. The adhesion of such surface was one order of magnitude higher in comparison with the aforesaid [31]. The surface chemistry of AA2024-T3 was dominated by chromate-based deoxidising step which resulted in fast smut dissolution, as well as the formation of a thin passivating overlayer containing chromium [34]. Alkaline cleaning removed the magnesium-rich layer from the surface of aluminium alloy AA7075-T6, resulting in a higher copper content of the surface [16]. Copper enrichment after chemical cleaning has been commonly observed on AA7075-T6 and AA2024-T3 surfaces [18–22]. Alkaline cleaning changed the composition of the native oxide layer consisting of MgO, $MgAl_2O_4$ and Al_2O_3, leading to Cu concentrations in the surface of the order of 3–7 times the bulk concentrations of Cu for both AA2024-T3 and AA7075-T6 [20]. The Cu enrichment affects the subsequent treatment of the surface using conversion coatings. For example, alkaline cleaning followed by acid activation using sulphuric acid increased the deposition rate and corrosion resistance of cerium conversion coatings on AA2024-T3 [29]. For AA7075-T6, a commercial cleaner at pH 9.1 removed the magnesium-rich outer oxide layer selectively, leaving behind the native Al-rich ~10 nm thick oxide [16]. The same alloy cleaning, using a commercial cleaner at pH 9.1 followed by alkaline activation, resulted in thicker cerium conversion coatings [16]. Campestrini et al. observed that the level of Cu enrichment in the form of particles at the AA2024-T3 alloy surface was dependent on the pre-treatment, with the least enrichment resulting from desmutting (30 s in nitric/hydrofluoric acid) and the highest after acid pickling (20 min in sulphuric/phosphoric acid) [18]. It was observed that the deoxidation of AA2024-T3 with various acids, such as HNO_3, H_2SO_4, H_3PO_4 + HF and with a combination of $Na_2S_2O_8$ + HF has a strong effect on the morphology and composition of alloy [35]. The presence of Cu has an accelerated effect on the subsequent deposition of a cerium-conversion coating [19]. Alkaline treatment also affects the surface composition of other aluminium alloys such as AA1010 [23], AA6061-T6 [24] and AA6060 [25].

Although the effects of pre-treatments have been reported as summarized above, a systematic approach involving both mechanical and chemical treatments is still lacking. The aim of the present study was to gain more understanding of the effects of various mechanical and chemical pre-treatments on the morphology, surface composition, water contact angle and electrochemical characteristics of AA7075-T6 and AA2024-T3. In our previous studies rare earth-based coatings were used for protecting these alloys [36–38]. In the study reported here we aimed to provide a basis for further optimization of conversion conditions. The mechanical pre-treatments tested were grinding under water and polishing under non-aqueous liquid. The chemical pre-treatments consisted of: alkaline cleaning using either a NaOH solution followed by desmutting in nitric acid, or by alkaline cleaning with a commercial SurTec cleaner (Bensheim, Germany) followed by desmutting in nitric acid. The purpose of alkaline cleaning was to remove surface contaminants and the surface oxide layer. This was followed by acid desmutting in nitric acid to remove residues of surface products or particle remnants. Surface characteristics and corrosion properties were analysed using electrochemical potentiodynamic polarization, scanning electron microscopy with energy dispersive X-ray analysis (SEM/EDS), X-ray photoelectron spectroscopy (XPS) and water contact angle measurements.

2. Experimental

2.1. Materials and chemicals

Aluminium alloys AA7075-T6 (Zn 5.81 wt%, Mg 2.55 wt%, Fe 0.21 wt%, Si 0.08 wt%, Cu 1.67 wt%, Al remaining) and AA2024-T3 (Cu 4.35 wt%, Mg 1.33 wt%, Fe 0.25 wt%, Mn 0.53 wt%, Zn 0.1 wt%, other 0.07 wt%, Al remaining), supplied by Kaiser Aluminum in the form of 1 mm thick sheet, were used as substrates.

For grinding, SiC papers ranging from 320 to P4000-grit were used, supplied by Struers. For polishing, diamond paste ranging from 15 to 1 μm (DP-paste P and MD-Nap cloth, supplied by Struers) and ethanol-based DP-Lubricant Blue, supplied by Struers, were used.

SurTec commercial cleaner (Bensheim, Germany) is a mixture of SurTec132 liquid recyclable builder and SurTec089 recyclable detergent component. The major component of SurTec132 is tetrapotassium pyrophosphate. It is a silicate-free, weak alkaline cleaner with a pH of 8.3. The ingredients of SurTec089 are nonionic surfactants alcohols—amines, coco alkyl and ethoxylated fatty alcohol.

0.01 M NaOH solution, pH 11.6 (99%, ApplicaChem) was used as a non-commercial cleaner. Desmutting of the surface was performed with 50% HNO_3 in water, pH = 1.5 (66%, Sigma Aldrich); Milli-Q Direct water with resistivity of 18.2 MΩ cm at 25 °C (Millipore, Billerica, MA) was used for rinsing and for solution preparation.

Electrochemical measurements were performed in 0.1 M NaCl (99.7%, Fisher Scientific), pH = 5.5.

2.2. Mechanical and chemical pre-treatments

The mechanical pre-treatments used in this study are summarized in Table 1. Following surface mechanical pre-treatment, chemical pre-treatment was performed using non-commercial and commercial cleaners, as summarized in Fig. 1. The following parameters were considered: time of immersion in NaOH or HNO_3 solutions, concentrations of SurTec132 and of SurTec089,

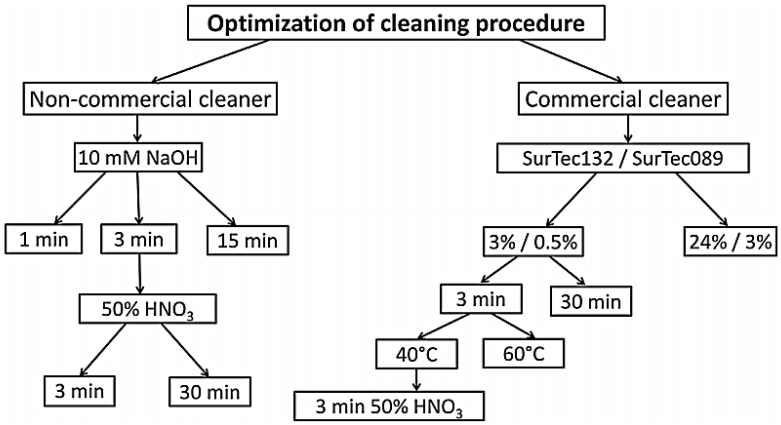


Fig. 1. Optimization of cleaning procedures.

Table 1
Mechanical pre-treatment of the substrate.

Grinding	Polishing
- Water-based	- Not water based
- Use of SiC paper successively up to 4000-grit	- Use of 15, 9, 3 and 1 μm diamond pastes
- Water rinsing	- EtOH-based lubricant rinsing
- Ultrasonic cleaning in EtOH, 5 min	- Ultrasonic cleaning in EtOH, 5 min
- Drying in a stream of nitrogen	- Drying in a stream of nitrogen

and time of immersion and temperature of a SurTec (ST) mixture. Abbreviations were used to identify the treatment, such as ST_x%_132_y%_089 for 3% SurTec132 + 0.5% SurTec089, where x and y are volume percentages of each SurTec (ST) cleaner.

2.3. Characterization

2.3.1. Surface analysis

X-ray photoelectron spectroscopy was carried out using a PHI-TFA XPS spectrometer (Physical Electronic Inc.). The vacuum during the XPS analysis was in the range of 10^{-9} mbar. The analysed area was 0.4 mm in diameter and the analysed depth about 3–5 nm. X-rays were provided from a monochromatic Al source at photon energy of 1486.6 eV. XPS spectra were analysed by Multipak software, version 8.0 (Physical Electronics Inc.). Experimental spectra were curve-fitted using Gaussian/Lorentzian shape of curves. As carbon was an adventitious surface contaminant, it was not taken into account when calculating the surface composition. After taking the spectra at the surface, sputter depth profiles were determined. An Ar^+ ion beam, with an energy of 4 keV and a raster of 3 mm × 3 mm, was used for etching. The sputtering rate was 2 nm/min, as determined on a Ni/Cr multilayer structure of known thickness.

Scanning electron microscopy (SEM) images in secondary electron mode were taken with a JEOL JSM-7600F microscope equipped with energy dispersive X-ray spectroscopy (EDS), supplied by Oxford Instruments INCA. The analysed area was a few micrometres in diameter and the analysed depth around 1 μm. Prior to analysis, samples were coated with a thin carbon layer to reduce the charging effect and then analysed at an energy of 15 kV.

Contact angles for deionised water drops on the sample surfaces were measured using a Krüss DSA 20 tensiometer (Krüss GmbH. Hamburg, Germany). Each contact angle value is the average of at least three measurements made at different locations.

2.3.2. Electrochemical measurements

Electrochemical measurements were performed in 0.1 M NaCl at room temperature in a three-electrode standard corrosion cell (PAR model K0047 Corrosion Cell Kit) with a volume 0.350 L. The working electrode was embedded in a Teflon holder (PAR model K0105 Flat Specimen Holder Kit) with an exposed area of 0.87 cm^2. A graphite electrode (area 7.54 cm^2) served as a counter electrode and a saturated calomel electrode (SCE) placed in a Luggin capillary was used as reference electrode (E = 0.242 V versus standard hydrogen electrode).

Electrochemical experiments were carried out with an Autolab PGSTAT 12 (Metrohm Autolab, Utrecht, Netherlands) potentiostat/galvanostat controlled by Nova 1.11 software. All potentials in the text refer to the SCE scale.

After 1-h stabilization at the open circuit potential (OCP), potentiodynamic polarization curves were recorded, starting at −250 mV vs. OCP up to −0.5 V SCE using a scan rate of 1 mV/s. Experiments were repeated at least three times. The most representative measurement that was chosen for plotting. In tabular form, results are given as mean ± standard deviation. Since, in chloride solution, the anodic current increased abruptly due to pitting corrosion, the corrosion current density, j_{corr}, was determined as the intersection of the cathodic slope and the line passing through the corrosion potential, E_{corr}.

3. Results and discussion

The study is divided into two parts: (i) the effect of mechanical pre-treatment, and (ii) the effect of chemical pre-treatment. The morphology, composition, water contact angle and corrosion properties of AA7075-T6 and AA2024-T3 samples were analysed.

3.1. Mechanical pre-treatments

3.1.1. SEM/EDS characterization

The effect of surface preparation on morphology and composition was investigated by SEM/EDS and XPS analyses. The SEM/EDS analysis was carried out at different locations on AA7075-T6 ground under water and on AA7075-T6 polished under non-aqueous liquid (Fig. 2, Table 2). Aluminium alloys have a heterogeneous structure with intermetallic particles [9,39–42]. Samples ground under water exhibited more surface defects and pulled-out grains, while the polished sample surfaces were smoother (Fig. 2). The composition at location 1 (Fig. 2a) of the sample ground under water

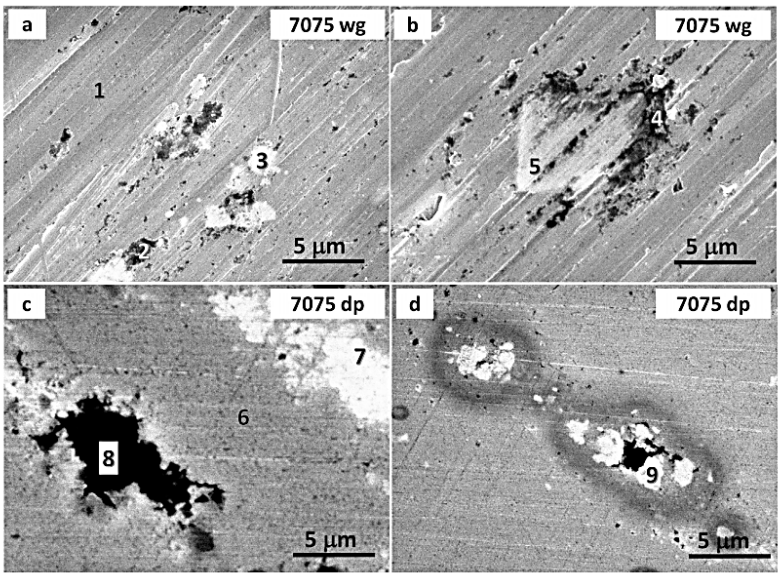


Fig. 2. SEM images of AA7075-T6 after (a, b) under water grinding and (c, d) diamond polishing. The numbers 1–8 denote locations where EDS analysis was carried out (Table 2). The abbreviation "wg" denotes the sample ground under water and "dp" sample diamond polished under non-aqueous liquid.

Table 2
Concentrations of elements obtained by EDS analysis at different locations on the surface of ground under water (locations 1–5) and of surface polished under non-aqueous liquid (locations 6–9) AA7075-T6 (SEM images in Fig. 2).

Location	at.% Al	at.% Mg	at.% Zn	at.% Cu	at.% O	at.% Fe	at.% Si
1	92.7	2.1	5.2	–	–	–	–
2	72.1	1.9	2.0	–	24.0	–	–
3	80.7	2.3	2.6	1.5	12.9	–	–
4	72.1	–	–	16.5	3.9	7.5	–
5	77.8	–	–	4.9	–	17.3	–
6	95.1	2.4	2.5	–	–	–	–
7	88.1	10.1	1.8	–	–	–	–
8	44.5	3.2	1.3	–	42.3	–	8.8
9	65.2	–	–	21.4	4.9	8.5	–

corresponds to that of a matrix alloy surface containing Al, Zn and Mg (Table 2). At location 2, in addition to Al, Zn and Mg, more oxygen was observed, showing that the oxide layer was thicker. Following grinding, a native oxide layer is immediately formed by self-passivation during air exposure. Copper is present in smaller, spherical Al-Cu-Mg IMs (location 3). The larger IMs, containing Fe and Cu, are Al-Cu-Fe particles (locations 4,5, Fig. 2b) with various amounts of Cu and Fe, respectively.

The concentrations of Al and Mg in the matrix of sample AA7075-T6 polished under non-aqueous liquid are similar to those in the matrix of the sample ground under water, but that of Zn is lower (location 6) (Fig. 2c, Table 2). The concentration of Mg was high at location 7, but not on the ground sample. Si concentration was increased at location 8 (Fig. 2c), which could be related to the remaining $MgSi_2$ particles or to surface contamination. Cu and Fe are present at location 9. Thus, in addition to the smoothness of the surface, the main difference observed between samples ground under water and polished under non-aqueous liquid is the higher concentration of Mg in the latter, AA7075-T6 sample (2.0–2.3 at.% in sample ground under water and 2.4–10.1 at.% in polished under non-aqueous liquid).

The differences in morphology and composition at different locations at the AA2024-T3 surface are presented in Fig. 3 and Table 3. The matrix of AA2024-T3 ground under water at location 1 consists of Al, Mg and Cu (Fig. 3a). Oxide is present at location 2. A larger IM particle (~10 µm), containing Al-Cu-Fe and some O, was observed at location 3, together with a high concentration of Cu. Iron is also present in the smaller particle at location 4, where the concentration of oxygen is highest. Particles 5, 6 and 7 are similar and consist of Al, Mg, Cu and O with different concentrations of O.

Compared to the sample ground under water, the surface of AA2024-T3 sample polished under non-aqueous liquid is relatively smooth (Fig. 3). Polishing appears to lead to a more homogeneous surface on AA2024-T3 than on AA7075-T6 (Fig. 3c,d). Mg was detected in amounts similar to those in the ground sample, while the amount of Cu was smaller (locations 8 and 9). Sites at locations 10 and 11 contain Fe, and, at location 12, Mg and a high content of O.

3.1.2. *X ray photoelectron spectroscopy*

Samples ground under water and samples polished under non-aqueous liquid were studied by XPS analysis. The X-ray spot size was 400 µm, so the results represent an average of the surface composition, including matrix and IMs. The surface of AA7075-T6 ground under water contains Al and O, and minor elements Mg, Zn, Si, Ca and N (Fig. 4a). Silicon is present in the alloy, but at a

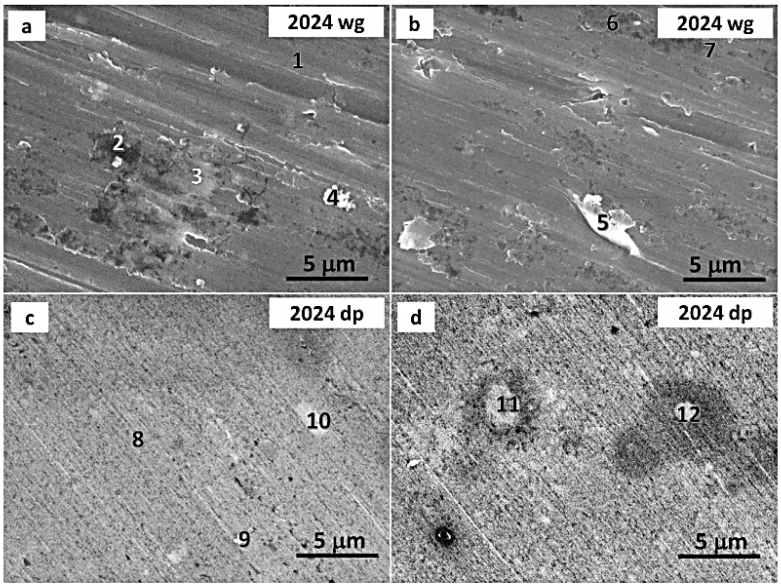


Fig. 3. SEM images of AA2024-T3-T3 after (a, b) under water grinding and (c, d) diamond polishing. The numbers 1–12 denote locations where EDS analysis was carried out (Table 3). The abbreviation "wg" denotes sample ground under water and "dp" sample diamond polished under non-aqueous liquid.

Table 3
Concentrations of elements obtained by EDS analysis at different locations on the surface ground under water (location 1–7) and polished under non-aqueous liquid (locations 8–12) AA2024-T3 (SEM images in Fig. 3).

Location	at.% Al	at.% Mg	at.% Cu	at.% O	at.% Fe
1	96.4	1.3	2.3	–	–
2	73.7	1.0	2.8	22.5	–
3	74.0	–	17.6	2.9	5.5
4	66.3	0.93	–	27.8	3.2
5	91.4	1.2	2.1	5.3	–
6	94.0	1.0	2.2	2.8	–
7	85.4	1.3	1.8	11.5	–
8	97.3	1.0	0.8	0.9	–
9	96.0	–	1.6	2.4	–
10	91.4	1.2	–	–	7.4
11	71.4	2.1	–	9.7	16.8
12	54.2	4.2	–	41.6	–

lower concentration than that detected here, so the increased concentration may be related partially to contamination. Ca and N are contaminants, presumably originating from grinding and/or water. Mg and Zn are constituents of IMs in the alloy, and are present in solid solution. The surface studied in the point EDS analysis is only a few micrometres in diameter, considerably less than that for XPS analysis. The results from point EDS (Table 2) and XPS analyses are thus expected to differ (Fig. 4a). Cu and Fe are not detected by XPS in the IMs, although they are present in the alloy and clearly identified by point EDS analysis. The reason for this lies in the smaller lateral resolution of XPS than that of EDS and, also, the smaller depth analysed. After polishing under non-aqueous liquid, the most important change is related to the increase in Mg content (Fig. 4a). Due its high reactivity, magnesium from the IMs can be dissolved in water, thus leading to selective leaching from the alloy. Magnesium dissolution is clearly reduced in non-aqueous liquid diamond polishing, when the surface contains a Mg content more similar to that in base alloy.

AA2024-T3 ground under water contains Al and O and minor elements Zn, Cu, Ca and Sn, the latter two being surface contaminants (Fig. 4b). Like those for AA7075-T6, XPS and point EDS analyses gave different results: (i) the content of Cu detected by XPS is much lower than that by EDS (Table 3), and (ii) Mg and Fe were not detected by XPS, although EDS confirmed their presence. In contrast to AA7075-T6, a smaller difference between samples AA2024-T3 ground under water and polished under non-aqueous liquid was observed (Fig. 4b). Both Cu and Zn could scarcely be detected.

High resolution XPS Al 2p curve-fitted spectra are presented in Fig. 5. The position of 2p peak in Al_2O_3 was reported at binding energies between 71.1 eV and 76.19 eV, while that of Al metal between 72.5 and 72.9 eV [43]. Aluminium is present mostly as the oxide, Al_2O_3, in both ground under water and polished under non-aqueous liquid AA7075-T6 and AA2024-T3, as shown by the intense peak at 74.3 eV. The metal Al peak is centred at 71.8 eV. The intensity of the metal peak is most pronounced on AA7075-T6 ground under water, which could indicate that, for this sample, self-passivation was the slowest. The oxygen peak corresponds mainly to oxide formation and is centred at 531.5 eV (results not shown).

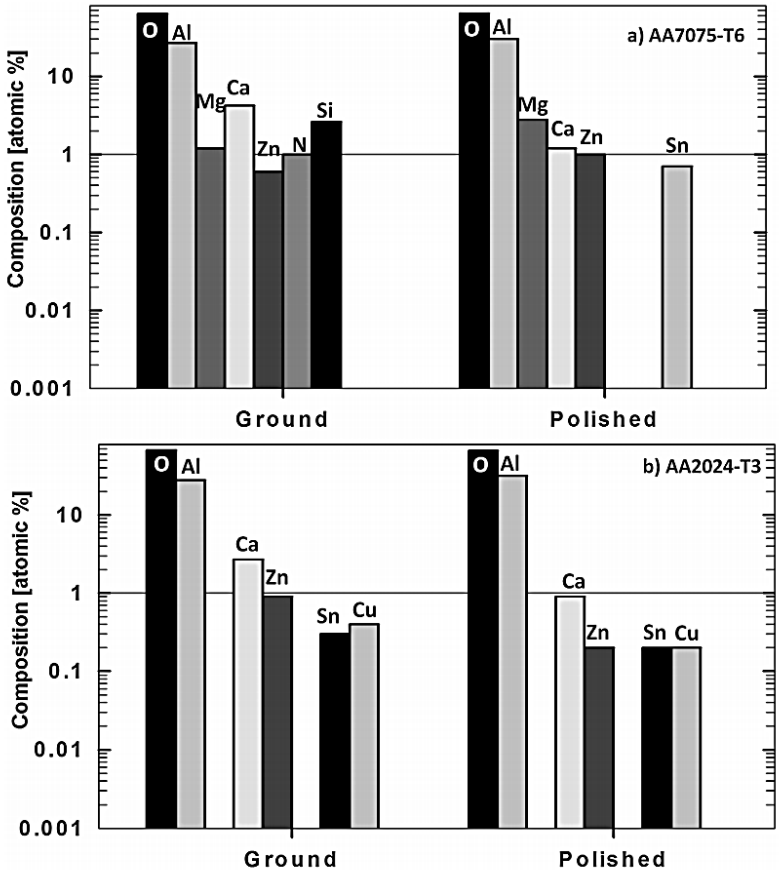


Fig. 4. Concentrations of elements obtained by XPS after different surface mechanical pre-treatments (under water grinding and under non-aqueous liquid diamond polishing) of (a) AA7075-T6 and (b) AA2024-T3.

3.1.3. Electrochemical measurements

Potentiodynamic polarization curves recorded for samples AA7075-T6 and AA2024-T3 ground under water and polished under non-aqueous liquid are presented in Fig. 6. The related electrochemical parameters are summarized in Table 4. The cathodic process corresponds to the reduction of oxygen that proceeds mainly on intermetallic particles, and the anodic process to pitting corrosion initiated on the intermetallics [8–12] with a breakdown potential slightly above E_{corr}. Depending on the type of alloy, one or two breakdown potentials were observed [8–12].

The effects of under water and under non-aqueous liquid mechanical treatment on polarization curves for AA7075-T6, an Al-Zn-Mg-Cu-based alloy, were related mainly to a distinct negative shift of E_{corr} (Fig. 6a). Mechanical pre-treatment under non-aqueous liquid preserves more Mg in the alloy than under water grinding and, since Mg is electrochemically more active, a negative potential shift occurred. The current density decreased, indicating that there are fewer cathodically active sites at the surface, where oxygen reduction proceeds. The increase of E_{corr} in the anodic range is slower than for the sample ground under water. For AA2024-T3, which is an Al-Cu-Mg-based alloy, the negative shift of E_{corr} is less pronounced, the current density is smaller in the cathodic range, and the increase of anodic current density is slower (Fig. 6b).

3.2. Chemical pre-treatment

Two alkaline treatments were used, (i) NaOH at pH 11.6 and (ii) commercial ST cleaner at pH 8.3. Since the pH values and compositions of these agents are different, the effect of the two treatments on the AA7075-T6 and AA2024-T3 is expected to differ. After the alkaline treatments, the surface was desmutted in nitric acid. These two treatments are denoted as NaOH/HNO_3 and ST/HNO_3. As a mechanical pre-treatment, under water grinding was used for both alloys.

The first step was optimization of the cleaning procedure as a function of immersion time in NaOH and in HNO_3. After cleaning using NaOH, all curves exhibited smaller corrosion current density compared to untreated sample (Fig. S1a in Supplement material). Immersion for 15 min was too long, since the curve differed considerably from those for other samples and the sample became dark brown. Among 3 and 5 min, the former was chosen for further experiments since the time of immersion is shorter (more suitable for industrial purposes) whilst the shape of curves is similar. In the case of HNO_3 treatment alone, 3 min of immersion was the most

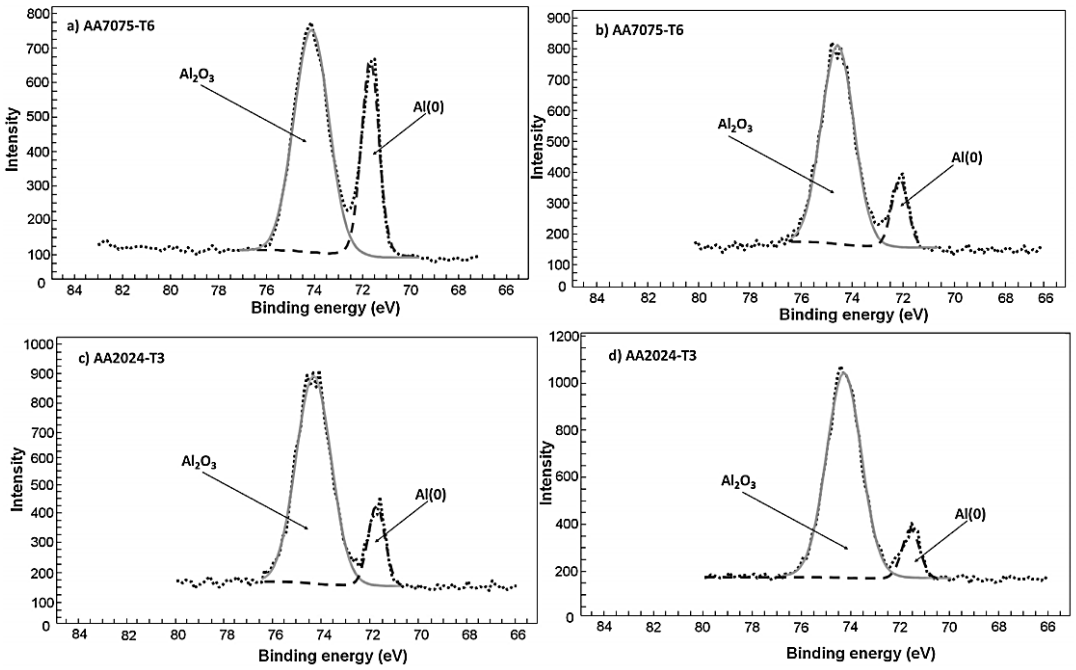


Fig. 5. Curve-fitted XPS Al 2p peaks of aluminium after different mechanical pre-treatments: (a) under water grinding and (b) under non-aqueous liquid diamond polishing AA7075-T6, (c) under water grinding and (d) under non-aqueous liquid diamond polishing AA2024-T3. Dotted lines represent experimental data, grey and dashed lines are fitted lines.

Table 4
Corrosion potentials, E_{corr}, corrosion current densities, j_{corr}, and cathodic Tafel slopes, β_c, for AA7075-T6 and AA2024-T3 determined from polarization curves in 0.1 M NaCl (Fig. 6) after different mechanical and chemical pre-treatments (ground under water, polished under non-aqueous liquid, ground under water and $NaOH/HNO_3$ and ground under water and ST/HNO_3). Results are given as mean ± standard deviation.

AA7075-T6	Ground	Polished	$NaOH_3/HNO_3$	ST/HNO_3
j_{corr} [μA/cm²]	2.4 ± 0.30	1.72 ± 0.05	0.9 ± 0.02	1.1 ± 0.08
E_{corr} [V vs. SCE]	−0.65 ± 0.01	−0.76 ± 0.02	−0.67 ± 0.01	−0.69 ± 0.01
β_c [mV/dec]	−380 ± 15	−290 ± 20	−240 ± 10	−340 ± 20
AA2024-T3	Ground	Polished	$NaOH/HNO_3$	ST/HNO_3
j_{corr} [μA/cm²]	2.0 ± 0.10	1.0 ± 0.03	0.55 ± 0.04	0.55 ± 0.03
E_{corr} [V vs. SCE]	−0.60 ± 0.02	−0.68 ± 0.01	−0.59 ± 0.01	−0.62 ± 0.01
β_c [mV/dec]	−410 ± 25	−340 ± 20	−220 ± 20	−210 ± 20

suitable, as after 30 s the curve was not significantly different than that of the untreated one (Fig. S1b in Supplement material). The selected alkaline/acid treatment was therefore 3 min of immersion in NaOH followed by 3 min in HNO_3.

The second step was optimization of the cleaning procedure as a function of immersion time in commercial SurTec cleaner and HNO_3 (Fig. S2 in Supplement material). 3 min in HNO_3 was always used as the acid desmutting step. The following parameters were optimized for alkaline cleaning: concentrations of ST132 and ST089; at selected concentration the immersion time and temperature of mixture were then tested (Fig. S2 in Supplement material). As for NaOH pre-treatment (Fig. S1a), all curves exhibited smaller corrosion current density than the untreated sample. Based on the difference compared to untreated sample and/or rationality in terms of time of immersion the following parameters were used: 3%ST132 and 0.5%ST089 mixture, an immersion time of 3 min and a desmutting temperature of 40 °C (Fig. S2 in Supplement material).

Electrochemical behaviour will be discussed further after the water contact angle, SEM/EDS and XPS results are presented below.

3.2.1. *Water contact angle and characterization by SEM/EDS*

The water contact angle (Θ) of the surface was affected less by chemical pre-treatment than by mechanical (ground under water) pre-treatment (Table 5). Treatment with $NaOH/HNO_3$ led to the surface of AA7075-T6 becoming super-hydrophilic (Θ < 10°), and almost super-hydrophilic (Θ = 10°), following ST/HNO treatment. The difference in contact angle between mechanically and chemically treated AA2024-T3 is smaller than that for AA7075-T6, the surface of which remained hydrophilic.

SEM/EDS analysis was performed to investigate the effect of chemical pre-treatment on the morphology of the surface. The SEM images of samples AA7075-T6 and AA2024-T3 ground under water presented in Figs. 2 a,b and 3 a,b were compared. A significant difference in the shape of intermetallic particles was observed after

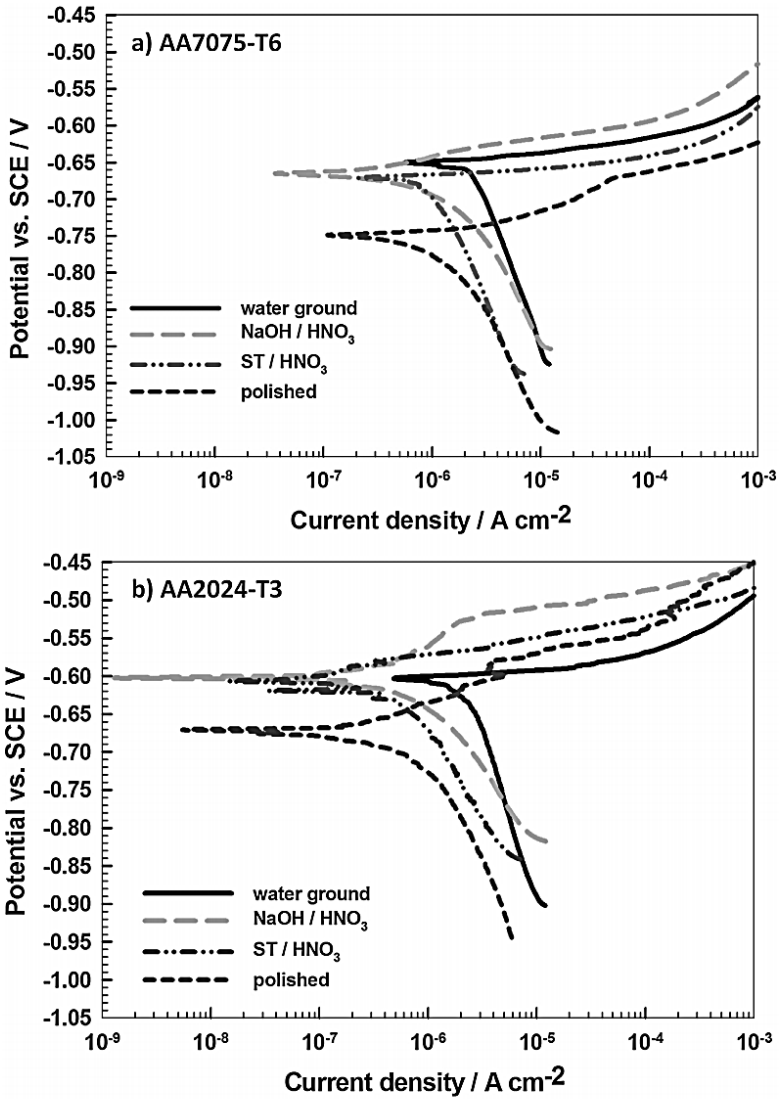


Fig. 6. Potentiodynamic polarization curves recorded in 0.1 M NaCl for (a) AA7075-T6 and (b) AA2024-T3 ground under water, polished under non-aqueous liquid, ground under water and $NaOH/HNO_3$ treated, and ground under water and ST/HNO_3 treated. d E/d t = 1 mV/s. Electrochemical parameters are given in Table 4.

Table 5
Values of contact angles of untreated (ground under water) AA7075-T6 and AA2024-T3, and of chemically treated alloys using $NaOH/HNO_3$ and ST/HNO_3.

Sample	Contact angle [°]
AA7075-T6_untreated	47
AA7075-T6_$NaOH/HNO_3$	8
AA7075-T6_ST/HNO_3	12
AA2024-T3_untreated	39
AA2024-T3_$NaOH/HNO_3$	25
AA2024-T3_ST/HNO_3	16

chemical treatment of AA7075-T6 (Fig. 7a,b). After $NaOH/HNO_3$ treatment, white, round deposits with a spongy-like appearance were observed at the surface (Fig. 7a, location 1). These deposits consist of copper, as evidenced by EDS (Table 6). Prolonged (20 h) immersion in NaOH solution leads to dealloying od S-phase and formation of bicontinuous dealloying morphology with flatter region with "Swiss cheese" morphology and near surface region of the porous structure [44]. At location 2, Cu was also detected, but together with Fe, thus corresponding to Cu-Fe-based IMs (Fig. 7a).

After treating AA7075-T6 with ST/HNO_3, no round, spongy deposits containing mainly Cu were detected (Fig. 7b). Again, Cu and Fe are present at location 3, probably related to IMs (Table 6). The oxidized matrix is seen at location 4.

Following $NaOH/HNO_3$ treatment the surface of AA2024-T3 was rough, consisting of micrometre-sized fragments (Fig. 7c). EDS

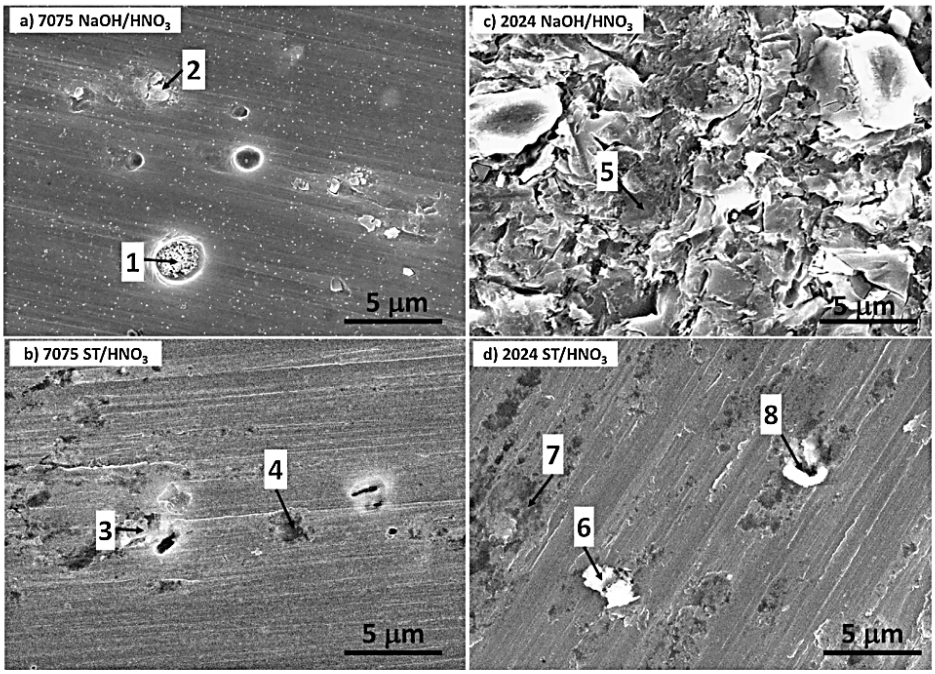


Fig. 7. SEM images of AA7075-T6 treated using (a) $NaOH/HNO_3$ and (b) ST/HNO_3 and images of AA2024-T3 treated using (c) $NaOH/HNO_3$ and (d) ST/HNO_3. The numbers 1–8 denote the locations where EDS analysis was carried out (Table 6).

analysis confirmed that only Al and O are present (Table 6, location 5). This result could indicate the product of etching, i.e. sodium aluminate, $NaAlO_2$, formed during exposure of Al_2O_3 to NaOH solution. No other element was detected. After ST/HNO_3 treatment, however, the surface appearance differed completely from that with $NaOH/HNO_3$, (Fig. 7d) and was more closely similar to that of the mechanically ground surface (Fig. 3a,b). Locations 6 and 8 consist of Al, Mg and Cu with a high concentration of oxygen. At location 7, Mg is not present and a high concentration of Cu was observed, in addition to Fe.

3.2.2. X ray photoelectron spectroscopy

The composition of AA7075-T6 ground under water, as determined from the XPS survey spectrum, includes the following elements: O, Al, Mg, Zn, Si, with contaminants Ca and N (Figs. 4 and 8). After chemical treatment the composition of the surface changed (Fig. 8). The effects of NaOH and $NaOH/HNO_3$ were studied separately (Fig. 8). After cleaning with NaOH, the content of Al was reduced and that of O and, especially of Mg, increased (Fig. 8a). The content of Ca decreased, while N and Si disappeared. The sputter depth profile following NaOH treatment (Fig. 8b,c) showed that, after etching with NaOH solution at pH 11.6, formation of Mg oxide occurs. The content of Mg at the surface of AA7075-T6 reached almost 15 at.%. At the same time, Al oxide was dissolved, leaving the surface enriched in Mg-oxide. The content of Cu and Zn was low at the surface but started to increase within depth of the layer. The thickness of the surface Mg-rich oxide layer was 36 nm (taking the depth at which the oxygen concentration drops to half that at the surface as a measure of layer thickness). This is in accordance with reports that subsequent activation in NaOH or Na_2CO_3 with pH >11.5 increases the thickness of the Mg-rich surface oxide to 20–60 nm [16].

The stability of individual elements and their compounds as a function of pH. According to the *E*-pH diagrams, aluminium oxide, which covers the matrix, is stable in the pH range 4–9.5, and will thus dissolve as AlO_2^- when using NaOH. For the Al–Mg–H_2O system it was reported that aluminium is stable at pH values up to pH 11.5 [16]. Magnesium, which is present in IMs and in alloy matrix as, for example, $MgZn_2$, Mg_2Al_3, Al_2CuMg, etc., is stable as $Mg(OH)_2$ at pH >11.5 and dissolves at lower pH values. At pH 11.6 oxides of Cu and Zn are at the upper edge of stability and their dissolution is expected to be less than that of Al; these elements dissolve in alkaline medium as $HCuO_2^-$ and $HZnO_2^-$.

After $NaOH/HNO_3$ treatment zinc is still present at the surface but magnesium disappeared, in accordance with the dissolution of Mg-rich layer at low pH (Fig. 8a). Instead, Cu peak appeared. Both Zn and Cu were detected at very low concentrations ($\leq$1 at.%). In contrast to point EDS analysis (Fig. 7a), the spot is much larger on XPS and local Cu deposits cannot be detected.

Compared to NaOH, which acts as an etching agent, ST cleaner is expected to have a milder etching effect, given its lower pH. After treatment with ST/HNO_3 the following elements were detected: O, Al, P, Si and Zn (Fig. 8a). The Zn content was smaller than after $NaOH/HNO_3$ treatment and Mg was no longer observed. Si remained at the surface. The level of phosphorus increased. Similar features, i.e., decrease in Zn and Mg and increase in Cu concentrations, were observed after alkaline cleaning of AA7075-T6 treated previously with commercial cleaners N-Kleen and Novaclean Al86 [18].

XPS spectra for Al, Mg, Cu and Zn, as major constituents of AA7075-T6, are interpreted in more detail using high resolution spectra (Fig. 9). Two peaks of Al were detected after both chemical treatments (Fig. 9a). The first peak, at 74.3 eV, was ascribed to the oxide Al_2O_3 and the second, at 71.8 eV, to aluminium metal, the

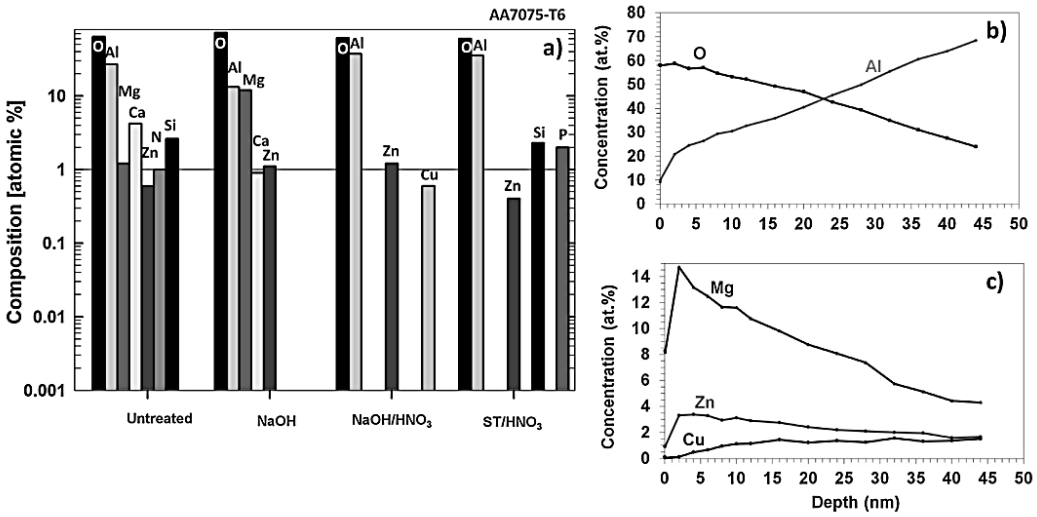


Fig. 8. a) The concentrations of elements obtained from survey XPS spectra for untreated, ground under water AA7075-T6 and AA7075-T6 treated using NaOH, $NaOH/HNO_3$ and ST/HNO_3. Sputter depth profile of the sample treated using NaOH showing b) Al and O, and c) minor elements at enlarged scale.

Table 6
Concentrations of elements obtained by EDS analysis at different locations on the AA7075-T6 surface ground under water (locations 1–4) and AA2024-T3 (locations 5–8) treated using $NaOH/HNO_3$ and ST/HNO_3 (SEM images in Fig. 8).

Location	at.% Al	at.% Mg	at.% Zn	at.% Cu	at.% O	at.% Fe
7075–1	70.4	3.5	–	18.1	8.0	–
7075–2	83.6	2.6	–	6.7	4.2	2.9
7075–3	68.5	–	–	19.2	3.4	8.9
7075–4	79.9	2.2	2.2	–	15.7	–
2024- 5	96.4	–	–	–	3.6	–
2024–6	47.3	2.1	–	5.1	45.5	–
2024–7	67.6	–	–	12.0	16.8	3.6
2024–8	82.3	1.0	–	2.4	14.3	–

intensity of oxide peak being similar or slightly higher than that of the metal. This indicates that the oxide layer is thin. The presence of oxide may be due to ineffective removal of surface product by chemical treatment, the formation of hydroxide/oxide film during chemical treatment, or its formation during air exposure after treatment. The shape of oxide part of the peak for the chemically untreated sample is quite broad indicating that two species may be present. As Mg is also detected in untreated sample (Fig. 9b) it may be assumed that in addition to Al_2O_3 peak it contains also contribution of Al bonded as $MgAl_2O_4$. For AA7075-T6, a commercial cleaner with pH 9.1, removed the magnesium-rich outer oxide layer selectively, leaving behind the native Al-rich ~10 nm thick oxide [16]. The peak of Mg was detected only for chemically untreated, ground under water sample (Fig. 9b), indicating that it is dissolved during the desmutting step. Its binding energy at 1304.8 eV can be related to $Mg(OH)_2$ (1302.7 eV) and $MgAl_2O_4$ (1304.0 eV) [43]. Two peaks appeared in the Zn $2p_{3/2}$ region, at 1020.9 eV and at 1022.4 eV (Fig. 9c). The latter peak may be related to the formation of ZnO or $Zn(OH)_2$ and is larger for the sample ground under water, indicating that chemical treatment removed ZnO from the surface. The peak of copper at 933.0 eV in the Cu $2p_{3/2}$ region appeared only for the sample treated with $NaOH/HNO_3$ (Fig. 9d). In XPS 2p spectra it is difficult to differentiate between Cu and Cu_2O, because of the small chemical shift [45,46]. These compounds can be differentiated based on the XPS Auger spectra [45]. However, due to the small content of Cu at the surface it is not possible to use the latter procedure here. Furthermore, the Auger Cu LMM spectrum overlaps with that of O 1s. In oxide, the full width at half maximum in oxides is greater than in metal [45,46]. Under these circumstances it cannot be determined unambiguously whether copper is present in its metal and/or oxide state. The P 2p peak is centred at a binding energy of 134.0 eV (results not shown) which can be related to phosphate and originates from the ST cleaning agent.

XPS analysis of the sample AA2024-T3 ground under water shows the presence of the elements O, Al, Zn, Cu, Ca and Sn, the latter two being contaminants (Fig. 10a). After treatment using NaOH, Zn was the only minor element remaining at the surface. On further treatment, with nitric acid, Zn dissolved and Cu remained at the surface. Depth profiles after NaOH treatment are presented in Fig. 10b,c. Mg is enriched and Cu depleted at the surface, but much less than for AA7075-T6 which is a Mg-based alloy. The thickness of the Al-rich oxide layer formed is thinner (26 nm) than that of the Mg-rich oxide layer formed at the surface of AA7075-T6 (Figs. 8 c and 10 c).

After treatment with $NaOH/HNO_3$, Zn dissolved and Cu remained at the surface (Fig. 10a) while, after ST/HNO_3 treatment, only Al and O were detected. In contrast to AA7075-T6, no phosphorus, originating from the ST cleaner, was present at the AA2024-T3 surface.

XPS spectra of Al, Cu and Zn were also investigated at high resolution (Fig. 11). Two Al peaks appeared at 74.3 eV and at 71.8 eV, related to Al_2O_3 and Al metal, respectively (Fig. 11a), the intensity

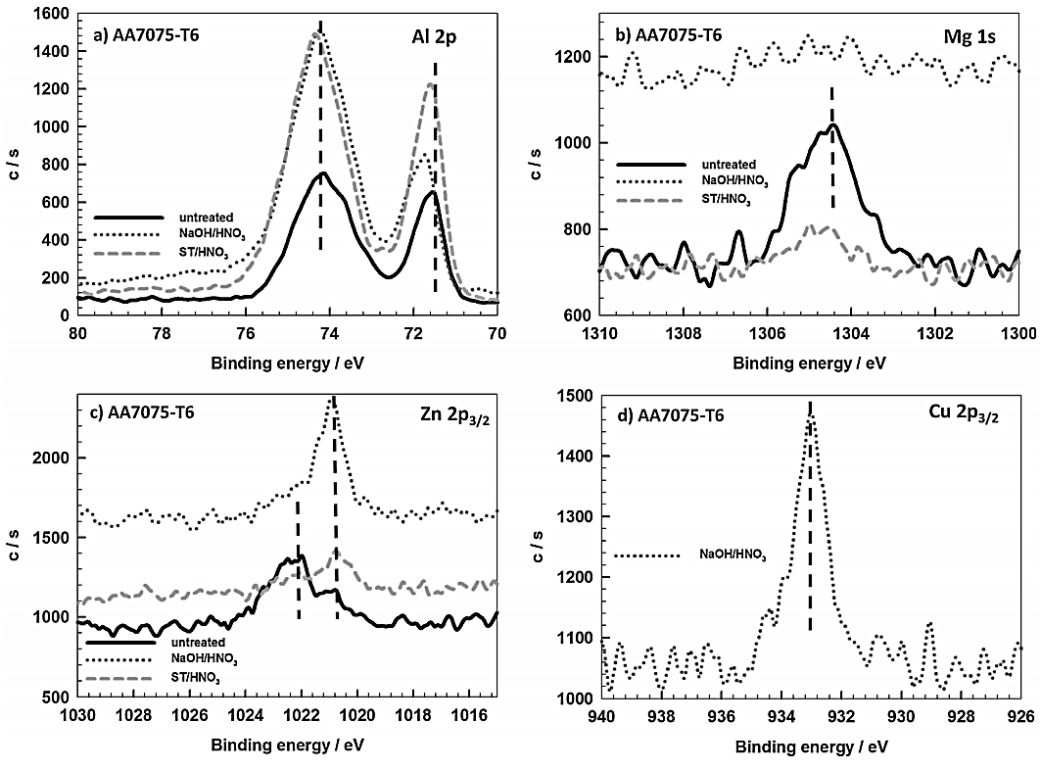


Fig. 9. High resolution XPS spectra of (a) Al 2p, (b) Mg 1s, (c) Zn $2p_{3/2}$ and (d) Cu $2p_{3/2}$ recorded for untreated, ground under water AA7075-T6 and AA7075-T6 treated using $NaOH/HNO_3$ and ST/HNO_3.

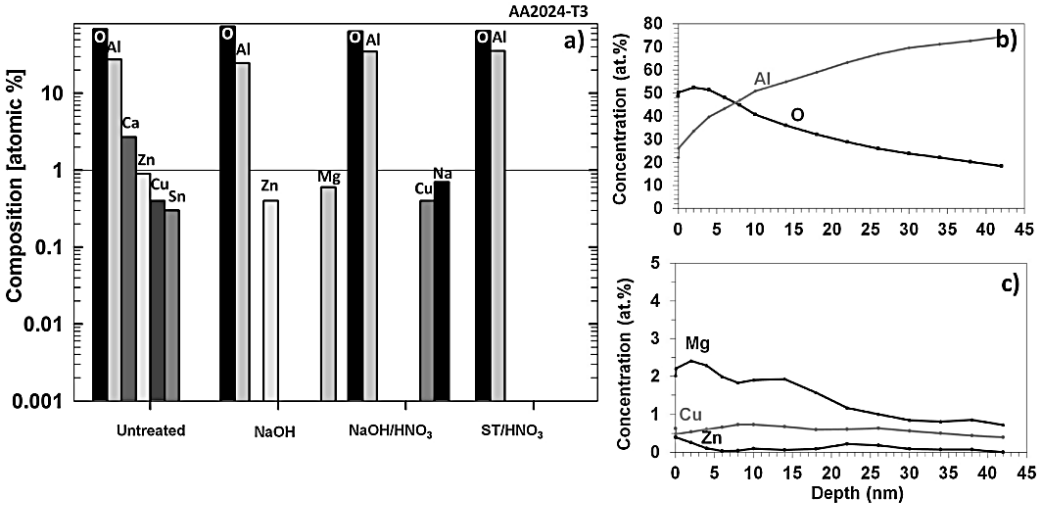


Fig. 10. (a) The concentrations of elements deduced from XPS survey spectra for untreated, ground under water AA2024-T3 and for AA2024-T3 treated using NaOH, $NaOH/HNO_3$ and ST/HNO_3. Sputter depth profile of the sample treated using NaOH showing b) Al and O, and c) minor elements at enlarged scale.

of the oxide part prevailing over the metal part. For AA2024-T3 it has been reported that treatment with 1.25 M NaOH and 2.8 M HNO_3 leads first to selective dissolution of Al in NaOH and then to enrichment of alloy elements such as Cu [47]. Subsequent treat-

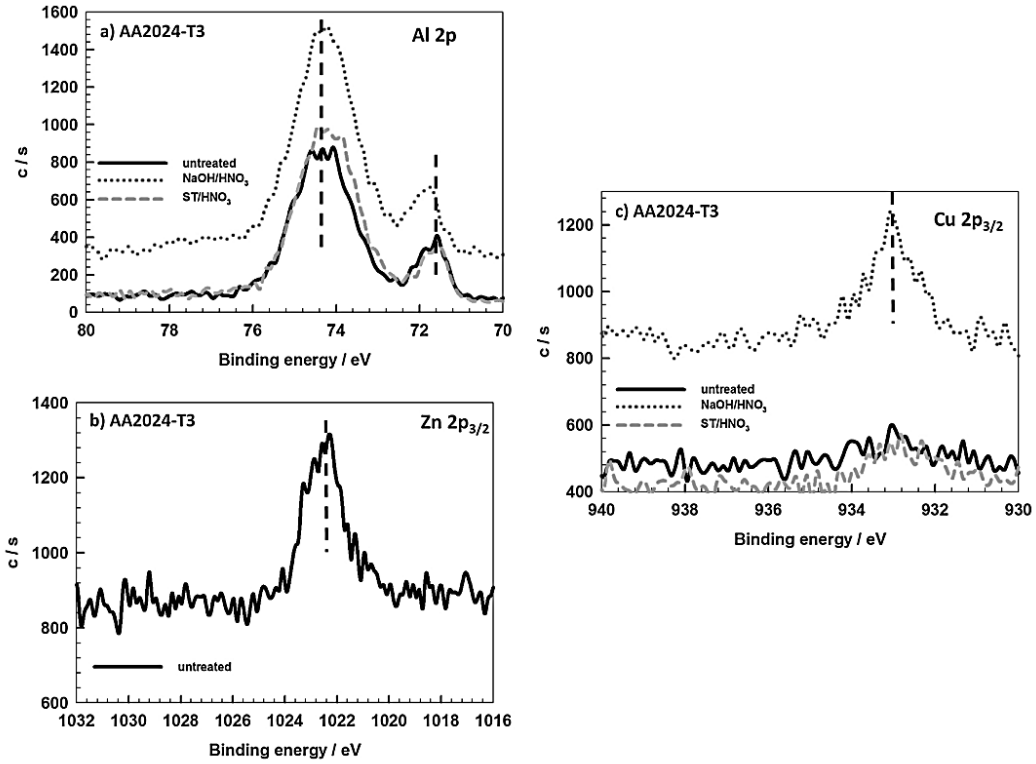


Fig. 11. High resolution XPS spectra of (a) Al 2p, (b) Zn $2p_{3/2}$ and (c) Cu $2p_{3/2}$ recorded for untreated, ground under water AA2024-T3 and for AA2024-T3 treated using $NaOH/HNO_3$ and ST/HNO_3.

ment in HNO_3 dissolved the excess residual layer and passivated the alloy matrix [47]. The peak of Zn appeared only in the chemically untreated sample. It is located at 1022.4 eV, in accordance with the presence of ZnO or $Zn(OH)_2$ (Fig. 11b). The peak of copper, centred at 933.0 eV, is observed only in samples cleaned with $NaOH/HNO_3$ (Fig. 11c). Its shape indicates that Cu may be in the oxide or metal state.

3.2.3. Electrochemical measurements

Polarization curves for AA7075-T6 and AA2024-T3, recorded following selected chemical treatments, are presented in Fig. 6. The related electrochemical parameters are presented in Table 4. Under water grinding, followed by chemical pre-treatment, resulted in a smaller current density in both cathodic and anodic ranges.

Compared to untreated, sample AA7075-T6 ground under water, the chemically treated samples showed smaller current densities in the cathodic region and slightly more negative E_{corr}. In the anodic region, the current density of the sample treated using $NaOH/HNO_3$ increased more slowly than the chemically untreated sample; the sample treated using ST/HNO_3 exhibits a curve similar to that of the untreated sample.

For AA2024-T3, the decrease in current density following $NaOH/HNO_3$ pre-treatment was more pronounced than for AA7075-T6 (Fig. 6b, Table 4). In the anodic region a narrow passive region was established, followed by an increase of current density at −0.52 V. Separate electrochemical measurements after treatment with NaOH and with $NaOH/HNO_3$ showed that a passive region was established after the latter treatment; i.e. NaOH does not passivate the surface but HNO_3 does (Fig. S3 in Supplement material). Furthermore, the surface passivation by HNO_3 is more pronounced for AA2024-T3 than for AA7075-T6. For the ST/HNO_3-treated AA2024-T3 sample the increase in current density was slower than for the chemically untreated sample, but no plateau was established as for the $NaOH/HNO_3$ treated sample. Similar results, showing a smaller current density of polarization curves for AA2024-T3 after treatment in $NaOH/HNO_3$, were obtained by Gharbi et al. [47].

A decrease in cathodic current density reflects a diminished reaction of oxygen reduction, implying the reduction of cathodic sites (more noble than aluminium alloy matrix) where oxygen reduction takes place. During alkaline treatment and acid desmutting, some of the intermetallic particles containing copper are removed, leading to decreased oxygen reduction. Consequently, the anodic reaction was also diminished. Enrichment of Cu in the form of remnants of intermetallic particles at the surface of aluminium alloys following chemical treatment has been reported [18,19] and is shown in the present work, especially for $NaOH/HNO_3$ treated AA7075-T6 (Fig. 7a). As the cathodic reaction takes place primarily at IMs containing copper [8], we would expect an increase in cathodic current due to presence of Cu remnants of intermetallic particles at the surface (Fig. 7a), and not the opposite, as shown in Fig. 6a [47]. This would be in accordance with the mechanism described by Buchheit et al. that, during de-alloying of Al_2CuMg, particles are isolated electrically from the matrix due to their detachment [48]. These particles are then not included in the faradaic process. Alternatively, Cu particles are passivated

during HNO_3 treatment, as proposed in [47]. Both these explanations appear to be plausible since, according to the XPS spectrum (Fig. 9d), it is ambiguous as to whether Cu is present in a metallic or an oxidized state.

4. Conclusions

Mechanical and chemical pre-treatments both have strong effects on the morphology, composition and wettability of the surfaces of AA7075-T6 and AA2024-T3. In consequence, they affect the corrosion properties of these alloys in sodium chloride solution.

1. Mechanical under water grinding of AA7075-T6 leads to preferential dissolution of Mg. Surfaces polished under non-aqueous liquid, however, contain a higher proportion of Mg than surface ground under water. Due to its high electrochemical activity, Mg shifts the corrosion potential of polished surface to more negative values. Mechanical treatment appears to affect less the surface composition of AA2024-T3.
2. Chemical treatment was carried out using alkaline NaOH solution and alkaline commercial cleaner, both followed by desmutting with HNO_3. For AA7075-T6, treatment using NaOH (pH = 11.6) results in enrichment of surfaces copper and dissolution of magnesium, as evidenced by XPS results. Copper deposits are present as spongy remnants of intermetallic particles. After treatment with commercial cleaner (pH = 8.3), the surface contained phosphorus originating from the commercial cleaner. Unlike the surface treated with $NaOH/HNO_3$, surface is morphologically more similar to that of a sample ground under water. Chemical treatment produces the super- or almost superhydrophilic surfaces.
3. For AA2024-T3, treatment using NaOH produces a rough layer at the surface, with complete removal of intermetallic particles. Commercial cleaner affects the surface morphology less. Both treated surfaces are hydrophilic.
4. In general, chemical treatment leads to a smaller current density in the polarization curves, probably due to removal of sites at which oxygen reduction takes place preferentially that at matrix and to the presence of the hydroxide/oxide layer that was formed during the desmutting with nitric acid. Copper deposits on AA7075-T6 do not increase the current density in the cathodic range, which indicates electrical isolation from the matrix and/or passivation due to oxide formation.
5. To summarize, the processes occurring during chemical treatments are complex and specific for each alloy. A further *in situ* study regarding the kinetics of dissolution of individual intermetallic particles would be necessary to understand these processes completely.

Acknowledgements

Financial support by the Slovenian Research Agency is acknowledged (research core funding No. P2-0393 and the project "Lightweight alloys based on aluminium as materials with increasing potential in transportation industry", ID J1-6734). The authors thank T. Filipič, MSc, for valuable technical help in XPS and SEM/EDS measurements and Prof. R.H. Pain for proof reading the manuscript. Cleaning agents were supplied by Mr. E. Kokalj of SurTec; fruitful comments and help are acknowledged. The authors thank Prof. G.S. Frankel of Fontana Corrosion Center, The Ohio State University for valuable comments and discussion of the manuscript.

Appendix A. Supplementary data

Supplementary data associated with this article can be found, in the online version, at http://dx.doi.org/10.1016/j.corsci.2017.02.018.

References

[1] C. Vargel, Corrosion of Aluminum, 1st ed., Elsevier Amsterdam, The Netherlands, 2004.
[2] J.R. Davis, Corrosion of Aluminum and Aluminum Alloys, ASM International, United States of America, 1999.
[3] G. Kufman, Introduction to Aluminum Alloys and Tempers, 1st ed., ASM International, United States of America, 2000.
[4] M.W. Kendig, R.G. Buchheit, Corrosion inhibition of aluminum and aluminum alloys by soluble chromates, chromate coatings, and chromate-free coatings, Corros 59 (2003) 379–400.
[5] J.W. Bibber, An overview of nonhexavalent chromium conversion coatings—Part I: aluminum and its alloys, Met. Finish. 99 (2001) 15–22.
[6] G.W. Critchlow, D.M. Brewis, Review of surface pretreatments for aluminium alloys, Int. J. Adhes. Adhes. 16 (1996) 255–275.
[7] P.G. Sheasby, R. Pinner, The Surface Treatment and Finishing of Aluminium and Its Alloys (Volumes 1 & 2), 6 har/cdr edition, ASM, International, Materials Park, Ohio, 2001 (Finishing publications).
[8] Q. Meng, G.S. Frankel, Effect of Cu content on corrosion behavior of 7xxx series aluminum alloys, J. Electrochem. Soc. 151 (2004) B271–B283.
[9] A. Laurino, Y. Liu, Corrosion behaviour of mechanically polished AA7075-T6 aluminium alloy, Surf. Interface Anal. 42 (2010) 185–188.
[10] W. Zhang, G.S. Frankel, Transitions between pitting and intergranular corrosion in AA2024, Electrochim. Acta 48 (2003) 1193–1210.
[11] G.S. Frankel, N. Sridhar, Understanding localized corrosion, Mater. Today 11 (2008) 38–44.
[12] Z. Zhao, G.S. Frankel, On the first breakdown in AA7075-T6, Corros. Sci. 49 (2007) 3064–3088.
[13] A. Afseth, J.H. Nordlien, G.M. Scamans, K. Nisancioglu, Influence of heat treatment and surface conditioning on filiform corrosion of aluminium alloys AA3005 and AA5754, Corros. Sci. 43 (2001) 2359–2377.
[14] A. Afseth, J.H. Nordlien, G.M. Scamans, K. Nisancioglu, Effect of thermo-mechanical processing on filiform corrosion of aluminium alloy AA3005, Corros. Sci. 44 (2002) 2491–2506.
[15] F. Eckermann, T. Suter, P.J. Uggowitzer, A. Afseth, A.J. Davenport, B.J. Connolly, M.H. Larsen, F.D. Carlo, P. Schmutz, In situ monitoring of corrosion processes within the bulk of AlMgSi alloys using X-ray microtomography, Corros. Sci. 50 (2008) 3455–3466.
[16] S. Joshi, W.G. Fahrenholtz, M.J. O'Keefe, Effect of alkaline cleaning and activation on aluminum alloy 7075-T6, Appl. Surf. Sci. 257 (2011) 1859–1863.
[17] Y. Liu, M.A. Arenas, A. de Frutos, J. de Damborenea, P. Conde, G.E. Thompson, P. Bailey, T.C.Q. Noakes, Influence of nitric acid pre-treatment on Al–Cu alloys, Electrochim. Acta 53 (2008) 4454–4460.
[18] R. Grilli, Conversion Coatings for Aluminium Alloys: a Surface Investigation for Corrosion Mechanisms, University of Surrey, United Kingdom, 2010.
[19] P. Campestrini, H. Terryn, A. Hovestad, J.H.W. de Wit, Formation of a cerium-based conversion coating on AA2024: relationship with the microstructure, Surf. Coat. Technol. 176 (2004) 365–381.
[20] C.E. Moffitt, D.M. Wieliczka, H.K. Yasuda, An XPS study of the elemental enrichment on aluminum alloy surfaces from chemical cleaning, Surf. Coat. Technol. 137 (2001) 188–196.
[21] Y. Liu, M.A. Arenas, S.J. Garcia-Vergara, T. Hashimoto, P. Skeldon, G.E. Thompson, H. Habazaki, P. Bailey, T.C.Q. Noakes, Behaviour of copper during alkaline corrosion of Al–Cu alloys, Corros. Sci. 50 (2008) 1475–1480.
[22] A. de Frutos, M.A. Arenas, Y. Liu, P. Skeldon, G.E. Thompson, J. de Damborenea, A. Conde, Influence of pre-treatments in cerium conversion treatment of AA2024-T3 and 7075-T6 alloys, Surf. Coat. Technol. 202 (2008) 3797–3807.
[23] S.S. Golru, M.M. Attar, B. Ramezanzadeh, Effects of different surface cleaning procedures on the superficial morphology and the adhesive strength of epoxy coating on aluminium alloy 1050, Prog. Org. Coat. 87 (2015) 52–60.
[24] N.J. Cherepy, T.H. Shen, A.P. Esposito, T.M. Tillotson, Characterization of an effective cleaning procedure for aluminum alloys: surface enhanced Raman spectroscopy and zeta potential analysis, J. Colloid Interface Sci. 282 (2005) 80–86.
[25] L. Fedrizzi, A. Bianchi, F. Deflorian, S. Rossi, P.L. Bonora, Effect of chemical cleaning on the corrosion behaviour of painted aluminium alloys, Electrochim. Acta 47 (2002) 2159–2168.
[26] B.L. Treu, S. Joshi, W.R. Pinc, M.J. O'Keefe, W.G. Fahrenholtz, Characterization of localized surface states of Al 7075-T6 during deposition of cerium-based conversion coatings, J. Electrochem. Soc. 157 (2010) C282–C287.
[27] W.G. Fahrenholtz, M.J. O'Keefe, H. Zhou, J.T. Grant, Characterization of cerium-based conversion coatings for corrosion protection of aluminum alloys, Surf. Coat. Technol. 155 (2002) 208–213.
[28] A.E. Hughes, J.D. Gorman, P.R. Miller, B.A. Sexton, P.J.K. Paterson, R.J. Taylor, Development of cerium-based conversion coatings on 2024-T3 Al alloy after rare-earth desmutting, Surf. Interface Anal. 36 (2004) 290–303.

[29] S. Joshi, W.G. Fahrenholtz, M.J. O'Keefe, Alkaline activation of Al 7075-T6 for deposition of cerium-based conversion coatings, Surf. Coat. Technol. 205 (2011) 4312–4319.
[30] W. Pinc, S. Geng, M. O'Keefe, W. Fahrenholtz, T. O'Keefe, Effects of acid and alkaline based surface preparations on spray deposited cerium based conversion coatings on Al 2024-T3, Appl. Surf. Sci. 255 (2009) 4061–4065.
[31] F.J. Monteiro, M.A. Barbosa, D.R. Gabe, D.H. Ross, Surface pretreatments of aluminium for electroplating, Surf. Coat. Technol. 35 (1988) 321–331.
[32] T.G. Harvey, Cerium-based conversion coatings on aluminium alloys: a process review, Corros. Eng. Sci. Technol. 48 (2013) 248–269.
[33] F.J. Monteiro, M.A. Barbosa, D.H. Ross, D.R. Gabe, Pretreatments of improve the adhesion of electrodeposits on aluminium, Surf. Interface Anal. 17 (1991) 519–528.
[34] A.E. Hughes, R.J. Taylor, K.J.H. Nelson, B.R.W. Hinton, L. Wilson, Characterisation of surface preparation of 2024 aluminium alloy for conversion coating, Mater. Sci. Technol. 12 (1996) 928–936.
[35] A.E. Hughes, G. Theodossiou, S. Elliott, T.G. Harvey, P.R. Miller, J.D. Gorman, P.J.K. Paterson, Study of deoxidation of 2024-T3 with various acids, Mater. Sci. Technol. 17 (2001) 1642–1652.
[36] P. Rodič, I. Milošev, Corrosion inhibition of pure aluminium and alloys AA2024-T3 and AA7075-T6 by cerium(III) and cerium(IV) salts, J. Electrochem. Soc. 163 (2016) C85–C93.
[37] I. Milošev, P. Rodič, Cerium chloride and acetate salts as corrosion inhibitors for aluminum alloy AA7075-T6 in sodium chloride solution, Corrosion 72 (2016) 1021–1034.
[38] B. Volarič, I. Milošev, Rare eath chloride and nitrate salts as individual and mixed inhibitors for aluminium alloy 7075-T6 in chloride solution, Corr Eng Sci Technol. (n.d.).
[39] R.G. Buchheit, Local dissolution phenomena associated with S phase (Al_2CuMg) particles in aluminum alloy 2024-T3, J. Electrochem. Soc. 144 (1997) 2621–2627.
[40] M. Gao, C.R. Feng, R.P. Wei, An analytical electron microscopy study of constituent particles in commercial 7075-T6 and 2024-T3 alloys, Metall. Mater. Trans. A. 29 (1998) 1145–1151.
[41] A.E. Hughes, A.M. Glenn, N. Wilson, A. Moffatt, A.J. Morton, R.G. Buchheit, A consistent description of intermetallic particle composition: an analysis of ten batches of AA2024-T3, Surf. Interface Anal. 45 (2013) 1558–1563.
[42] A.E. Hughes, C. MacRae, N. Wilson, A. Torpy, T.H. Muster, A.M. Glenn, Sheet AA2024-T3: a new investigation of microstructure and composition, Surf. Interface Anal. 42 (2010) 334–338.
[43] NIST X-ray Photoelectron Spectroscopy (XPS) Database, Version 3.5, (n.d.). https://srdata.nist.gov/xps/ (Accessed 7 November 2016).
[44] N. Dimitrov, J.A. Mann, M. Vukmirovic, K. Sieradzki, Dealloying of Al_2CuMg in alkaline media, J. Electrochem. Soc. 147 (2000) 3283–3285.
[45] I. Milošev, H.H. Strehblow, Electrochemical behavior of Cu-xZn alloys in borate buffer solution at pH 9.2, J. Electrochem. Soc. 150 (2003) B517–B524.
[46] M.C. Biesinger, L.W.M. Lau, A.R. Gerson, R.S.C. Smart, Resolving surface chemical states in XPS analysis of first row transition metals, oxides and hydroxides: Sc, Ti, V, Cu and Zn, Appl. Surf. Sci. 257 (2010) 887–898.
[47] O. Gharbi, N. Birbilis, K. Ogle, In-situ monitoring of alloy dissolution and residual film formation during the pretreatment of Al-alloy AA2024-T3, J. Electrochem. Soc. 163 (2016) C240–C251.
[48] R.G. Buchheit, M.A. Martinez, L.P. Montes, Evidence for Cu ion formation by dissolution and dealloying the Al_2CuMg intermetallic compound in rotating ring-disk collection experiments, J. Electrochem. Soc. 147 (2000) 119–124.

Chapter 3

Hybrid Sol-Gel Coatings Based on GPTMS/TEOS Containing Colloidal SiO_2 and Cerium Nitrate for Increasing Corrosion Protection of Aluminum Alloy 7075-T6

One of the promising replacements for chromate conversion coatings for corrosion protection of aluminum alloys are hybrid sol-gel coatings. In the present chapter hybrid sol-gel coatings were based on organic silane precursor (3-glycidyloxypropyl) trimethoxysilane (GPTMS) and inorganic tetraethoxysilane (TEOS) and were applied on aluminum alloy AA7075-T6. To achieve barrier property, SiO_2 nanoparticles (Ludox) were added to the precursor's solution. Their addition increases the coating thickness, density and reinforcement. Moreover, their addition offers the control of viscosity of sol. However, they do not ensure an active corrosion protection of AA7075-T6. Additionally, corrosion inhibitor cerium nitrate $Ce(NO_3)_3$ was incorporated into the hybrid sol-gel coating, leading to an active corrosion protection. The observed improvement of corrosion properties is attributed to the combination of the barrier properties of SiO_2 nanoparticles with the active corrosion protection of $Ce(NO_3)_3$. The opening of the epoxy rings of GPTMS and the completion of hydrolysis and the condensation of sol during the synthesis were confirmed and the high degree of cross-linking between GPTMS and TEOS was achieved *in situ*, during the synthesis of sol. Moreover, the effect of the curing process on coating was investigated and confirmed. In this chapter the synthesis of hybrid-sol gel coating was optimized and the properties of developed coatings gave a promising replacement for chromate conversion coatings.

In Figure 1.9 a Graphical abstract of Chapter 3 is present.

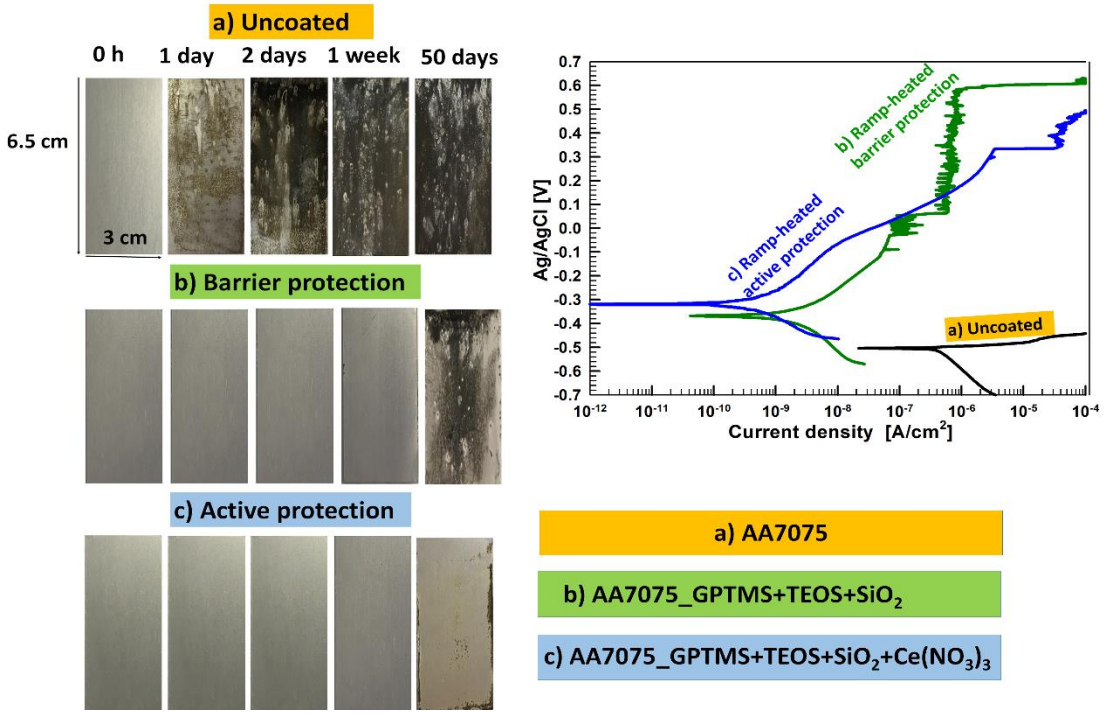


Figure 1.9: Graphical abstract of chapter 3.

This chapter addresses thesis Objective 2), 3) and 5) from Chapter 1.6.

Regarding my contribution: I made a literature overview of the topic, co-formulated the basic idea for the object of the investigation, co-planned, co-designed and performed the experiments and jointly prepared the manuscript with co-authors.

Journal of Sol-Gel Science and Technology (2018) 85:546–557
https://doi.org/10.1007/s10971-017-4577-7

ORIGINAL PAPER: INDUSTRIAL AND TECHNOLOGICAL APPLICATIONS OF SOL-GEL AND HYBRID MATERIALS

Hybrid sol–gel coatings based on GPTMS/TEOS containing colloidal SiO_2 and cerium nitrate for increasing corrosion protection of aluminium alloy 7075-T6

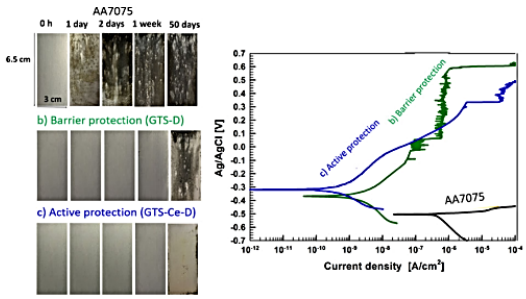
Urša Tiringer[1,2] · Ingrid Milošev[1] · Alicia Durán[3] · Yolanda Castro[3]

Received: 15 November 2017 / Accepted: 26 December 2017 / Published online: 30 January 2018
© Springer Science+Business Media, LLC, part of Springer Nature 2018

Abstract

One of the promising candidates to replace the chromate conversion coatings for corrosion protection of aluminium alloy AA7075 are the hybrid sol–gel coatings. In the present work hybrid silica sol–gel coatings doped with cerium nitrate were prepared and characterized. Tetraethoxysilane (TEOS) and 3-glycidoxypropyl-trimethoxysilane (GPTMS) were used as precursors. Silica SiO_2 (Ludox) particles were added to achieve a barrier properties of coating, while $Ce(NO_3)_3{\cdot}6H_2O$ was added in order to obtain an active corrosion protection. Optimization of sol synthesis was based on the results of ATR-FTIR spectroscopy and UV–vis–NIR spectroscopy. Opening of epoxy rings and completion of hydrolysis and the condensation reactions during the synthesis process were confirmed. Coatings were characterized through thickness, water contact angle, roughness, adhesion, electrochemical properties (potentiodynamic and electrochemical impedance spectroscopy) and the response to prolonged immersion time in 0.1 M NaCl. The high degree of cross-linking of Si–O–Si network structure and high density was achieved during the synthesis of the sol. Moreover, the results showed that the curing process and the incorporation of cerium nitrate into the hybrid sol–gel coating affected to the corrosion properties of the coating. The observed enhancement in corrosion protection properties is attributed to the combination of the barrier properties of the silica matrix with the active protection of the cerium nitrate.

Graphical Abstract



Keywords Aluminium alloy · Sol–gel coatings · Corrosion protection · Barrier properties · SiO_2 nanoparticles · Cerium inhibitor

✉ Yolanda Castro
castro@icv.csic.es

[1] Department of Physical and Organic Chemistry, Jožef Stefan Institute, Jamova c. 39, 1000 Ljubljana, Slovenia

[2] Jožef Stefan Postgraduate School, Jamova c. 39, 1000 Ljubljana, Slovenia

[3] Campus de Cantoblanco, Instituto de Cerámica y Vidrio (CSIC), 28049 Madrid, Spain

1 Introduction

Aluminium AA7075 alloy-T6 has been used in many technological applications, such as the aircraft and automotive industries [1, 2]. Its most important advantages are its low density, high strength-to-weight ratio and physical properties. However, AA7075 has a complex chemical composition with numerous intermetallics containing Zn, Mg and Cu (IMs). IMs comprise particles with different electrochemical activities, some of them being less noble ($MgZn_2$, Mg_2Si) and the other more noble (Al_2Cu, Al_7Cu_2Fe, and S-phase Al_2CuMg after initial dealloying of Mg) compared to aluminium oxide matrix [3]. IMs in AA7075 are the sites where localized corrosion starts as a result of the high potential difference between particular IMs and surrounding matrix, resulting in galvanic corrosion/localized attack when alloy is immersed in NaCl solution [3–5]. chromate conversion coatings (CCCs) have provided effective corrosion protection of aluminium alloys for many years. However, they are based on hexavalent chromium which is highly toxic and are therefore banned or strongly restricted.

To replace CCCs, many surface treatments have been proposed; the sol–gel processes is one of the most promising and environmentally friendly [2, 6–18]. Sol–gel technology offers important advantages such as cost effectiveness and simple application procedures easily adaptable in industry [15]. A great number of sol–gel coatings are based on silicon precursors because of their low reactivity, easy handling and availability [19]. The first studies dealing with sol–gel methodology were based on inorganic silane sol–gel coatings which offer good mechanical properties and promote good adhesion between the metal substrate and organic coatings, leading to low oxygen diffusion [13]. However, these inorganic coatings contain micropores and microcracks and, moreover, high temperatures are required to obtain dense coatings [10]. Thus, pure inorganic sol–gel coatings cannot prevent the ingress of corrosive species through defects to the metal substrate. Hybrid coatings are usually prepared with a combination of inorganic and organic polymerization [20–23] and improve the overall performance of the coating as they combine inorganic and organic components; the former offering good mechanical properties, and the organic components increasing the flexibility and ductility of coatings, with decreased treatment temperature [10, 14, 24–26].

The aim of the present work was to develop hybrid coatings that offer a barrier behaviour and active corrosion protection of aluminium alloy AA7075-T6. To prevent changes in alloy microstructure, this alloy should not be treated above 120 °C [27]. Two silicon-based components have been used: the inorganic component being tetraethoxysilane (TEOS) and the organic component, (3-glycidyloxypropyl) trimethoxysilane (GPTMS).

GPTMS is one of the most common hybrid silanes used as binder in paints or as a filler in inorganic and composite materials [28]. It is also used as a coupling agent for epoxy bonded aircraft repairs [29]. The deposition of GPTMS on metallic substrates was studied, but the corrosion resistance of such coatings was poor [29]. The polymerization of epoxy groups of GPTMS is used to link the organic and inorganic parts of hybrid coatings, leading to films with good chemical, thermal and mechanical resistance [30]. Cross-linking between two networks can be achieved by direct reaction of silanols with epoxy rings or by condensation of silanols with the hydroxyl of the opened epoxy rings [30]. On the other side, one main advantage of epoxy-based sol–gel coatings is their compatibility with and bonding to the epoxy-based primer or top-coats usually used for the aircraft structure [31]. The epoxy group of GPTMS can promote cross-linking with inorganic networks such as silicon-based in TEOS, resulting in better mechanical properties, corrosion resistance and flexibility of coatings [32–38]. In particular, the lower treatment temperature required for curing hybrid coatings respecting inorganic films is associated with a reduction of microcracks in the coating [10, 14, 26, 39]. The epoxy ring can be opened and polymerized to form a linear poly(ethylene oxide) organic matrix [40]. In many cases the opening of epoxy ring is thermally catalyzed [39], but it can also be opened at room temperature by the addition of amine curing agents (DETA), each hydrogen of the amine being capable of opening and linking to one epoxy group [30], leading to the formation of diol, alkoxy alcohol or polyether products [41–43]. The opening of the epoxy ring can also be monitored by fourier transform infrared spectroscopy (FTIR) and/or ultraviolet-visible-near infra-red spectroscopy (UV-vis-NIR).

In order to improve the densification of hybrid sol–gel coatings, several routes can be considered, one being the incorporation of silica (SiO_2) nanoparticles into the sol–gel coating to obtained so-called hybrid silica coatings [23]. Addition of SiO_2 particles has been reported to increase the barrier effect by increasing the coating thickness, density and reinforcement [44–50]. The effect depends on the concentration and dispersion of the nanoparticles in the coating [51, 52]. Santana et al. [44] reported high anti-corrosion performance and thicker coatings for higher amounts of SiO_2 nanoparticles incorporated into a GPTMS/TEOS sol, with molar ratios TEOS/GPTMS/SiO_2 = 42/18/40. In contrast, Suegama et al. considered that the concentration of SiO_2 particles of BTSPA (bis-(trimethoxysilylpropyl) amine) that achieved the best corrosion properties of coating was 300 ppm, with a molar ratio of BTSPA to SiO_2 of 91:9 [53]. Incorporation of higher colloidal silica led to worse corrosion protection. The addition of nanoparticles always increased the viscosity of sols [54].

To obtain active corrosion protection, inhibitors have to be incorporated into the coatings. According to Hinton et al. [55, 56], many salts of rare earth ions such as Ce^{3+}, Y^{3+}, La^{3+}, Pr^{3+} and Nd^{3+}, are successful corrosion inhibitors for aluminium alloys. The inhibitory action of rare earth compounds is based on the deposition of their insoluble hydroxides at cathodic sites on the surface that diminishes the corrosion reaction at the surface. When corrosion occurs, reduction of oxygen takes place at the cathodic sites, OH^- ions are formed and pH increases. In the case of cerium, precipitation of the hydroxide $Ce(OH)_3$ occurs, which can be further oxidized to $Ce(OH)_4$ [16, 53, 54].

The aim of this work was to improve the corrosion resistance of AA7075-T6 substrates through the deposition of hybrid coatings able to ensure passive and active corrosion protection. The incorporation of colloidal silica nanoparticles increases the densification of the coating provoking a higher barrier effect, and the incorporation of $Ce(NO_3)_3$ in the sol leads to an active corrosion protection by slow release of Ce inhibitor from the coating. The novelty of the work is associated with the modification of the sol–gel synthesis process where the cross-linking degree of silicon-based hybrid matrix was improved through the organic and inorganic polymerization in situ during the synthesis of the sol. The effect of curing ramp in the densification of the coating was also studied, observing significant changes in the corrosion resistance.

2 Experimental procedure

2.1 Substrate preparation

Aluminium alloy AA7075-T6 (Zn 5.81 wt%, Mg 2.55 wt%, Fe 0.21 wt%, Si 0.08 wt%, Cu 1.67 wt%, the remaining, Al) with dimensions of $30 \times 65 \times 2$ mm, supplied by Kaiser Aluminum, was used as substrate. Before deposition, the alloy sheets were pre-cleaned using an alkaline cleaning solution (Metaclean T2001—Chemie Vertrieb Hannover GmbH & Co KG), an alkaline etching solution (Turco Liquid Aluminetch Nr.2—Turco Chemie GmbH) and, finally, an acid etching solution (Turco Liquid Smutgo NC —Turco Chemie GmbH). This procedure enables removal of the oxide layer and intermetallic particles on the metal surface. Prior to depositing the coating, the samples were rinsed with deionized water.

2.2 Hybrid sol–gel synthesis and characterization

Alkoxide precursors and all reagents were used as received, without further purification. First, a hybrid silica sol was prepared under acidic conditions at room temperature by mixing tetraethoxysilane (TEOS, Aldrich, 99%) and 3-(glycidyloxypropyl)trimethoxysilane (GPTMS, ABCR, 98%) with a suspension of colloidal SiO_2 nanoparticles (Ludox-4S, Aldrich, aqueous suspension 40 wt.%, particle size 20 nm, pH 9). The solution was stirred for 30 min, after which 0.6 mL of concentrated nitric acid HNO_3 (VWR, 65%) was added to 100 mL of solution to catalyze the hydrolysis and the condensation reactions. Finally, absolute ethanol (EtOH, Panreac, 99.8%) was added to the solution to give a final silica concentration of 120 g/L, with 64 g/L of colloidal particles, labelled as 120 (64). The final molar ratio of the hybrid silica sol (denoted as GTS) was TEOS/GPTMS/SiO_2 = 0.4/0.46/0.14 and the pH of the sol was 5. Secondly, a hybrid silica-Ce sol, incorporating cerium nitrate ($Ce(NO_3)_3 \cdot 6\ H_2O$, Aldrich, 98%) (denoted as GTS-Ce) was prepared as inhibitor sol. Cerium was added at the end of the synthesis. The final molar ratio of hybrid silica-Ce sol was TEOS/GPTMS/SiO_2/Ce = 0.39/0.44/0.12/0.05 and pH value was 4.

The sols were characterized by FTIR and UV-vis-NIR spectroscopy. FTIR spectra were recorded between 650 and 4000 cm^{-1}, using a Perkin Elmer Spectrum 100 spectrometer with an Attenuated Total Reflectance (ATR) accessory, with a resolution of 2 cm^{-1}. UV-vis-NIR spectra were recorded between 2500 and 2000 nm with a Perkin Elmer (Lambda 950) spectrophotometer, with a resolution of 2 nm. All spectra were normalized and presented as absorbance [%].

The viscosity of sols was monitored during one month using an A&D Vibro Viscosimeter SV-10 to evaluate the stability of the sols.

2.3 Deposition and curing of the coatings

Following synthesis, sols were deposited on glass slides and on AA7075 substrates. The deposition was carried out by dip-coating at a withdrawal rate of 30 cm/min. The same basic notation (GTS, GTS-Ce) is used for sols and deposited coatings. Coatings were prepared as single coatings of GTS (denoted as GTS-M) and of GTS-Ce (denoted as GTS-Ce-M), or as double coatings of two GTS layers (denoted as GTS-D) and two GTS-Ce layers (denoted as GTS-Ce-D). For double coatings, the first layer was dried with hot air (100 °C) for 3 min before applying the second layer.

Finally, coatings were cured for 1 h at 120 °C, using two different routes: (i) introducing the samples directly at the maximum temperature (denoted as GTS and GTS-Ce), or (ii) using a heating and cooling rate of 5 °C/min (denoted as GTS-R and GTS-Ce-R).

2.4 Characterization of the coatings

The coating thickness was measured on coated glass slides by Spectroscopic Ellipsometer (J.A. Woollam Co., Inc, EC-400, M-2000U Software: WVASE32). The spectral band

was recorded from 250 to 900 nm at incident angles between 50° and 60°. The data were fitted using the WVASE32 software with a Cauchy model. The hydrophilic/hydrophobic behaviour of the films was determined by measuring the water contact angle, using the Easy Drop Standard 'Drop Shape Analysis System' Kruss DSA 100 equipment under ambient laboratory conditions. Three measurements were performed on each sample and the results are presented as average ± standard deviation.

The roughness of coated AA7075 samples was measured using a roughness-metre (Taylor-Hobson Surtronic 3+ Roughness, UK). In the work, the value considered was the arithmetic mean (Ra) that corresponds with the measurement between the peaks and depressions travelled by the active tip of the device. This value was calculated from at least three individual measurements at different sites on the surface. The results are presented as average ± standard deviation.

An adhesion test was performed following the ASTM D3359 standard and using a Cross Hatch Adhesion Tester, (NEUTREK Instruments Company). The measurement was performed using a multi-blade cutting tool to make a lattice pattern with several cuts in each direction on the coating. The tape was then applied over the pattern and removed. The evaluation is based on six-step classifications, from 0 to 5 A, where a higher number indicates less peeling or coating removal.

The corrosion properties of coatings were evaluated by potentiodynamic polarization measurements and electrochemical impedance spectroscopy (EIS) in 0.1 M NaCl at room temperature. For potentiodynamic polarization measurements a Gamry FAS2 Femtostat was used, with a typical three-electrode configuration. Ag/AgCl was used as the reference electrode (0.192 V vs. standard hydrogen electrode), a large area platinum wire as a counter electrode and the tested material as the working electrode. The sample was placed at the bottom of the cell, exposing an area of 0.78 cm^2. Before each polarization test the samples were immersed in the electrolyte for 1 h at the open circuit potential (E_{oc}), to reach equilibrium. E_{oc} is the equilibrium potential of the metal in the absence of electrical connections [57]. Potentiodynamic polarization curves were scanned starting at −250 mv vs. E_{oc} up to 1 V at a scan rate of 1 mv/s. Experiments were repeated at least three times and the most representative measurement was chosen for plotting. The results are presented as average ± standard deviation (Table 1). The electrochemical data were fitted using Z_{view} software to deduce the corrosion potential (E_{corr}) and the corrosion current density (j_{corr}). E_{corr} corresponds with the potential at which the rate of anodic dissolution of electrode is equal to the rate of cathodic reactions. The j_{corr} is the current at the E_{corr} and it is associated with the corrosion rate [57]. The j_{corr} was determined as the intersection of the cathodic slope and the line passing through the E_{corr}.

Table 1 The main bands in TEOS, GPTMS, GTS and GTS-Ce spectra

Precursors and sols	Frequency (cm^{-1})
GPTMS	1250, 1076, 907, 814, 776
TEOS	1165, 1098, 1074, 957, 782
GTS (GPTMS/TEOS/SiO_2) sol	1128, 1086, 1042, 879
GTS-Ce (GPTMS/TEOS/SiO_2/Ce$(NO_3)_3$) sol	1128, 1086, 1042, 879

The corrosion performance of coatings was also tested using EIS in a 0.1 M NaCl aqueous solution at room temperature. An AUTOLAB PGSTAT 12 potentiostat/galvanostat, controlled by NOVA 1.11 software, was used for measurements made in a three-electrode standard corrosion cell (PAR Flat cell K0235, volume 250 mL). An Ag/AgCl electrode was the reference electrode (0.192 V vs. standard hydrogen electrode), the platinum mesh was a counter electrode and the tested material embedded in a Teflon holder was a working electrode. The area exposed to the corrosion medium was 1 cm^2. All potentials in the text are given with respect to an Ag/AgCl electrode. The EIS were performed at open circuit potential with an ac excitation voltage of 10 mV in the range from 10^{-2} to 10^5 Hz. The impedance response of a system can be described in terms of real (Z_{real}) and imaginary components (Z_{imag}), respectively. For data analysis, the calculated impedance is expressed as Nyquist plot and/or Bode plot. The variation of Z_{real} and Z_{imag} were used to assess the electrochemical behaviour and corrosion resistance of the uncoated and coated samples.

Corrosion properties were also monitored using an immersion test carried out in 0.1 M NaCl at room temperature. Samples were placed in a DURAN glass flask with a solution volume of 250 mL. The area of sample exposed to electrolyte was 1450 mm^2, according to the standard guide for laboratory immersion corrosion testing of metals (NACE TMO169/G31). Immersed samples were monitored for 1 month, and then inspected visually for corrosion damage.

3 Results and discussion

The sol–gel synthesis was followed by ATR-FTIR and UV-vis-NIR spectroscopies and by viscometer; the characterization of the coatings included measurements of thickness, contact angle, roughness, adhesion, electrochemical tests and immersion test.

3.1 Synthesis and characterization of the sols

FTIR spectra of GTS and GTS-Ce sols were compared to TEOS and GPTMS precursors, in order to analyze the inorganic and organic polymerization. The region from 700 to 1300 cm^{-1} was studied in detail (Fig. 1), since it contains

the principal bands associated with the hydrolysis and condensation reactions of silica [9]. In the spectrum of TEOS, the most intense bands are situated at 1165, 1098, 1074, 960, 814 and 778 cm^{-1} (Fig. 1 and Table 1). Bands at 1165 and 960 cm^{-1} correspond to $-CH_3$ rocking; those at 1098 and 1074 cm^{-1} are associated with the asymmetric and symmetric stretching bands of Si−O−C, respectively. The spectrum of GPTMS exhibits strong bands similar to those identified in the TEOS precursor; two characteristic bands of epoxy groups at 1250 and 910 cm^{-1} [40, 46, 58] were also identified. The band at 910 cm^{-1} is associated with anti-symmetric epoxy ring deformation [40] and the smaller one at 1250 cm^{-1} (Fig. 1d) is assigned with the ring breathing. The opening of epoxy rings was followed by analyzing the evolution of 910 cm^{-1} band.

In the spectrum of GTS sol, the bands at 814 and at 776 cm^{-1} associated with Si−O−CH_3 stretching, were absent, indicating completion of hydrolysis, the $-CH_3$ groups being replaced by −OH groups [59]. The band at 906 cm^{-1} was also absent, indicating that the epoxy rings were opened and organic polymerization has started. The non-appearance of this band is the result of the chemical bonding between organic silane (from GPTMS) and inorganic silicate (from TEOS) [39, 40] and the corresponding formation of a hybrid network. The spectrum of GTS contains the most intense bands at 879, 1042, 1086 and 1128 cm^{-1}, associated with the formation of Si−O−Si bonds, typical of inorganic polymerization [60]. The small band at 800 cm^{-1}, observed in Fig. 2a, is assigned to a rocking vibration of SiO_2 [61].

GTS-Ce sol, obtained following a similar process but incorporating cerium nitrate, exhibits a spectrum similar to that of GTS (Fig. 1 and Table 1), which confirms that inorganic and organic polymerization have taken place. The incorporation of $Ce(NO_3)_3$ does not affect the hydrolysis and condensation reactions.

The UV-vis-NIR absorption spectra of GPTMS, GTS and GTS-Ce sols are presented in Fig. 2. The broad peak between 2100 and 2200 nm in the spectrum of GPTMS is assigned to epoxy rings [62, 63]. These bands disappear in GTS and GTS-Ce sols, indicating the opening of the epoxy rings, agreeing with FTIR analysis. This confirms that the organic polymerization has started before the thermal treatment of the coating. During the synthesis process, and especially after nitric acid is added to the precursors, the sol suffers a strong exothermic reaction; the increase in temperature is enough to open the epoxy rings and initiate the organic polymerization. The polymerization continues during the synthesis, in the liquid state, resulting in a more cross-linked and dense Si−O−Si network and, consequently, leading to denser coatings [64].

The viscosity of sols GTS and GTS-Ce remained almost unchanged for at least 3 weeks (Table 2). A Newtonian behaviour is observed likely associated with the small particle size of the colloidal silica and the high dilution of the sols [65]. Sols can be used up to 3 weeks.

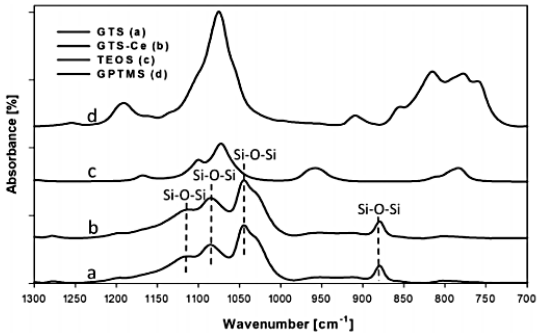


Fig. 1 FTIR spectra of TEOS, GPTMS, GTS and GTS-Ce sols

Table 2 Viscosity of GTS and GTS-Ce sols over 1 month

Time [days]; temperature [°C]	GTS η [mPa s]	GTS-Ce η [mPa s]
1 day ; 24.0	3.9 ± 0.6	3.8 ± 0.8
7 days; 25.8	4.2 ± 0.8	4.2 ± 0.5
14 days; 24.7	4.3 ± 0.8	4.3 ± 0.5
21 days; 24.2	4.7 ± 0.9	5.5 ± 0.6
31 days; 23.3	5.8 ± 0.9	6.0 ± 0.7

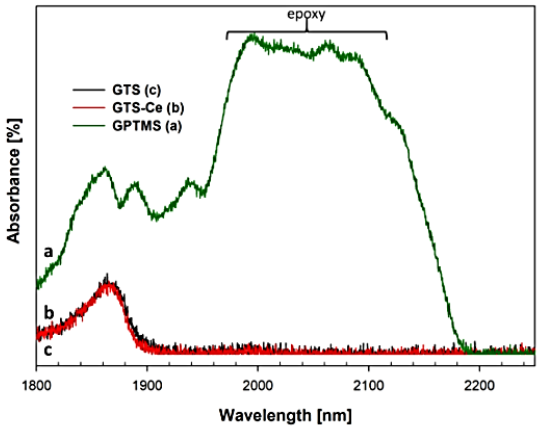


Fig. 2 UV-vis-NIR spectra of GPTMS, GTS and GTS-Ce sols

3.2 Characterization of the coatings

The thickness of single and double GTS and GTS-Ce coatings deposited on glass slides and cured at 120 °C with and without ramp was measured by ellipsometry (Table 3).

Table 3 Thickness of hybrid silica (GTS) and silica-Ce (GTS-Ce) coatings deposited on glass slides prepared as mono (M) and double (D) layers and cured without (M) or with ramp (R) procedure

Coating	Thickness [μm]
GTS-M	4.2 ± 0.4
GTS-M-R	3.1 ± 0.2
GTS-D	7.2 ± 0.3
GTS-D-R	5.3 ± 0.4
GTS-Ce-M	5.1 ± 0.6
GTS-Ce-M-R	3.4 ± 0.5
GTS-Ce-D	8.6 ± 0.8
GTS-Ce-D-R	7.0 ± 0.7

Homogenous coatings 4.2 μm thick were obtained from GTS sol cured at 120 °C without a ramp. When using a heating ramp the thickness was smaller, 3.1 μm, indicating that denser coatings are obtained in this conditions because of controlled elimination of the solvents; consequently, a more cross-linked 'network' structure is formed. For coatings obtained without ramp, a higher porosity and lower density is expected. For double coatings thickness of 7.2 or 5.3 μm are obtained, depending on whether the ramp procedure was used or not.

The incorporation of cerium nitrate increases the thickness from 4.2 to 5.1 μm for single coatings treated without ramp, with further contraction—from 3.1 μm to 3.4 μm—when ramp is used. For double coatings, an increment of thickness is also observed, up to 8.6 or 7 μm, depending on the curing process. In both cases, the incorporation of cerium acts inhibiting the densification of the hybrid silicon-based network and increasing the porosity of the coatings [66, 67].

Only double coatings (GTS-D, GTS-D-R, GTS-Ce-D, GTS-Ce-D-R) were selected for further analysis, since thicker films will offer better corrosion properties.

Contact angles and surface roughness of uncoated sample AA7075 and of samples coated using double coatings hybrid coatings with and without cerium and at different curing procedures are summarized in Table 5. Two elements are considered to explain the results: coating composition and curing procedure. Compared to uncoated substrate, a coating based on GTS exhibits much less roughness, 0.08 μm compared to 0.3 μm, while GTS-Ce films showed a greater roughness, 0.4 μm (Table 4); this may be correlated with the porosity and inhomogeneity of the GTS-Ce coatings compared to that without Ce [66, 67]. The incorporation of cerium provokes the increase of thickness and roughness of coatings, coming from a porous structure [64]. The interaction of the cerium with the hybrid network usually leads to considerable defects in the coatings, affecting their barrier properties and reducing the protection performance. This effect could be partially counter-rested by incorporating SiO_2 nanoparticles. Considering the effect of the curing process, less roughness was obtained for ramp curing, likely related to a more uniform evaporation of solvents during the controlled heating, this leading to a denser and rigid structure.

Table 4 Contact angles and surface roughness of substrate AA7075-T6 uncoated and coated using hybrid silica (GTS) and silica-Ce (GTS-Ce) coatings and cured without ramp procedure (GTS-D and GTS-Ce-D) and with ramp procedure (GTS-D-R and GTS-Ce-D-R)

Substrate/ Coating	Contact angle [°]	Roughness (Ra) [μm]
AA7075	48 ± 3	0.3 ± 0.1
GTS-D	52 ± 2	0.08 ± 0.09
GTS-D-R	67 ± 4	0.05 ± 0.04
GTS-Ce-D	67 ± 1	0.4 ± 0.2
GTS-Ce-D-R	80 ± 4	0.3 ± 0.3

All the coatings are hydrophilic, with contact angles between 48° and 67°, except for the GTS-Ce-D-R coating, with a contact angle of 80° (Table 4). In general, contact angles of ramp-heated coatings are greater than those obtained without a ramp associated with the difference in roughness (Table 4).

Adhesion of the coatings is an important factor to promote an appropriate deposition of primer and top-coats to achieve the final protective system. The adhesion of GTS-D-R and GTS-Ce-D-R coatings is rated as 5 A (desirable adhesion), according to the ASTM D3359 standard, the edge of the cuts is completely smooth and none of the squares of the lattice is detached. The excellent adhesion of sol–gel films to the aluminium alloy is the result of strong covalent bonds and the mechanical interlocking between the coating and the roughened surface [59].

3.3 Potentiodynamic polarization measurements

Electrochemical properties of uncoated AA7075-T6 and of coated (GTS-D, GTS-D-R, GTS-Ce-D, GTS-Ce-D-R) samples were studied by potentiodynamic measurements in 0.1 M NaCl. The effects of the coating composition and of the curing procedure on the barrier behaviour were studied as well as the inhibition properties of hybrid sol–gel coatings deposited on the aluminium alloy.

The effect of coating composition was firstly investigated. Uncoated AA7075-T6 immersed in chloride solutions is susceptible to localized corrosion (Fig. 3). In the cathodic range oxygen reduction takes place, while in the anodic range pitting corrosion immediately initiates above E_{corr} [1, 2]. In hybrid silica GTS-D coatings treated without ramp corrosion current density ($j_{corr} = 60\ nA/cm^2$) is smaller than that for the bare AA7075 alloy ($j_{corr} = 510\ nA/cm^2$),

but the E_{oc} and E_{corr} remain similar (Table 5). The decrease of current density is associated with the addition of silica nanoparticles which increase the density of the coating and fill pores thus increasing the barrier effect [53]. The shape of the curve did not change much compared to that of uncoated substrate; the cathodic current density is smaller by more than one order of magnitude, the change on the anodic side being less pronounced. However, in the presence of cerium (GTS-Ce-D) E_{oc} shifts in a positive direction by 40 mV compared to uncoated 7075-T6, thus indicating the effect on the anodic reaction (Table 5). The curve of the GTS-Ce-D coating is different to those of uncoated and GTS-D coated substrates. The corrosion current density decreased from 60 nA/cm^2 for GTS-D to 1.4 nA/cm^2 for GTS-Ce-D, respectively. Significant changes occur in the anodic range where a broad pseudo-passive (or barrier) range is established (Fig. 3). The presence of cerium obviously generates a barrier range in the anodic part likely related to the deposition of cerium hydroxides, oxides on the cathodic sites and subsequent reduction of anodic reaction [68–70]. In the case of AA7075-T6 the cathodic sites are those containing copper [5, 66]. Two breakdown potentials were observed on the curve of GTS-Ce-D (Fig. 3, Table 5). The first at −0.18 V ($\Delta E = 0.31$ V), may be associated with the initiation of coating breakdown due to initial ingress of electrolyte and establishment of conductive paths in the coating related to release of cerium. The current density increases for over two orders of magnitude but then another current density plateau is established, possibly related to the temporary blockage of individual pores. The second breakdown at 0 V ($\Delta E = 0.49$ V) may be related to the point at which the electrolyte, through the pores, reached the inner interface with the substrate. The use of a ramp in the curing process affects significantly the E_{oc} values and the potentiodynamic curves (Fig. 3). Positive shifts of E_{oc} by 180 and 210 mV, compared to curing without the ramp procedure, are observed in GTS-D and GTS-Ce-D, respectively (Table 5). Further, the GTS-D-R coating has a j_{corr} of 4.3 nA/cm^2, much smaller than that corresponding to AA7075 alloy ($j_{corr} = 510$ nA/cm^2) and GTS-D without ramp ($j_{corr} = 60$ nA/cm^2). Following the E_{corr} a broad pseudo-passive range was established. Similar as for the GTS-Ce-D curve, two breakdown potentials are observed for GTS-D-R curve (Fig. 3, Table 5), i.e. at 0.08 and 0.60 V.

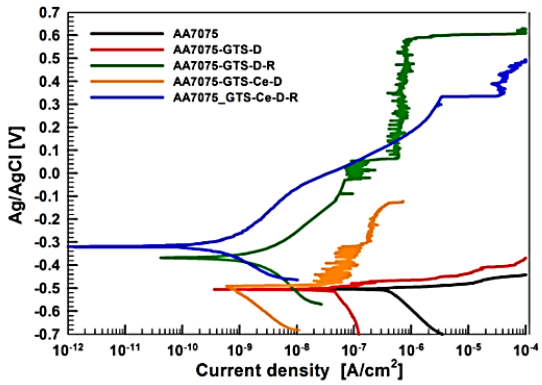


Fig. 3 Potentiodynamic polarization curves recorded in 0.1 M NaCl, after 1 h of stabilization, with a scan rate of 1 mV/s, for AA7075-T6 both uncoated and coated by hybrid silica coatings (GTS) and for silica-Ce coatings (GTS-Ce) subjected to curing with (GTS-D-R and GTS-Ce-D-R) and without ramp (GTS-D and GTS-Ce-D)

The smaller current density and more positive corrosion potential of ramp-cured coatings might be the result of denser coatings. The difference in density was previously confirmed by the lower thickness and roughness, and higher water contact angles of ramp-cured coatings (Tables 3 and 4). For the coating containing cerium the improvement is even more significant, resulting in a value of j_{corr} below 1 nA/cm^2. Pseudo-passive region with constant current density extends up to 0 V ($\Delta E = 0.33$ V) (Table 5), when it starts to increase slowly; thus, the breakdown potential becomes difficult to define. Continuous current density

Table 5 Electrochemical corrosion parameters (open circuit potential, corrosion current density and corrosion potential) for AA7075-T6, uncoated and coated by hybrid silica (GTS-D-R), and silica-Ce (GTS-Ce-D-R) coatings cured using the ramp procedure

Sample	E_{oc} [V vs. Ag/AgCl]	j_{corr} [nA/cm^2]	E_{corr} [V vs. Ag/AgCl]	β_c [mV/dec]	E_{pitt} [V]	ΔE [V]
AA7075-T6	−0.53 ± 0.04	510 ± 115	−0.52 ± 0.03	−200 ± 20	/	/
GTS-D	−0.52 ± 0.04	60 ± 41	−0.51 ± 0.02	−480 ± 35	/	/
GTS-D-R	−0.34 ± 0.02	4.3 ± 1.5	-0.36 ± 0.03	−210 ± 25	0.14 ± 0.05	0.5
					0.6 ± 0.04	0.98
GTS-Ce-D	−0.49 ± 0.02	1.4 ± 0.66	−0.49 ± 0.01	−180 ± 20	−0.22 ± 0.08	0.27
					0 ± 0.04	0.49
GTS-Ce-D-R	−0.28 ± 0.01	0.87 ± 0.15	−0.33 ± 0.005	140 ± 25	0 ± 0.06	0.33

E_{oc} denotes the values after 1 h stabilization, j_{corr} and E_{corr} were deduced from potentiodynamic measurements made in 0.1 M NaCl solution (Fig. 5)

increase may be related to a progressive release of cerium from the coating leaving behind a porous structure more susceptible to electrolyte ingress.

Based on these results, the ramp-heated samples (GTS-D-R and GTS-Ce-D-R coatings) showed better corrosion behaviour and were therefore investigated by the EIS and immersion test. In general, the addition of silica nanoparticles combined with the use of curing ramp allows reinforcing and promoting densification the hybrid silicon-based network. The addition of Ce as inhibitors generates an active corrosion protection that complements the barrier passive effect.

3.4 Electrochemical impedance spectroscopy

AA7075-T6, both uncoated and coated by GTS-D-R and GTS-Ce-D-R coatings, were studied by Nyquist plots obtained from EIS measurements, after different time of immersion in 0.1 M NaCl (Fig. 4). The Nyquist plots of uncoated AA7075 (Fig. 4a) after 1 h of immersion displayed semicircle at higher frequency followed by Warburg impedance at lower frequencies. Semicircle is the most typical shape of Nyquist plot and reflects the equivalent circuit for the interface between electrode and electrolyte, under equilibrium conditions. Warburg impedance is a general impedance which represents a resistance to mass transfer; i.e. diffusion controlled process. A Warburg impedance typically exhibits a 45° slope [71]. The diameter of the semicircle associated with the polarization resistance is in the range of 4 Kohm; data are scattered at low frequency, presumably due to the instability of the layer formed. Higher values Z_{real} are observed for uncoated AA7075 after 2 and 7 days of immersion as a result of the gradual formation of an oxide layer during the course of immersion [72]. This layer is not highly protective and is subjected to localized corrosion accompanied by the diffusion of soluble species [73].

For the sample coated with GTS (Fig. 4b) the shape of the plots changed and the response characteristic for barrier-type layer was observed up to 2 days of immersion. Moreover, values of Z_{real} at the lowest frequency are more than one order of magnitude higher compared to uncoated AA7075. However, after 4 days of immersion, the barrier properties are progressively degraded, the semicircle appearing with reduced Z_{real} (inset in Fig. 4b). For the samples coated with GTS-Ce-D-R (Fig. 4c) the barrier-type response is lower compared to GTS-D-R coatings and Z_{real} values at low frequencies progressively decrease for longer immersion times. In contrast, in the coating with cerium, the drop in Z_{real} value is not so big, indicating that the addition of cerium retards the degradation of the coating in chloride solution. This results can be related with the action of cerium ions in the coatings which affects the electrochemical

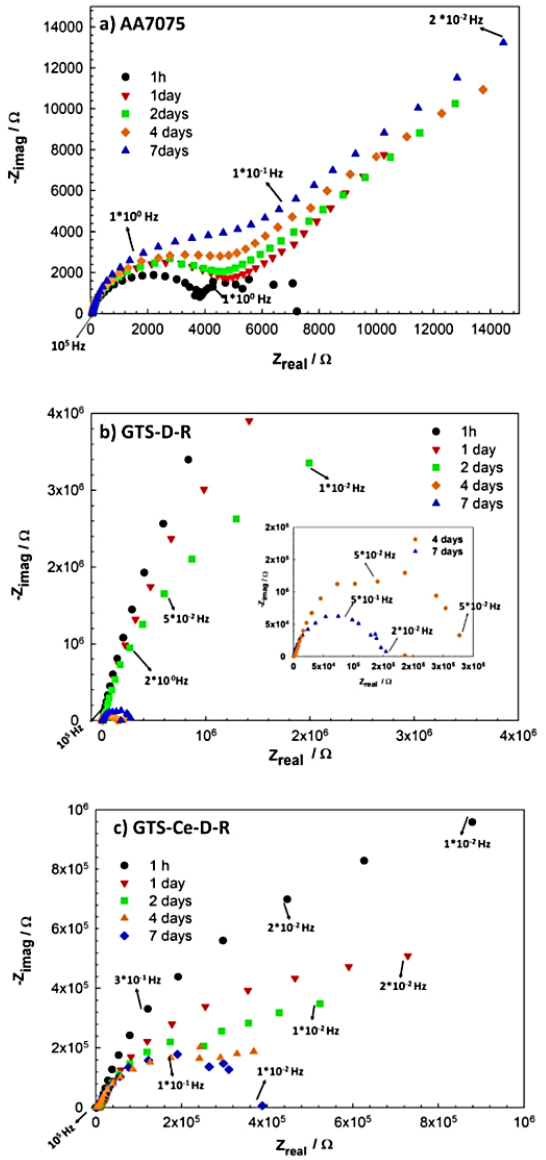


Fig. 4 EIS Nyquist plots of the uncoated AA7075 (**a**), coated with hybrid silica GTS-D-R (**b**) and with hybrid silica-Ce GTS-Ce-D-R (**c**) coatings, after different immersion times in 0.1 M NaCl. Coatings were cured using ramp procedure

response; it was shown that Ce can migrate [65, 66]. Further precipitating on cathodic sites as $Ce(OH)_3$ and/or $Ce(OH)_2$ forming the so-called 'local barrier' that blocks the cathodic sites and lead to related oxygen reduction reaction [74]. EIS measurements are in accordance with PD measurements (Fig. 3) where it was noticed that, compared to GTS-D-R, the GTS-Ce-D-R exhibits reduced current density in a broad

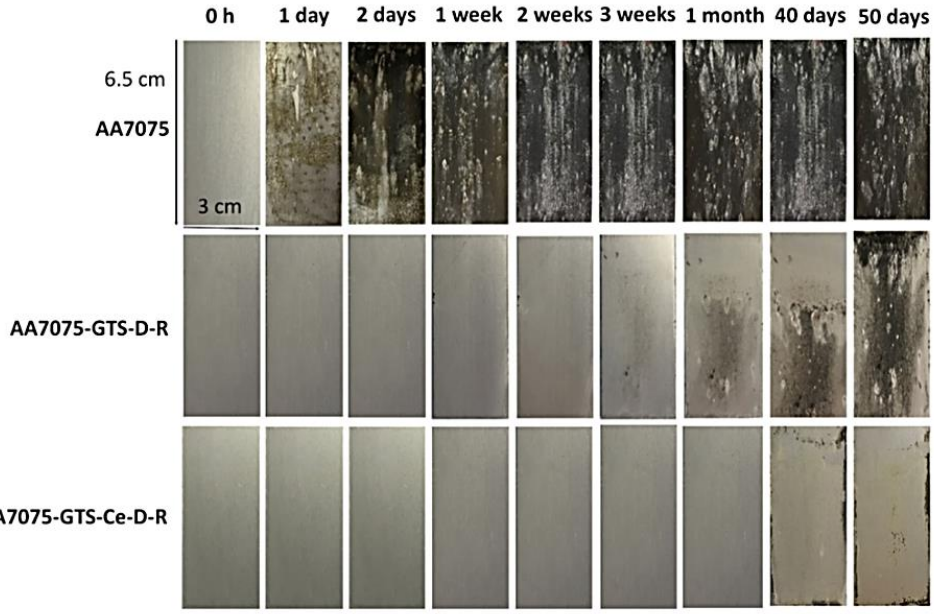


Fig. 5 Images of AA7075-T6 substrate uncoated and coated by hybrid silica GTS-D-R and by silica-Ce GTS-Ce-D-R coatings during an immersion test for 50 days in 0.1 M NaCl at room temperature. Images were taken after different times of immersion. Coatings were cured using ramp procedure

potential range [66, 67, 75]. The decrease of barrier effect with the immersion time, is associated to the presence of porosity and defects in the hybrid silica network produced for the incorporation of cerium as observed in the measurements described above [64].

3.5 Immersion test

AA7075-T6, both uncoated and coated by GTS-D-R and GTS-Ce-D-R coatings, were immersed for 50 days in 0.1 M NaCl at room temperature (Fig. 5). This alternative immersion test used as a standard lab test (NACE TMO169/G31) provides relevant information about corrosion process and is able to foreseen the behaviour of the alloy when exposed to natural outdoor environments.

Corrosion of the uncoated sample was visible after 1 day of immersion, resulting from galvanic and pitting corrosion. In contrast, corrosion of the GTS-D-R coated samples was only visible after 1 week of immersion, primarily at the boundaries of the sample, as a consequence of the higher density of defects in the borders. Corrosion at the sample surface was visible after 3 weeks of immersion, as a result of chloride attack. The long-standing corrosion resistance of GTS-D-R coating is due to its good barrier properties which are the result of thickness and density sufficient to withstand chloride attack. On the other hand, the GTS-Ce-D-R coating, doped with cerium, remained virtually undamaged for 40 days, when corrosion was noted at the surface. The difference between GTS-D-R and GTS-Ce-D-R coated samples is due to the presence of cerium in GTS-Ce which acts as a corrosion inhibitor of AA7075 alloy. The presence of tetravalent cerium compound at the coating surface is confirmed by the characteristic light yellow colour of GTS-Ce-D-R coating after 40 days of immersion. This finding confirms that $Ce(NO_3)_3$ added in the hybrid coating migrated to the coating surface, as also confirmed using glow discharge optical emission spectroscopy [66].

4 Conclusions

Hybrid sol–gel coatings, based on TEOS and GPTMS precursors and containing SiO_2 particles and cerium(III) nitrate were synthesized to provide a barrier and active corrosion protection of aluminium alloy AA7075 in 0.1 M NaCl. As AA7075-T6 is otherwise poorly corrosion resistant, these novel coatings offer an important progress for its protection in chloride containing solutions.

The aperture of the epoxy ring during synthesis process, indicative of polymerization, was confirmed by ATR-FTIR, UV-vis-NIR and C^{13}NMR; the reactions of hydrolysis and condensation were completed and sol was easily deposited on the substrate. The curing procedure affects the coating properties: curing using a heating ramp results in lower

roughness, reduced thickness and higher density of the coating. Double coatings exhibited better properties than monolayer coatings.

Incorporation of cerium in the coatings increases the roughness and thickness associated with a more porous network. Such porous network enables a release and migration of incorporated cerium ions which has a beneficial effect on the long-term corrosion resistance of the coatings.

The potentiodynamic polarization curves recorded in 0.1 M NaCl showed that coatings containing cerium and cured with heating ramp exhibit enhanced corrosion properties. Long-term EIS measurements confirmed that the presence of cerium allows controlling the degradation of the coatings. Coatings prepared with ramp-cured coatings doped with cerium remained undamaged for 40 days in chloride solution. These coatings are a good candidate to be applied on AA7075-T3 alloy combined with the deposition of an organic topcoat.

Acknowledgements The authors acknowledge financial support from the Slovenian Research Agency (research core funding No. P2-0393 and the project 'Lightweight alloys based on aluminium as materials with increasing potential in transportation industry', ID J1-6734). The authors thank Aritz Iglesias, Desiré Ruiz and Eva Peiteado for the technical help at ICV (CSIC). The authors also thank Sheila Omar for all helpful advices. The measurements of sol viscosity were performed at the Nanotesla Institute Ljubljana. The authors thank Dr. Branka Mušič and Adis Šahinović for discussion and comments. The authors thank Prof. R.H. Pain for proof reading the manuscript.

Compliance with ethical standards

Conflict of interest The authors declare that thay have no conflict of interest.

References

1. Vargel C (2004) Corrosion of aluminum. 1st edn. Elsevier, Amsterdam, The Netherlands
2. Davis JR (1999) Corrosion of aluminum and aluminum alloys. ASM International, Novelty, OHIO, USA
3. Buchheit RG (1995) A compilation of corrosion potentials reported for intermetallic phases in aluminum alloys. J Electrochem Soc 142:3994–3996
4. Milošev I, Rodič P (2016) Cerium chloride and acetate salts as corrosion inhibitors for aluminum alloy AA7075-T6 in sodium chloride solution. Corrosion 72:1021–1034
5. Birbilis N, Buchheit RG (2008) Investigation and discussion of characteristics for intermetallic phases common to aAluminum alloys as a function of solution pH. J Electrochem Soc 155: C117–C126
6. Kufman G (2000) Introduction to aluminum alloys and tempers. 1st edn. ASM International, USA
7. Kendig MW, Buchheit RG (2003) Corrosion inhibition of aluminum and aluminum alloys by soluble chromates, chromate coatings, and chromate-free coatings. Corrosion 59:379–400
8. Bibber JW (2001) An overview of nonhexavalent chromium conversion coatings—Part I: aluminum and its alloys. Met Finish 99:15–22
9. Chou TP, Chandrasekaran C, Cao GZ (2003) Sol-gel-derived hybrid coatings for corrosion protection. J Sol-Gel Sci Technol 26:321–327
10. Figueira RB, Silva CJR, Pereira EV (2014) Organic–inorganic hybrid sol–gel coatings for metal corrosion protection: a review of recent progress. J Coat Technol Res 12:1–35
11. Rodič P, Iskra J, Milošev I (2014) A hybrid organic–inorganic sol–gel coating for protecting aluminium alloy 7075-T6 against corrosion in Harrison's solution. J Sol-Gel Sci Technol 70:90–103
12. Twite RL, Bierwagen GP (1998) Review of alternatives to chromate for corrosion protection of aluminum aerospace alloys. Prog Org Coat 33:91–100
13. Zheng S, Li J (2010) Inorganic–organic sol gel hybrid coatings for corrosion protection of metals. J Sol-Gel Sci Technol 54:174–187
14. Wen J, Wilkes GL (1996) Organic/Inorganic hybrid network materials by the sol−gel approach. Chem Mater 8:1667–1681
15. Wang H, Akid R (2008) Encapsulated cerium nitrate inhibitors to provide high-performance anti-corrosion sol–gel coatings on mild steel. Corros Sci 50:1142–1148
16. Brinker CJ, Hurd CJ, Schunk PR, Frye GC, Ashley CS (1992) Review of sol-gel thin film formation. J Non-Cryst Solids 147:424–436
17. Metroke TL, Parkhill RL, Knobbe ET (2001) Passivation of metal alloys using sol–gel-derived materials—a review. Prog Org Coat 41:233–238
18. Livage J, Ganguli D (2001) Sol–gel electrochromic coatings and devices: a review. Sol Energy Mater Sol Cells 68:365–381
19. Brinker CJ, Scherer GW (2013) Sol-Gel science: the physics and chemistry of sol-gel processing. Academic Press, Cambridge, Massachusetts, USA
20. Guglielmi M (1997) Sol-gel coatings on metals. J Sol-Gel Sci Technol 8:443–449
21. Han Y-H, Taylor A, Mantle MD, Knowles KM (2007) Sol–gel-derived organic–inorganic hybrid materials. J Non-Cryst Solids 353:313–320
22. Mosa J, Durán A, Aparicio M (2009) Proton conducting sol–gel sulfonated membranes produced from 2-allylphenol, 3-glycidoxypropyl trimethoxysilane and tetraethyl orthosilicate. J Power Sources 192:138–143
23. Voevodin NN, Kurdziel JW, Mantz R (2006) Corrosion protection for aerospace aluminum alloys by modified self-assembled nanophase particle (MSNAP) sol–gel. Surf Coat Technol 201:1080–1084
24. Pirhady Tavandashti N, Sanjabi S, Shahrabi T (2011) Evolution of corrosion protection performance of hybrid silica based sol–gel nanocoatings by doping inorganic inhibitor. Mater Corros 62:411–415
25. Schottner G (2001) Hybrid sol−gel-derived polymers: applications of multifunctional materials. Chem Mater 13:3422–3435
26. Zheludkevich ML, Salvado IM, Ferreira MGS (2005) Sol–gel coatings for corrosion protection of metals. J Mater Chem 15:5099–5111
27. Rosero-Navarro NC, Curioni M, Castro Y, Aparicio M, Thompson GE, Durán A (2011) Glass-like CexOy sol–gel coatings for corrosion protection of aluminium and magnesium alloys. Surf Coat Technol 206:257–264
28. Zomorodian A, Brusciotti F, Fernandes A, Carmezim MJ, Moura e Silva T, JCS Fernandes, Montemor MF (2012) Anti-corrosion performance of a new silane coating for corrosion protection of AZ31 magnesium alloy in Hank's solution. Surf Coat Technol 206:4368–4375
29. Underhill PR, Goring G, DuQuesnay DL (1998) The drying of 3-glycidoxypropyltrimethoxy silane. Appl Surf Sci 134:247–253
30. Davis SR, Brough AR, Atkinson A (2003) Formation of silica/epoxy hybrid network polymers. J Non-Cryst Solids 315:197–205

31. Lakshmi RV, Yoganandan G, Mohan AVN, Basu BJ (2014) Effect of surface pre-treatment by silanization on corrosion protection of AA2024-T3 alloy by sol–gel nanocomposite coatings. Surf Coat Technol 240:353–360
32. Wang H, Akid R (2007) A room temperature cured sol–gel anticorrosion pre-treatment for Al 2024-T3 alloys. Corros Sci 49:4491–4503
33. Zheludkevich ML, Serra R, Montemor MF, Miranda Salvado IM, Ferreira MGS (2006) Corrosion protective properties of nanostructured sol–gel hybrid coatings to AA2024-T3. Surf Coat Technol 200:3084–3094
34. Zheludkevich ML, Serra R, Montemor MF, Yasakau KA, Miranda Salvado IM, Ferreira MGS (2005) Nanostructured sol–gel coatings doped with cerium nitrate as pre-treatments for AA2024-T3: corrosion protection performance. Electrochim Acta 51:208–217
35. Roussi E, Tsetsekou A, Tsiourvas D, Karantonis A (2011) Novel hybrid organo-silicate corrosion resistant coatings based on hyperbranched polymers. Surf Coat Technol 205:3235–3244
36. Schem M, Schmidt T, Gerwann J, Wittmar M, Veith M, Thompson GE, Molchan IS, Hashimoto T, Skeldon P, Phani AR, Santucci S, Zheludkevich ML (2009) CeO2-filled sol–gel coatings for corrosion protection of AA2024-T3 aluminium alloy. Corros Sci 51:2304–2315
37. Wang H, Akid R, Gobara M (2010) Scratch-resistant anticorrosion sol–gel coating for the protection of AZ31 magnesium alloy via a low temperature sol–gel route. Corros Sci 52:2565–2570
38. Khramov AN, Balbyshev VN, Voevodin NN, Donley MS (2003) Nanostructured sol–gel derived conversion coatings based on epoxy- and amino-silanes. Prog Org Coat 47:207–213
39. Milošev I, Kapun B, Rodič P, Iskra J (2015) Hybrid sol–gel coating agents based on zirconium(IV) propoxide and epoxysilane. J Sol-Gel Sci Technol 74:447–459
40. Zandi-zand R, Ershad-langroudi A, Rahimi A (2005) Silica based organic–inorganic hybrid nanocomposite coatings for corrosion protection. Prog Org Coat 53:286–291
41. Sakka S (2005) Handbook of sol-gel science and technology. 2. Characterization and properties of sol-gel materials and products. Springer Science & Business Media
42. Innocenzi P, Brusatin G, Babonneau F (2000) Competitive polymerization between organic and Inorganic networks in hybrid materials. Chem Mater 12:3726–3732
43. Metroke TL, Kachurina O, Knobbe ET (2002) Spectroscopic and corrosion resistance characterization of GLYMO–TEOS Ormosil coatings for aluminum alloy corrosion inhibition. Prog Org Coat 44:295–305
44. Santana I, Pepe A, Jimenez-Pique E, Pellice S, Milošev I, Ceré S (2015) Corrosion protection of carbon steel by silica-based hybrid coatings containing cerium salts: effect of silica nanoparticle content. Surf Coat Technol 265:106–116
45. Ballarre J, Manjubala I, H Schreiner W, Orellano JC, Fratzl P, Ceré S (2010) Improving the osteointegration and bone-implant interface by incorporation of bioactive particles in sol-gel coatings of stainless steel implants. Acta Biomater 6:1601–1609
46. Vreugdenhil AJ, Balbyshev VN, Donley MS (2001) Nanostructured silicon sol-gel surface treatments for Al 2024-T3 protection. J Coat Technol 73:35–43.
47. Peres RN, Cardoso ESF, Montemor MF, Melo HG, Benedetti AV, Suegama PH (2016) Influence of the addition of SiO2 nanoparticles to a hybrid coating applied on an AZ31 alloy for early corrosion protection. Surf Coat Technol 303(Part B):372–384
48. Durán A, Castro Y, Aparicio M, Conde A, Damborenea JJ (2007) Protection and surface modification of metals with sol–gel coatings. Int Mater Rev 52:175–192
49. Voevodin NN, Grebasch NT, Soto WS, Kasten LS, Grant JT, Arnold FE, Donley MS (2001) An organically modified zirconate film as a corrosion-resistant treatment for aluminum 2024-T3. Prog Org Coat 41:287–293
50. Rosero-Navarro NC, Pellice SA, Castro Y, Aparicio M, Durán A (2009) Improved corrosion resistance of AA2024 alloys through hybrid organic–inorganic sol–gel coatings produced from sols with controlled polymerisation. Surf Coat Technol 203:1897–1903
51. Khelifa F, Druart M-E, Habibi Y, Bénard F, Leclère P, Olivier M, Dubois P (2013) Sol–gel incorporation of silica nanofillers for tuning the anti-corrosion protection of acrylate-based coatings. Prog Org Coat 76:900–911
52. Suegama PH, de Melo HG, Recco AAC, Tschiptschin AP, Aoki IV (2008) Corrosion behavior of carbon steel protected with single and bi-layer of silane films filled with silica nanoparticles. Surf Coat Technol 202:2850–2858
53. Suegama PH, Recco AAC, Tschiptschin AP, Aoki IV (2007) Influence of silica nanoparticles added to an organosilane film on carbon steel electrochemical and tribological behaviour. Prog Org Coat 60:90–98
54. Iribarren-Mateos JI, Buj-Corral I, Vivancos-Calvet J, Alemán C, Iribarren JI, Armelin E (2015) Silane and epoxy coatings: a bilayer system to protect AA2024 alloy. Prog Org Coat 81:47–57
55. Hinton BRW (1992) Corrosion inhibition with rare earth metal salts. J Alloy Compd 180:15–25
56. Hinton BRW, Arnott DR, Ryan NE (1984) Inhibition of aluminum alloy corrosion by cerous cations. ResearchGate 7:211–217
57. Revie RW, Uhlig HH (2008) Corrosion and corrosion control. Wiley, Hoboken, NJ
58. Zhong X, Li Q, Hu J, Yang X, Luo F, Dai Y (2010) Effect of cerium concentration on microstructure, morphology and corrosion resistance of cerium–silica hybrid coatings on magnesium alloy AZ91D. Prog Org Coat 69:52–56
59. Rahimi H, Mozaffarinia R, Hojjati Najafabadi A (2013) Corrosion and wear resistance characterization of environmentally friendly sol–gel hybrid nanocomposite coating on AA5083. J Mater Sci Technol 29:603–608
60. Balgude D, Konge K, Sabnis A (2013) Synthesis and characterization of sol–gel derived CNSL based hybrid anti-corrosive coatings. J Sol-Gel Sci Technol 69:155–165
61. Scopel WL, Fantini MCA, Alayo MI, Pereyra I (2002) Local order structure of a-SiOxNy:H grown by PECVD. Braz J Phys 32:366–368
62. Mosa J, Durán A, Aparicio M (2010) Epoxy-polystyrene-silica sol–gel membranes with high proton conductivity by combination of sulfonation and tungstophosphoric acid doping. J Membr Sci 361:135–142
63. Crivello JV, Liu S (2000) Photoinitiated cationic polymerization of epoxy alcohol monomers. J Polym Sci Part Polym Chem 38:389–401
64. Cambon J-B, Esteban J, Ansart F, Bonino J-P, Turq V, Santagneli SH, Santilli CV, Pulcinelli SH (2012) Effect of cerium on structure modifications of a hybrid sol–gel coating, its mechanical properties and anti-corrosion behavior. Mater Res Bull 47:3170–3176
65. Castro Y, Ferrari B, Moreno R, Durán A (2004) Coatings produced by electrophoretic deposition from nano-particulate silica sol–gel suspensions. Surf Coat Technol 182:199–203
66. Paussa L, Rosero-Navarro NC, Andreatta F, Castro Y, Duran A, Aparicio M, Fedrizzi L (2010) Inhibition effect of cerium in hybrid sol–gel films on aluminium alloy AA2024. Surf Interface Anal 42:299–305
67. Rosero-Navarro NC, Pellice SA, Durán A, Aparicio M (2008) Effects of Ce-containing sol–gel coatings reinforced with SiO2 nanoparticles on the protection of AA2024. Corros Sci 50:1283–1291

68. Volarič B, Milošev I (2017) Rare earth chloride and nitrate salts as individual and mixed inhibitors for aluminium alloy 7075-T6 in chloride solution. Corros Eng Sci Technol 52:201–211.
69. Volaric B, Rodic P, Milosev I (2015) Cerium and lanthanum salts used as individual and combined inhibitors for corrosion protection of AA7075-T6 in chloride solution. Meet Abstr 2015-02:685–685
70. Rodič P, Milošev I (2016) Corrosion inhibition of pure aluminium and alloys AA2024-T3 and AA7075-T6 by cerium(III) and cerium(IV) salts. J Electrochem Soc 163:C85–C93
71. Marcus P, Mansfeld F B (2005) Analytical methods in corrosion science and engineering. CRC Press. https://www.crcpress.com/Analytical-Methods-In-Corrosion-Science-and-Engineering/Marcus-Mansfeld/p/book/9780824759520. Accessed 4 Dec 2017
72. Rosace G, Guido E, Colleoni C, Brucale M, Piperopoulos E, Milone C, Plutino MR (2017) Halochromic resorufin-GPTMS hybrid sol-gel: chemical-physical properties and use as pH sensor fabric coating. Sens Actuators B Chem 241:85–95
73. Mansfeld F, Wang Y (1995) Development of "stainless" aluminum alloys by surface modification. Mater Sci Eng A 198:51–61
74. Rosero-Navarro NC, Paussa L, Andreatta F, Castro Y, Durán A, Aparicio M, Fedrizzi L (2010) Optimization of hybrid sol–gel coatings by combination of layers with complementary properties for corrosion protection of AA2024. Prog Org Coat 69:167–174
75. Lakshmi RV, Aruna ST, Sampath S (2017) Ceria nanoparticles vis-à-vis cerium nitrate as corrosion inhibitors for silica-alumina hybrid sol-gel coating. Appl Surf Sci 393:397–404

Chapter 4

Self-Healing Effect of Hybrid Sol-Gel Coatings Based on GPTMS, TEOS, SiO_2 Nanoparticles and $Ce(NO_3)_3$ Applied on Aluminum Alloy 7075-T6

In the present chapter hybrid sol-gel coatings from Chapter 3, based on silane precursors (3-glycidyloxypropyl) trimethoxysilane (GPTMS), tetraethoxysilane (TEOS), SiO_2 nanoparticles and $Ce(NO_3)_3$ as corrosion inhibitor, were improved by developing a multi-layer system. A bi-layer system of two sols was applied on aluminum alloy 7075-T6, where the first layer was doped with $Ce(NO_3)_3$ and the second was un-doped. It was confirmed that the addition of cerium has a role in self-healing only if it is locked within the first layer of multilayer coating. Self-healing effect was confirmed by immersion of un-scribed and scribed coating in a sodium chloride solution by using several techniques. Based on the high efficiency of such bilayer coating it can be stated that it represents an alternative to chromate conversion coating.

In Figure 1.10 a graphical abstract.

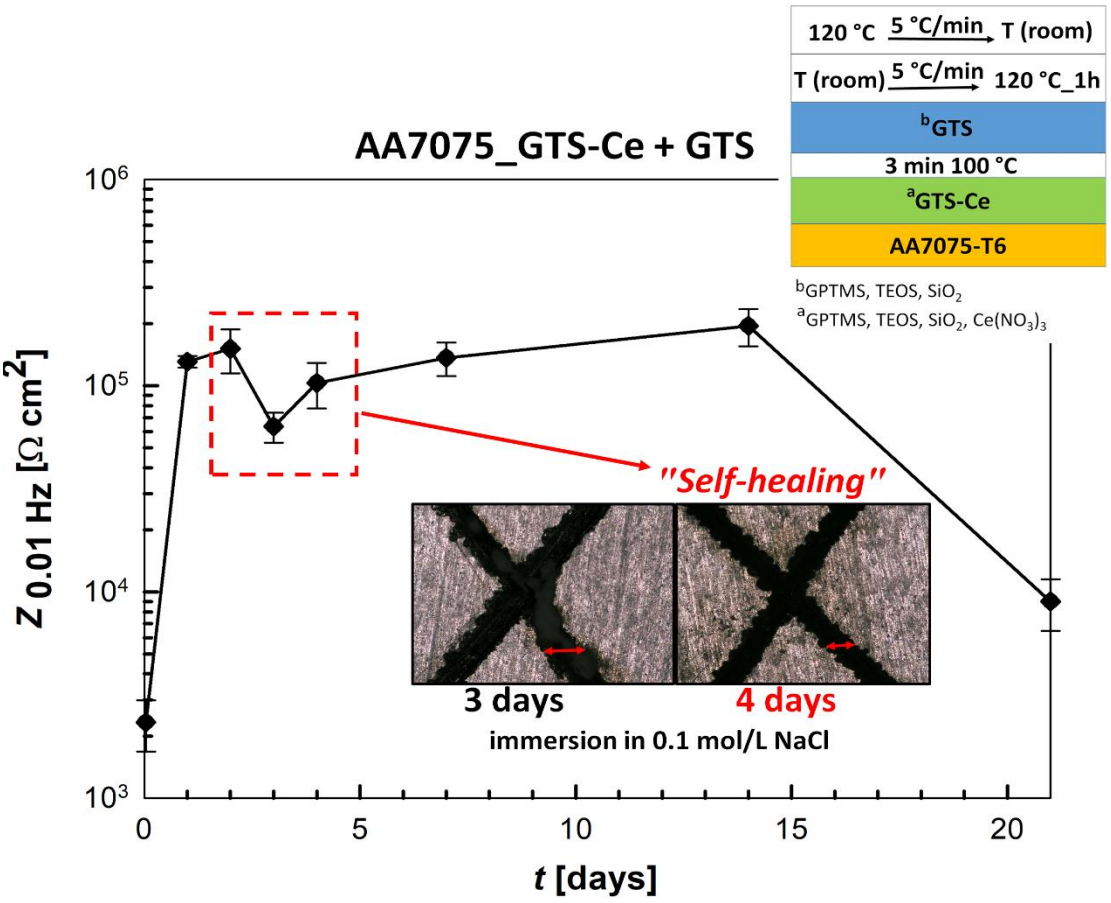


Figure 10: Graphical abstract of Chapter 4.

This chapter addresses thesis Objectives 4) and 5) from Chapter 1.6.

Regarding my contribution: I made a literature overview of the topic, co-formulated the basic idea for the object of the investigation, co-planned, co-designed and performed the experiments and jointly prepared the manuscript with co-authors.

Journal of The Electrochemical Society, **165** (5) C213-C225 (2018) C213

Self-Healing Effect of Hybrid Sol-Gel Coatings Based on GPTMS, TEOS, SiO_2 Nanoparticles and $Ce(NO_3)_3$ Applied on Aluminum Alloy 7075-T6

Urša Tiringer,[1,2] Alicia Durán,[3] Yolanda Castro,[3] and Ingrid Milošev [1,*,z]

[1] *Department of Physical and Organic Chemistry, Jožef Stefan Institute, SI-1000 Ljubljana, Slovenia*
[2] *Jožef Stefan Postgraduate School, SI-1000 Ljubljana, Slovenia*
[3] *Instituto de Cerámica y Vidrio (CSIC), Campus de Cantoblanco, 28049 Madrid, Spain*

Aluminum alloy AA7075-T6 is most commonly used in the aircraft and automotive industries. Due to the presence of intermetallic particles, AA7075-T6 is susceptible to localized corrosion in chloride solutions. In the present work multilayer hybrid sol-gel coatings, based on silane precursors 3-glycidyloxypropyl(trimethoxysilane) (GPTMS) and tetraethoxysilane (TEOS), were used to protect AA7075-T6 from corrosion. To enrich the barrier properties of the coating, SiO_2 nanoparticles were added to the GPTMS/TEOS sol-gel solution. Inhibition and a self-healing effect were achieved by doping $Ce(NO_3)_3$ in the coating. A multi-layer system was applied on the substrate composed of a first layer doped with $Ce(NO_3)_3$ and the second, undoped sol-gel layer. The addition of cerium increases the lifespan of hybrid sol-gel coating and has a role in self-healing if it is locked within the first layer of the multilayer coating. The self-healing effect was confirmed by immersion of unscribed and scribed coated substrates in 0.1 mol/L NaCl by using the immersion test, electrochemical impedance spectroscopy, X-ray photoelectron spectroscopy and scanning electron microscopy with chemical analysis.

© The Author(s) 2018. Published by ECS. This is an open access article distributed under the terms of the Creative Commons Attribution Non-Commercial No Derivatives 4.0 License (CC BY-NC-ND, http://creativecommons.org/licenses/by-nc-nd/4.0/), which permits non-commercial reuse, distribution, and reproduction in any medium, provided the original work is not changed in any way and is properly cited. For permission for commercial reuse, please email: oa@electrochem.org. [DOI: 10.1149/2.0211805jes]

BY-NC-ND

Manuscript submitted December 5, 2017; revised manuscript received March 6, 2018. Published March 17, 2018.

Due to increasing demand for light-weight metals to reduce fuel consumption and, consequently, CO_2 emission, aluminum alloy AA7075-T6 is very attractive in automotive and aircraft industries. In addition to its low density, its advantages are high strength-to-weight ratio and good mechanical properties.[1–3] However, due to the presence of zinc and copper intermetallic particles, AA7075-T6 readily undergoes localized corrosion, which limits its use in more aggressive environments. Chromate conversion coatings (CCCs), which were used for decades as providing the most effective corrosion protection of aluminum alloys, are limited, in the European Union.[4] Many surface treatments have been proposed to replace CCCs, the sol-gel process being one of the most promising and environmentally friendly.[5–12] In hybrid sol-gel coatings, which combine inorganic and organic compounds, the inorganic compound provides mechanical support, while the organic compound adds to flexibility and decreases treatment temperature.[8,12–15] Hybrid sol-gel coatings achieve protection of underlying substrate by acting as barrier coatings. Addition of silica nanoparticles (SiO_2) into sol-gel coating has been reported to additionally increase the barrier effect by increasing the coating thickness, density and reinforcement.[16–23] Still, if these coatings do not contain corrosion inhibitors they lack the ability to inhibit the corrosion process once it commences, i.e. they do not show active inhibition ability resulting in a self-healing of the coating.

To obtain an active corrosion protection, corrosion inhibitors can be incorporated into sol-gel coating. According to Hinton et al.,[24,25] many salts of rare earth ions such as Ce^{3+}, Y^{3+}, La^{3+}, Pr^{3+} and Nd^{3+}, are successful corrosion inhibitors for aluminum alloys, Ce^{3+} being the most efficient. When added directly to corrosive solution, e.g. chloride solution, earth salts hydrolyse and can then precipitate at the metal surface once the conditions for precipitation are established; in the case of Ce, cerium (III) hydroxide $Ce(OH)_3$ precipitates at the cathodic sites at the surface where the pH increases due to formation of OH^- ions during the reduction of oxygen.[26,27] $Ce(OH)_3$ formed can be further oxidized to $Ce(OH)_4$ and insoluble CeO_2, which acts as a protective barrier to oxygen and lowers the cathodic activity by hindering the transfer of electrons from the anodic to cathodic sites.[28–30] The addition of corrosion inhibitors, including cerium, to the formulation based on precursors, such as tetramethylorthosilicate (TMOS), tetraethoxysilane (TEOS), methyltrimethoxysilane (MTMS), 3-glycidoxypropyltrimethoxysilane (GPTMS), etc.[8] has been shown to provide self-healing properties when these coatings are applied on aluminum alloys.[21,29,31–35] Thus, when the coating is mechanically damaged or local defects are present, the inhibitor is released and act in such a way to repair the damage or retard the corrosion process. The most probable self-healing mechanism involves the formation of $Ce(OH)_2^{2+}$ ions which can migrate to the damaged sites where are converted into highly insoluble $Ce(OH)_4/CeO_2$.[28,36–38] Another possibility to express self-healing ability in silane hybrid sol-gel coating was pre-treatment of aluminum alloy in a $1{\cdot}10^{-3}$ mol/L $Ce(NO_3)_3$ solution.[37]

The possible drawback of direct incorporation of cerium ions into the hybrid coating is the generation of high porosity and consequently fast release of inhibitor into the solution which prevents the long-term self-healing ability.[39–41] Further, the increased roughness of cerium containing coatings was noticed and ascribed to a superficial agglomeration/precipitation of cerium containing nanoparticles.[32] This implicates that there exist an optimal content of Ce which would not deteriorate the coating stability but yet provide a self-healing ability for a reasonably long period of time upon exposure to chloride solution. This task is difficult to achieve, as shown in our previous study.[40,41] When using monolayer sol-gel coating doped with cerium to obtain barrier and active protection, the long-term coating stability can be jeopardized.[16,40–42] Namely, the inhibition effect was observed, but a fast deterioration of the barrier properties of the coating occurred after 24 hours in 0.35 wt% NaCl.[16] A multi-layer sol-gel hybrid coating, based on TEOS, methacryloxypropyl trimethoxysilane (MPS), ethylene glycol dimethacrylate (EGDMA) and glycidyl methacrylate (GMA) containing an intermediate cerium doped layer was shown to greatly improve the corrosion properties of AA2024.[32] It was further showed that the barrier and active protection of coatings were improved in multi-layer coating, based on TEOS, GPTMS and SiO_2 nanoparticles, where cerium was in the top layer, but the self-healing ability of such coatings applied on carbon steel was not confirmed.[16]

In the present work three types of multi-layer hybrid sol-gel coatings were developed based on the inorganic precursor TEOS, organic precursor GPTMS, SiO_2 nanoparticles and corrosion inhibitor $Ce(NO_3)_3$. The aim was to develop a coating system that would prevent the leaching of cerium ions from the coating. Thus, a multilayer

*Electrochemical Society Member.
[z]E-mail: ingrid.milosev@ijs.si

system of two different coatings was used: the first layer was doped with cerium, while the second was undoped to increase the stability of cerium in the underlying layer. This multi-layer system was expected to enable self-healing through migration of cerium ions to damaged sites and the recovery of damaged sites (i.e. self-healing) in the course of prolonged immersion in chloride containing electrolyte. We planned the experiments in such a manner as to prove the self-healing effect particularly on scribed coatings. A further novelty of the present work is the type of aluminum alloy used, i.e. AA7075-T6 which is difficult to protect due to its high susceptibility for localized corrosion in chloride environment.

Experimental

Metal substrate preparation.—Aluminum alloy AA7075-T6 (Zn 5.81 wt%, Mg 2.55 wt%, Cu 1.67 wt%, Fe 0.21 wt%, Si 0.08 wt%, the remaining Al) with dimensions of 30 mm × 65 mm × 2 mm, supplied by Kaiser Aluminum, was subjected to a three-step cleaning procedure including alkaline cleaning (Metaclean T2001 – Chemie Vertrieb Hannover GmbH & Co KG), an alkaline etching (Turco Liquid Aluminetch Nr.2 – Turco Chemie GmbH) and a final step of acid desmutting (Turco Liquid Smutgo NC – Turco Chemie GmbH). After each step samples were rinsed with deionized water.

Synthesis of hybrid sols and coatings deposition.—The schematic presentation of sol synthesis and coating deposition and curing are presented in Figs. 1 and 2a. Two hybrid sols were prepared, one undoped and the other doped with cerium (Fig. 1). The first sol was prepared at room temperature by mixing tetraethoxysilane (TEOS, Aldrich, 99%) and 3-(glycidyloxypropyl)trimethoxy silane (GPTMS, ABCR, 98%) with a colloidal silica (SiO_2) suspension (Ludox-4S, Aldrich, aqueous suspension 40 wt%, particle size 20 nm, pH 9). After 30 minutes of stirring, 0.6 mL of concentrated nitric acid HNO_3 (VWR, 65%) was added to 100 mL of solution as a catalyst. Finally, absolute ethanol (EtOH, Panreac, 99.8%) was added as a dissolvent. The final silica concentration was 120 g/L, with 64 g/L of colloidal particles, labelled as 120 (64). The molar ratio of the first hybrid sol was $TEOS/GPTMS/SiO_2 = 0.4/0.46/0.14$ and it was denoted as GTS.

The second sol was prepared following the same process, but incorporating cerium as a corrosion inhibitor. Cerium nitrate ($Ce(NO_3)_3 .6\ H_2O$, Aldrich, 98%), dissolved in EtOH, was added before addition of the catalyst (HNO_3). The molar ratio of the second sol was $TEOS/GPTMS/SiO_2/Ce = 0.39/0.44/0.12/0.05$, denoted as GTS-Ce.

After synthesis, sols were immediately deposited on AA7075-T6 substrate by dip-coating at a withdrawal rate of 30 cm/min. Three different coatings were prepared (Fig. 2a). The first coating was prepared by the deposition of two layers of GTS sols (denoted as GTS), and the second by the deposition of two layers of GTS-Ce sols (denoted as GTS-Ce). Before depositing the second layer the first layer was dried using a hot air gun at 100°C for 3 minutes. The third coating was the combination of GTS-Ce and GTS sols (denoted as GTS-Ce+GTS). Each sol was deposited as a single layer, with intermediate curing using a hot air gun at 100°C for 3 minutes.

Finally, the coatings were cured as follows: using a ramp of 5°C/min from room temperature up to the curing temperature of 120°C, cured for 1 h, and then cooled down with the same rate 5°C/min to reach room temperature (Fig. 2a).

Coating characterization.—The coating thickness was measured on coated glass-slides by Spectroscopic Ellipsometer (J.A. Woollam Co., Inc, EC-400, M-2000 U Software: WVASE32). The spectral band was recorded from 250 nm to 900 nm at incident angles between 50° and 60°. The data were fitted using the WVASE32 software with a Cauchy model. Three measurements were performed for each sample at different sites and the mean value was deduced for each coating.

The morphology and composition of coatings were analyzed using a field emission scanning electron microscope (FE-SEM, JEOL JSM-7600F) equipped with energy dispersive X-ray spectrometer (EDS, Oxford Instruments INCA). The diameter of the analyzed area was a few micrometres and the analyzed depth around 1 μm. Prior to analysis, samples were coated with a carbon layer to reduce the charging effect. Images were recorded in a compositional mode using an energy of 15 kV. EDS mapping was performed with a resolution of 512 lines.

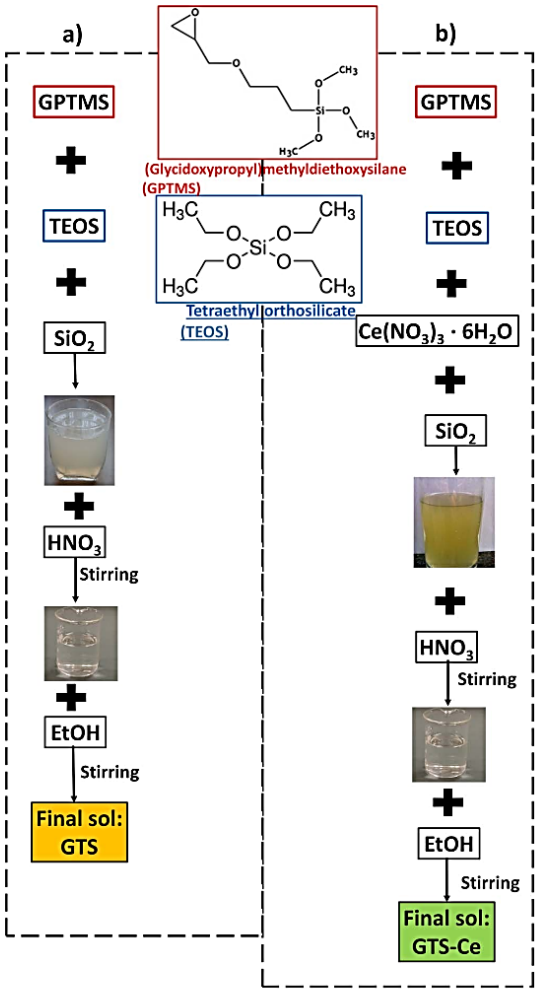


Figure 1. Schematic presentation of synthesis of hybrid sols GTS and GTS-Ce.

Ultraviolet-visible (UV-vis) spectra (Perkin with Elmer Lambda 950 spectrophotometer) were acquired between 200 and 700 nm for coatings deposited on SiO_2 substrates. Spectrum for the uncoated SiO_2 substrate was recorded for reference.

X-ray photoelectron spectroscopy (XPS) was carried out using a PHI-TFA XPS spectrometer (Physical Electronic Inc.). The vacuum during the XPS analysis was in the range of 10^{-9} mbar. The analyzed area was 0.4 mm in diameter and the depth about 3–5 nm. X-rays were provided from a monochromatic Al source at photon energy of 1486.6 eV. XPS spectra were analyzed by Multipak software, version 8.0 (Physical Electronics Inc.). The elemental composition was determined from survey spectra. An Ar^+ ion beam, with an energy of 4 keV and a raster of 3 mm × 3 mm, was used for etching. The sputtering rate was 2 nm/min, as determined on a Ni/Cr multilayer structure of known thickness.

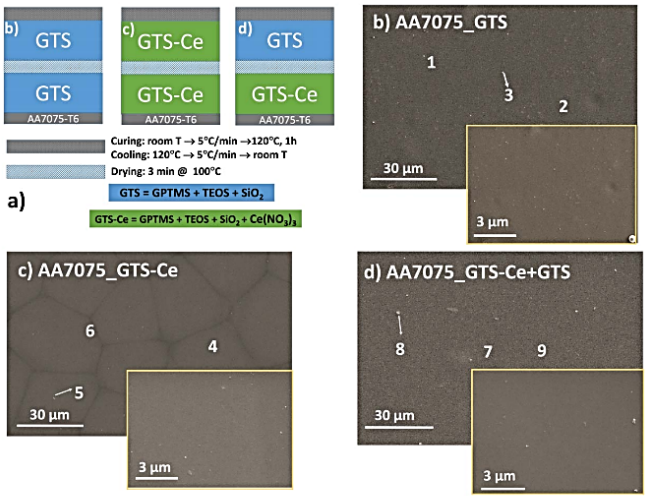


Figure 2. (a) Schematic presentation of the coatings GTS, GTS-Ce and GTS-Ce+GTS and drying and curing treatments. SEM images of AA7075-T6 coated with (b) GTS, (c) GTS-Ce and (d) GTS-Ce+GTS coatings. The numbers 1–9 denote locations where EDS analysis was carried out (Table I). Note that all coatings are bilayer coatings.

Corrosion behavior of coatings.—The corrosion performance of uncoated and coated AA7075-T6 substrates was tested using electrochemical impedance spectroscopy (EIS) in a 0.1 mol/L NaCl aqueous solution at room temperature. An AUTOLAB PGSTAT 12 potentiostat/galvanostat, controlled by NOVA 1.11 software, was used for measurements made in a three-electrode standard corrosion cell (PAR Flat cell K0235, volume 250 mL). An Ag/AgCl/saturated KCl electrode was the reference electrode (0.192 V versus standard hydrogen electrode), the platinum mesh was a counter electrode and the tested material embedded in a Teflon holder was a working electrode. The area exposed to the corrosion medium was 1 cm^2. All potentials in the text are given with respect to an Ag/AgCl electrode. The EIS were performed at open circuit potential with an ac excitation voltage of 10 mV in the range from 10^{-2} Hz to 10^5 Hz. Corrosion resistance was assessed by determining the modulus of impedance, Z, from the Bode plot (Z vs. frequency) at a frequency of 10^{-2} Hz. Experiments were repeated at least three times and the most highly representative measurement was chosen for plotting.

The development of corrosion process on uncoated and coated substrates were also monitored by an immersion test carried out in 0.1 mol/L NaCl at room temperature. Samples were placed in a DURAN glass flask containing 300 mL NaCl solution. The area of sample exposed to electrolyte was 1450 mm^2, giving a ratio of 0.207, thus in accordance with the "Standard guide for laboratory immersion corrosion testing of metals" (NACE TMO 169/631). Immersed samples were monitored for 80 days.

Evaluation of the self-healing effect on scribed coatings.—To evaluate the self-healing property of coatings, the samples were scribed and the course of self-healing process was followed using different methods. Two types of scribe were created: (i) a cross shaped scribe, with a depth of over 7 µm, made with a diamond tip; the depth of the scribe was larger than the coating depth and reached the underlying substrate, and (ii) cross shaped indents, with a depth around 2–4 µm, made using a Vickers diamond indenter within the coating depth. The indents were made using a Fisherscope H100C tester at the indentation load 2 N. The depth of the scribe was determined by the profilometer (model Bruker DektakXT). The radius of the stylus was 2 µm; it was used at a force of 30 mN. Map resolution was 10 µm/trace, scanned at a spot size of 1 mm × 1 mm. The vertical analysis range was 65.5 µm and the vertical resolution 0.167 µm/point. Data was processed using Bruker Vision 64 and TalyMap Gold 6.2 software. Three measurements were performed at different sites of the scribe and the mean value was determined.

Scribed GTS, GTS-Ce and GTS-Ce+GTS coatings were exposed to the 0.1 mol/L NaCl solution for various immersion times to follow the self-healing. EIS spectra were recorded during the course of immersion. The morphological changes at the scribe were monitored as a function of immersion time using an optical microscope (Olympus BX51). The magnification and light were controlled and kept constant throughout the experiment. At the end of the immersion test, SEM/EDS and XPS analyses were carried out.

Results and Discussion

The morphology, composition and corrosion properties of the uncoated and coated AA7075-T6 samples were analyzed. The study was divided into three parts: (i) characterization of as-prepared coatings, (ii) corrosion behavior of unscribed coatings and (iii) corrosion behavior of scribed coatings.

Coating characterization.—*Ellipsometry.*—The thickness of GTS, GTS-Ce and GTS-Ce+GTS coatings deposited on glass-slides was measured by ellipsometry. The total thickness of GTS coating was 5.3 ± 0.4 µm, of GTS-Ce was 7.0 ± 0.7 µm and of GTS-Ce + GTS coating was 6.0 ± 0.6 µm. The GTS-Ce coating was thicker as a result of the presence of cerium, which was ascribed to increased porosity, i.e. free volumes in the hybrid network, as will be described below.[44–46]

SEM/EDS analysis.—The morphology and composition of different coatings applied on AA7075-T6 were investigated by SEM/EDS analysis (Fig. 2, Table I). The surface of the GTS coating applied on AA7075-T6 was shown by SEM/EDS analysis to be homogeneous (Fig. 2b). EDS analysis shows Si and O as only elements of the coatings; Al and alloying elements were not detected, since the coating thickness was greater than 5 µm.[43] The concentrations of Si and O at locations 1, 2 and 3 were similar, indicating homogeneous composition over the surface. At the surface of GTS-Ce coating in addition to Si and O, a small concentration of Ce (up to 1 at.%) was identified at all three locations 4, 5 and 6 (Fig. 2c, Table I). Although the coating was homogeneous as GTS, some underlying structure in the form of grains is evident (Fig. 2c). This may be caused by the incorporation of cerium. It has been shown that the addition of cerium affects the structure of the hybrid sols in several ways: Ce promotes inorganic and organic polymerization of the network and the process of opening of the epoxy ring.[46] The degree of this effect is, however, dependent on Ce concentration in the sol. When Ce is present at low concen-

Table I. Concentrations of elements obtained by EDS analysis at various locations on the AA7075-T6 alloy coated with GTS (locations 1–3), GTS-Ce (locations 4–6) and GTS-Ce+GTS (locations 7–9) coatings. Locations are denoted on SEM images in Fig. 2.

Location	Si [at.%]	O [at.%]	Ce [at.%]
1	37.7	62.3	/
2	34.7	65.3	/
3	33.3	66.7	/
4	35.3	63.8	0.9
5	35.3	64.0	0.7
6	36.9	62.5	0.6
7	35.1	64.9	/
8	37.4	62.6	/
9	33.8	66.2	/

tration, the condensation and polymerization of both inorganic and organic networks are favored. When present at higher concentrations (> 0.01 mol/L), the polymerization of inorganic network is favored and may lead to destabilization of the Si−O−Si structure and possible creation of free volumes (pores) in the hybrid.[46] Atomic radius of Ce is larger than that of Si (185 and 110 pm, respectively) which is another factor which can cause internal stress. The Ce concentration used herein is 0.05 mol/L, which may already be in the range when destabilization of the network may occur leading to the structure observed in Fig. 2c. However, this higher Ce concentration may be beneficial for the self-healing effect, as will be shown below. The surface of the GTS-Ce+GTS coating was homogeneous and similar to that of GTS, as confirmed by EDS analysis (Fig. 2d). The absence of cerium at the surface of the GTS-Ce+GTS coating confirms that the deposition of the second layer (GTS) completely covered the underlying GTS-Ce layer. No structure similar to that in GTS-Ce (Fig. 2c) was observed indicating that the outer GTS layer does not destabilize the coating structure and that incorporated cerium was locked in the inner layer, closer to metal surface.

EDS analysis confirmed the presence of cerium but it could not differentiate between two oxidation states Ce^{3+} and Ce^{4+}. UV-vis analysis is explored for that purpose. UV-vis spectra recorded on uncoated SiO_2 substrate and substrates coated with GTS-Ce and with GTS-Ce+GTS coatings are presented in Fig. 3. The GTS-Ce coating absorbs some visible light in the range from 300 to 500 nm. Since Ce^{3+} ions are colorless and Ce^{4+} are yellow, this coating contains at least some amount of cerium ions in Ce^{4+} oxidation state. Although Ce is added in the sol in the form of Ce^{3+}, during the sol-gel synthesis

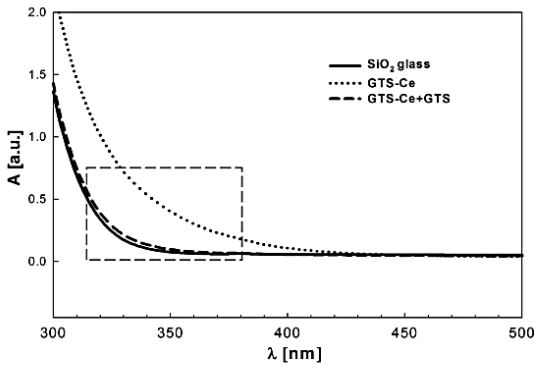


Figure 3. UV-vis-NIR spectra of uncoated SiO_2 and SiO_2 coated with GTS-Ce and GTS-Ce+GTS in the range from 300 to 700 nm. Coatings were cured from a room temperature, with a ramp of 5°C/min, up to the 120°C and cured for 1 hour at 120°C.

and especially during curing process at 120°C it can be partially oxidized to Ce^{4+}, as evident by slightly yellow coloration of the coating. In contrast, UV-vis spectrum for the GTS-Ce+GTS coating shows only a slightly different curve compared to substrate, i.e. no evidence of Ce(IV). After curing at 120°C, the coating remained colorless and not yellow as GTS-Ce coating. Although both coatings (GTS-Ce and GTS-Ce+GTS) contain GTS-Ce as an inner layer (Fig. 2a), the difference between two coatings arises from the curing procedure. Namely, whilst GTS-Ce coating was finally cured for 1 h at 120°C where oxidation of Ce^{3+} to Ce^{4+} can take place, in the case of GTS-Ce+GTS coating the final curing does not affect the underlying GTS-Ce layer and Ce remained mainly as colorless Ce^{3+}. Intermediate drying for 3 min at 100°C was not sufficient to produce significant amount of Ce^{4+} species.

Corrosion behavior of unscribed coatings in nacl solution.—*Electrochemical impedance analysis.*—EIS as a non-destructive method was used to in situ follow the electrochemical properties of the uncoated and coated substrates. The magnitudes of the impedance, $|Z|$, and the phase angle, ϕ, as a function of the frequency, f, (Bode plots) for uncoated and variously coated AA7075-T6 substrates are presented for different immersion time up to 25 days (Fig. 4). The uncoated AA7075-T6 sample shows an EIS spectrum (Figs. 4a, 4b) typical of pitting corrosion, as described by Mansfeld and Wang,[47] i.e. transmission line type impedance and a minimum in the phase angle at lower frequencies. The plot of $|Z|$ vs. f shows transmission at frequencies of 10^1 to 10^0, depending on the immersion time (Fig. 4a). With prolonged immersion the transition shifted to lower frequencies and the impedance increased within one order of magnitude. This may be related to the gradual formation of an oxide layer during the course of immersion which offers a certain degree of protection. In consequence, the maximum of the ϕ vs. f plot shifted to lower frequencies (Fig. 4b) and the phase angle at the lowest frequencies increased.

Coated substrates showed different Bode plots from those of uncoated substrate. The results are interpreted qualitatively in accordance with the modelling of physicochemical processes reported for aluminum alloys coated with hybrid sol-gel coatings incorporating $Ce(NO_3)_3$.[31,48–50] In general, in Bode plots of $|Z|$ vs. f three distinct regions are evident: high frequency range related to the outer part of the coating at the coating/electrolyte interface, intermediate frequency range related to the inner part of the coating and intermediate oxide-based layer formed between Al substrate and sol-gel coating (natural aluminum oxide layer Al−O−Al and Al−O−Si bonds[51] at the substrate/coating interface), and low frequency range related to corrosion process at the inner metal/sol-gel coating interface. During immersion, the pore resistance of the coating as well as the resistance of the intermediate oxide layer are important for compactness of the interface between the substrate and sol-gel coating. Stable and dense interface prevents the formation of conductive pathways and electrolyte ingress to the substrate. This process then leads to the local corrosion process expressed by the double layer capacitance and charge transfer resistance at the low frequency side.

On the immersion, two time constants are present in Bode plots for the GTS coating, at high frequency of 10^5 Hz and intermediate frequency of 1 Hz (Figs. 4c, 4d), related to the sol-gel coating and intermediate oxide layer. Coatings shows some barrier effect evidenced by increased Z in the low frequency range. After 2 days of immersion, a low frequency resistive part appeared, as reflected in the progressive decrease in impedance, probably related to the cracks formed in the intermediate oxide layer that allow ingress of electrolyte. In the ϕ vs. f plot, signs of corrosion at the inner substrate/coating interface (low frequency) were visible at the same time (Fig. 4d). On the high frequency side, reflecting the coating capacitance, the value of ϕ also decreased, indicating deterioration of the coating that progressed further at longer immersion times.

Similar to GTS, the GTS-Ce coating (Figs. 4e, 4f) also shows barrier protection. However, at the low frequency part (inner interface substrate/coating) the resistive part was smaller, and the ϕ vs. f plot showed that the ϕ values were initially much lower, indicating lower

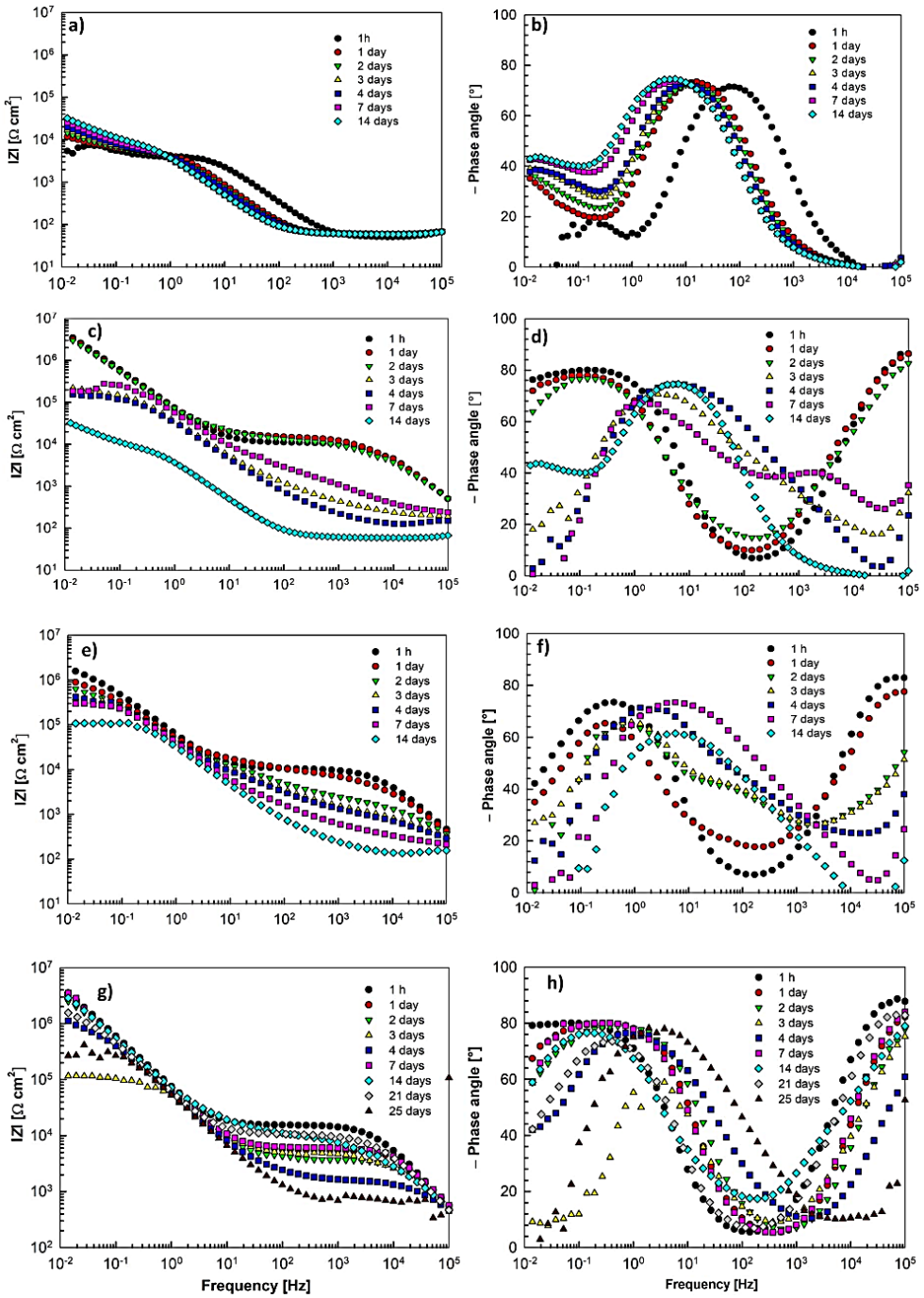


Figure 4. Bode plots of magnitude of impedance and phase angle recorded after various immersion times in 0.1 mol/L NaCl (from 1 h to 25 days) for (a, b) uncoated AA7075-T6, and for AA7075-T6 coated with (c, d) GTS, (e, f) GTS-Ce, and (g, h) GTS-Ce+GTS coatings.

stability of this coating. This may be related to the incorporation of Ce which may destabilize the structure of the coating[46] and/or to progressive release of cerium from the coating which, at the same time, leaves the porous structure underseath susceptible to corrosion.

Finally, the GTS-Ce+GTS coating exhibited behavior that can be attributed to barrier effect and self-healing. Namely, on immersion and up to the following 3 days, trend in the $|Z|$ vs. f plot (Fig. 4g) was similar to that for the GTS coating, i.e. progressive appearance of resistive behavior at low and intermediate frequencies. However, the values of ϕ were high, around $-80°$, in both high and low frequency regions, indicating stability of the coating (Fig. 4h). After 4 days, the impedance at low frequencies started to increase again, and the values of ϕ at the maximum were high and remained so at low frequencies, which may be ascribed to high charge transfer resistance of Ce-containing multilayer coating.[50] Only after 25 days were signs of corrosion noted — Z at low frequency decreased (Fig. 4g) and ϕ values formed a peak with low values on both low and high frequency sides (Fig. 4h).[48,49]

The impedance value determined at 0.01 Hz in the Bode plot of modulus of impedance vs. frequency was chosen as the parameter representing the corrosion resistance of the coating.[52] Values of $Z_{0.01\ Hz}$ as a function of immersion time are presented for uncoated and coated samples (Fig. 5). The $Z_{0.01\ Hz}$ value of uncoated sample AA7075-T6 gradually increased with time over the first 14 days for approximately one order of magnitude, reaching $2{\cdot}10^4\ \Omega\ cm^2$. The uncoated AA7075-T6 surface is in direct contact with the electrolyte solution and becomes covered by an oxide that gradually forms and acts protectively for a certain period of time.[53] On immersion, the $Z_{0.01\ Hz}$ value of the GTS coated substrate was larger, by more than two orders of magnitude ($Z_{0.01\ Hz} = 4{\cdot}10^6\ \Omega\ cm^2$), than that of the uncoated sample, confirming the barrier protective properties of the coating. After 3 days of immersion the $Z_{0.01\ Hz}$ values decreased gradually, which may be the result of the porous nature of the coating and the diffusion of the chloride anions into the coating where they interact with the substrate. Z values of the GTS-Ce coated sample were, at the beginning of immersion, similar to those of the GTS coating ($1.5{\cdot}10^6\ \Omega\ cm^2$). After 1 day of immersion, however, the value of $Z_{0.01\ Hz}$ decreased, indicating that the almost all cerium was released from the

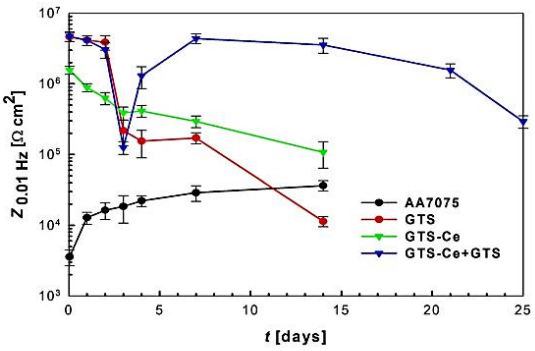


Figure 5. Values of $Z_{0.01\ Hz}$ (impedance at 0.01 Hz determined from Bode plots, Fig. 4) for uncoated and variously coated AA7075-T6 as a function of immersion time in 0.1 mol/L NaCl.

coating. At immersion times longer than 14 days, uncoated and GTS and GTS-Ce coated samples deteriorated but the latter coating still showed higher impedance indicating beneficial effect of Ce addition.

The trend of the $Z_{0.01\ Hz}$ value of the GTS-Ce+GTS coating, however, was different. At the beginning of immersion the value of Z was large, similar to that for the GTS coating ($4{\cdot}10^6\ \Omega\ cm^2$). After 3 days of immersion it was reduced to $10^5\ \Omega\ cm^2$. After 4 days of immersion, however, it again increased, almost to its initial value of $2{\cdot}10^6\ \Omega\ cm^2$ and remained stable for up to 21 days of immersion. After 25 days of immersion, the value of $Z_{0.01\ Hz}$ decreased to $2{\cdot}10^5\ \Omega\ cm^2$ but remained larger compared to other two coatings.

Immersion testing.—The lifespan of differently coated AA7075-T6 samples was followed using the NACE TMO 169/631 immersion test in 0.1 mol/L NaCl for up to 80 days (Fig. 6). Pitting and galvanic corrosion of an uncoated sample was visible after 1 day of immersion. Corrosion of a GTS coating was visible on the borders after

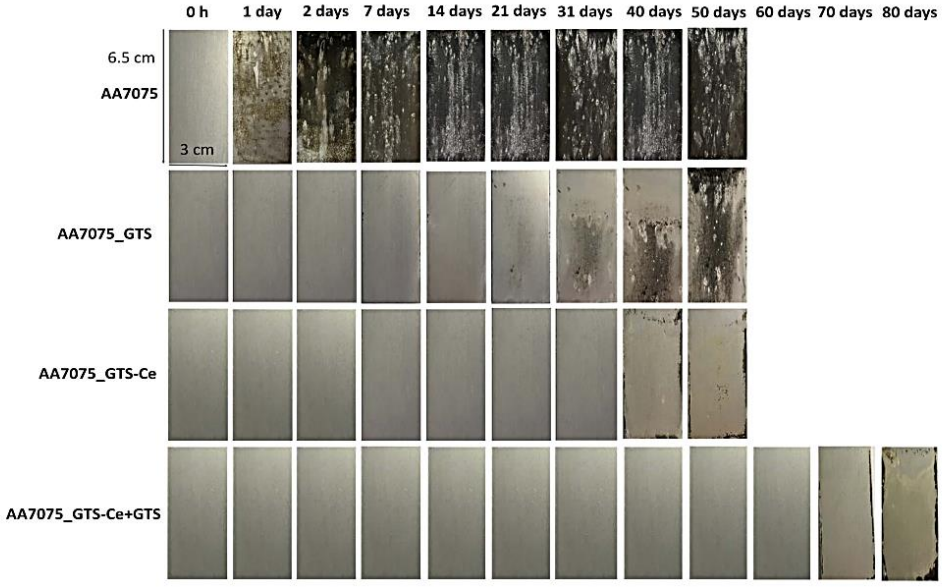


Figure 6. Images of uncoated AA7075-T6 and AA7075-T6 with GTS, GTS-Ce and GTS-Ce+GTS coatings during an immersion test in 0.1 mol/L NaCl at room temperature. Images were taken after different times of immersion up to 80 days (NACE TMO 169/631 immersion test).

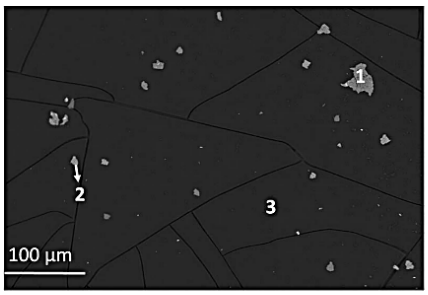


Figure 7. SEM image of AA7075-T6 coated with GTS-Ce+GTS after 4 days of immersion in 0.1 mol/L NaCl. The numbers 1, 2 and 3 on the SEM image denote locations where EDS analysis was carried out (given in Supplement materials as Fig. S1). The SEM image was taken in compositional mode.

7 days and was spread throughout the surface after 21 days. The corrosion resistance of the GTS coating is the result of its good barrier properties.[43] The GTS-Ce coating remained undamaged for 40 days of immersion, which may the result of the active corrosion inhibition caused by cerium. The longest period of resistance to corrosion was observed for samples coated with a GTS-Ce+GTS coating which remained virtually undamaged up to 70 days of immersion, at which point corrosion was observed on the borders. Based on EIS results (Figs. 4, 5) and immersion test (Fig. 6), an efficient protection is observed to GTS-Ce+GTS coating. Thus, even when some pits were formed during 70 days of immersion, they were healed by the action of cerium ions.

SEM/EDS analyses.—To study the role of cerium in the self-healing effect in more detail, AA7075-T6 prepared with a GTS-Ce+GTS coating was immersed for 4 days in 0.1 mol/L NaCl. Samples were then inspected using SEM/EDS (Fig. 7 and Fig. S1). After immersion, numerous bright deposits were shown to be present at the surface. Since images were recorded in compositional mode, the brightness is related to atomic mass. These bright deposits (Fig. 7) contained cerium and oxygen (Fig. S1, spectra at locations 1 and 2), indicating the formation of cerium hydroxide or oxide. In addition to Ce and O, Si was detected as a major element of the surrounding coating. It is known that the deposition of Ce-oxides proceeds at the cathodic sites at the surface which are, in the case of AA7075-T6, Cu-containing intermetallic particles (IMPs).[54–59] The fact that no Cu could be identified at the intermetallic particles proves that the deposits of Ce hydroxide/oxide are thicker than is the EDS analysis depth, i.e. several micrometers. At the surrounding surface, where no

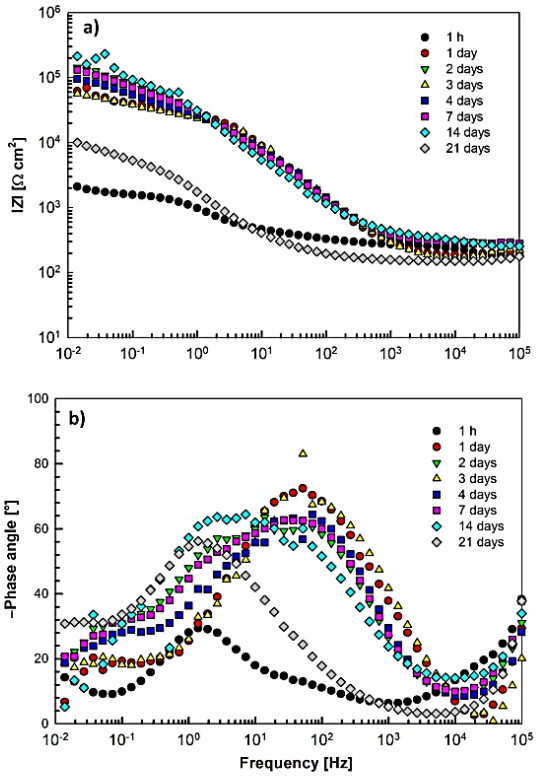


Figure 9. Bode plots of the magnitude of (a) impedance and (b) phase angle for a scribed GTS-Ce+GTS coating deposited on AA7075-T6 after various immersion times in 0.1 mol/L NaCl.

bright deposits were formed, no Ce was detected (or the deposits were too thin to be detected by EDS) but only Si and O (Fig. S1, location 3). The presence of Ce in the deposits indicates that it was concentrated at particular sites at the surface, presumably at IMPs which are sites where cathodic reduction of oxygen proceeds and leads to release of hydroxyl ions and consequent increase in pH; a local pH increase to about 8.5 enables the precipitation of cerium oxide and /or hydroxide.[26,27,36]

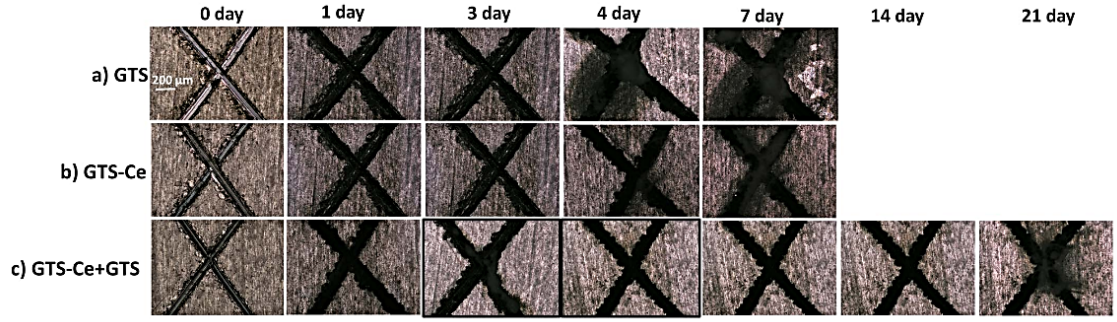


Figure 8. Optical microscope images of the cross shaped scribe on AA7075-T6 coated with (a) GTS, GTS-Ce and (c) GTS-Ce+GTS coatings after various immersion times in 0.1 mol/L NaCl. The depth of the scribe (~7 µm) was larger than the coating depth. The scale 200 µm (a, 0 day) is the same for all presented images.

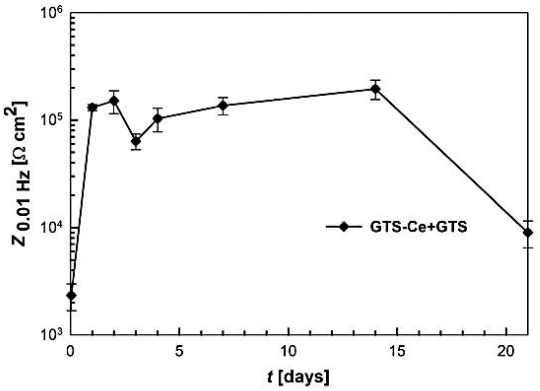


Figure 10. The impedance at 0.01 Hz, determined from Bode plots, of the magnitude of impedance vs. frequency recorded for a scribed GTS-Ce+GTS coating deposited on AA7075-T6 after various immersion times in 0.1 mol/L NaCl.

Corrosion behavior of scribed coatings in nacl solution.—The self-healing property of the coatings was addressed directly, using a cross-shaped scribe made at the surface. Scribe simulates the damage on/inside the coating, First, set of experiments was performed on GTS, GTS-Ce and GTS-Ce+GTS coatings scribed throughout the coating with a depth of 7.5 ± 0.4 μm, as determined by the profilometer. Self-healing ability was evaluated following immersion in 0.1 mol/L NaCl for up to 21 days. The propagation of the corrosion damage and self-healing process was monitored using optical microscope images of the scribe (Fig. 8). Secondly, EIS, SEM/EDS and XPS analyses were carried out at the scribed GTS-Ce+GTS coating (Figs. 9–17).

Immersion testing.—Corrosion on GTS and GTS-Ce at the scribe started after 4 days of immersion and spread over the surface (Figs. 8a, 8b). The width of the scribe on the GTS-Ce+GTS coating increased over 3 days of immersion and some corrosion products were observed (Fig. 8c). However, after 4 days of immersion the width of the scribe was diminished, indicating self-healing of the damage zone. Corrosion of the GTS-Ce+GTS coating was visible only after 21 days of immersion. Based on the obtained results, further study of the self-healing effect was concentrated on the GTS-Ce+GTS coating as GTS and GTS-Ce coatings did not show evidence of self-healing ability.

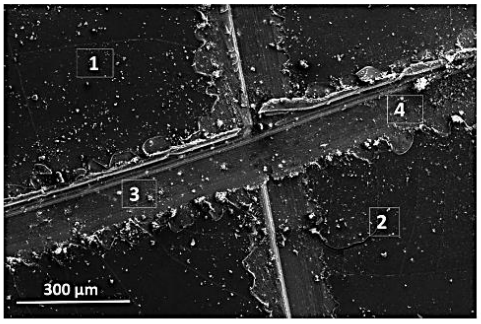


Figure 11. SEM/EDS analysis of the cross-shaped scribe on coating GTS-Ce+GTS, applied on AA7075-T6, after 4 days of immersion in 0.1 mol/L NaCl. The numbers 1–4 denote locations where EDS was carried out (Table II). The depth of the scribe (~7 μm) was larger than the coating depth.

Electrochemical impedance analysis.—The corrosion properties of scribed GTS-Ce+GTS coatings were followed in situ during 21 days immersion in 0.1 mol/L NaCl using EIS. The dependence of the magnitude of impedance and phase angle on the frequency (Bode plots) after different immersion times is shown in Fig. 9. The corrosion resistance is represented by the values of the magnitude of the impedance determined at 0.01 Hz as a function of immersion time (Fig. 10). The shape of EIS spectra changed with increasing time of immersion. The most significant changes took place within 1 day of immersion, confirming improved corrosion resistance and an increase in $Z_{0.01\ Hz}$ value by more than one order of magnitude. With increasing immersion time up to 4 days the impedance plot changed to a more capacitive shape, with a pronounced linear range at the intermediate frequencies (Fig. 9a). At the same time the phase angle plot changed from that centered at intermediate frequencies to a plateau at the low frequencies (Fig. 9b). After 4 days immersion, a broad plateau extending up to 1 Hz is formed (Fig. 9a), reaching a phase angle of −70°

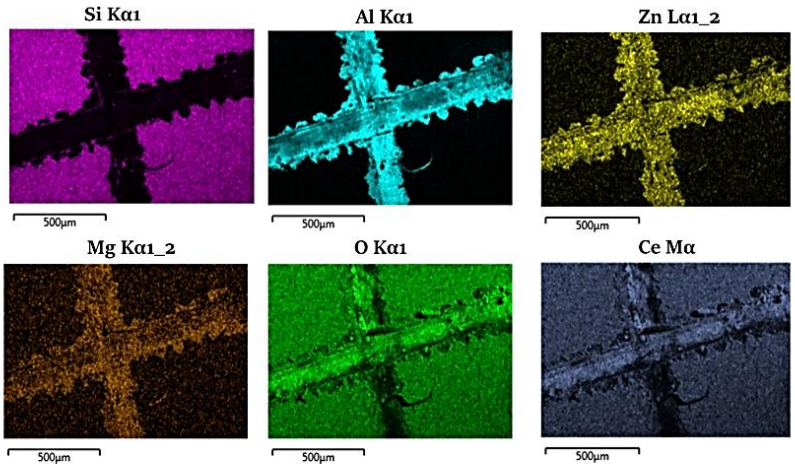


Figure 12. EDS mapping of cross-shaped scribed on GTS-Ce+GTS coating deposited on AA7075-T6 after 4 days of immersion in 0.1 mol/L NaCl (SEM image on Fig. 11). The depth of the scribe (~7 μm) was larger than the coating depth.

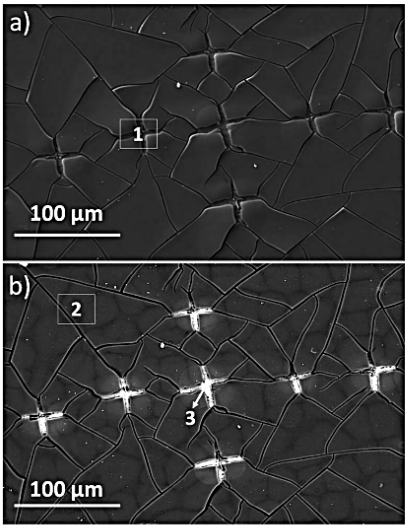


Figure 13. SEM images of cross-shaped Vicker's indents on a GTS-Ce+GTS coating deposited on AA7075-T6: (a) as-prepared, and (b) after being exposed to 0.1 mol/L NaCl for 4 days. The numbers 1–3 denote locations where EDS spectra were recorded (given in Supplement material as Fig. S2). The depth of the scribe (~2–4 µm) was smaller than the coating depth but the indentations induced cracks.

(Fig. 9b). Spectra remained similar up to 14 days but, at longer immersion times, the beginning of dissolution is observed as a progressive reduction of $|Z|$ and ϕ at the low frequency side.

The value of $Z_{0.01\,Hz}$ of the scribed GTS-Ce+GTS coating increased gradually from $2{\cdot}10^3$ Ω cm^2 to 10^5 Ω cm^2 in the first 2 days (Fig. 10). After 3 days, a small drop in the value of $Z_{0.01\,Hz}$ was observed ($6{\cdot}10^4$ Ω cm^2), indicating that the corrosion process had commenced. After 4 days, however, the $Z_{0.01\,Hz}$ value regained its previous value (10^5 Ω cm^2) and then remained stable up to 14 days of immersion, confirming the healing of the scribed damage. After 21 days of immersion it again dropped to a smaller value ($9{\cdot}10^3$ Ω cm^2), indicating that the corrosion process proceeded gradually.

SEM/EDS and XPS analyses.—SEM analysis of the scribed zone after 4 days of immersion in 0.1 mol/L NaCl is presented in Fig. 11 accompanied by EDS analysis at locations 1–4 (Table II). Cerium was deposited on the surface at locations 1 and 2 and also within the scribe, at locations 3 and 4. Therefore, self-healing of the damage site observed during immersion is related to the deposition of cerium.

The presence of Ce was additionally corroborated using EDS mapping of the cross-shaped scribe (Fig. 12). Silicon and oxygen, the main components of the coatings, were detected only outside the scribe, since the coating was removed at the scribe. Aluminum and the alloying elements zinc and magnesium were identified within the scribe. Oxygen is also detected in the scribe associated with Al and Ce oxide/hydroxides formed during immersion. Finally, cerium was observed outside and inside the scribe, although in higher concentration in the latter site. This results evidences that the migration of Ce from the interior layer of the coating occurred and results in the deposition of Ce compound, not only on the surface, but also on the damaged area.

Second set of experiments was carried out on GTS-Ce+GTS sample scribe damaged within the coating, i.e. at indentations 2 to 4 µm deep, without reaching the underlying substrate. However, the indentation procedure itself damaged the coating and induced cracks (Fig. 13a) although the depth of indents did not reach the substrate, as evident by EDS spectrum (Fig. S2, spectrum 1) showing only Si. No such cracks were observed when using diamond blade (Fig. 11). The sample was then again immersed in 0.1 mol/L NaCl for 4 days and analyzed by SEM (Fig. 13b) and EDS at labelled positions (Fig. S2, spectra 2 and 3). Cerium was deposited mainly within the scribed

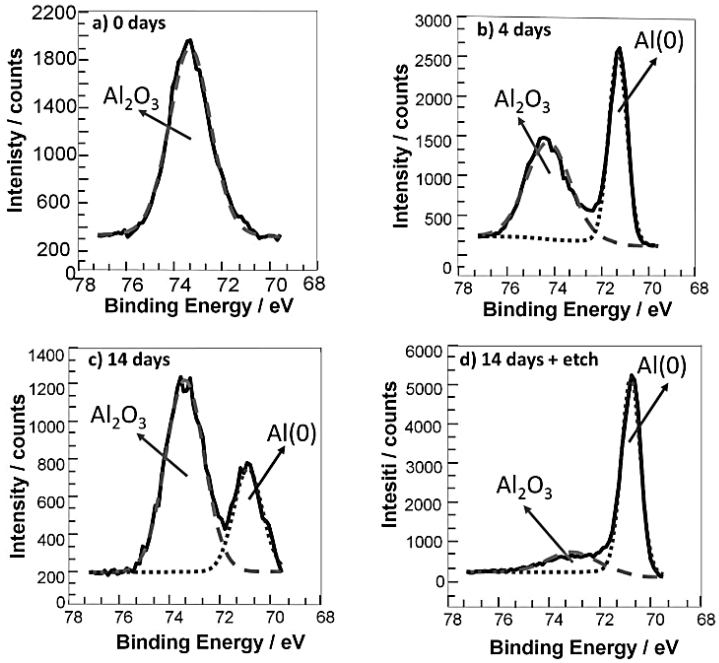


Figure 14. High resolution XPS Al 2p spectra recorded within a cross-shaped scribe on a GTS-Ce+GTS coating on AA7075-T6, before after 4 and 14 days immersion in 0.1 mol/L NaCl. After 14 days immersion the layer was etched using Ar^+ to reveal cerium deposits buried under aluminum oxide layer. Intensity of individual component peaks (expressed as%) is given in Table III. Solid curve denotes experimental data, and dashed and dotted curves are curve fitted component peaks.

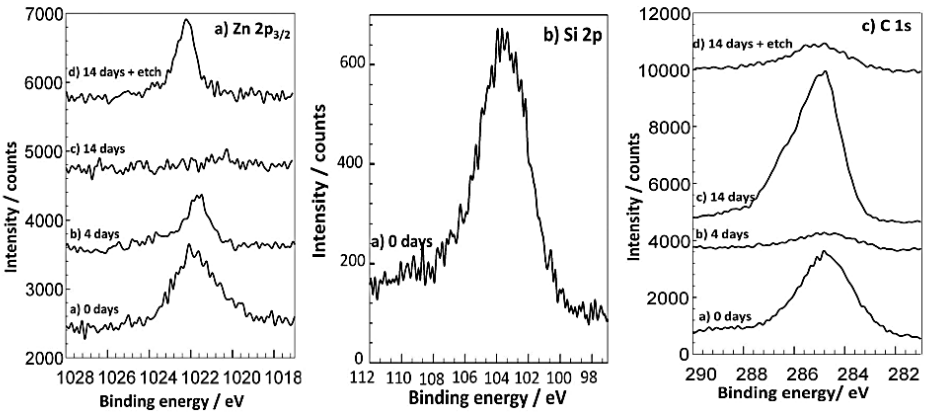


Figure 15. Non-normalized high resolution XPS (a) Zn $2p_{3/2}$, (b) Si 2p and (c) C 1 s spectra recorded within a cross-shaped scribe on a GTS-Ce+GTS coating on AA7075-T6, before and after 4 and 14 days immersion in 0.1 mol/L NaCl. After 14 days immersion the layer was etched using Ar^+ to reveal cerium deposits buried under aluminum oxide layer.

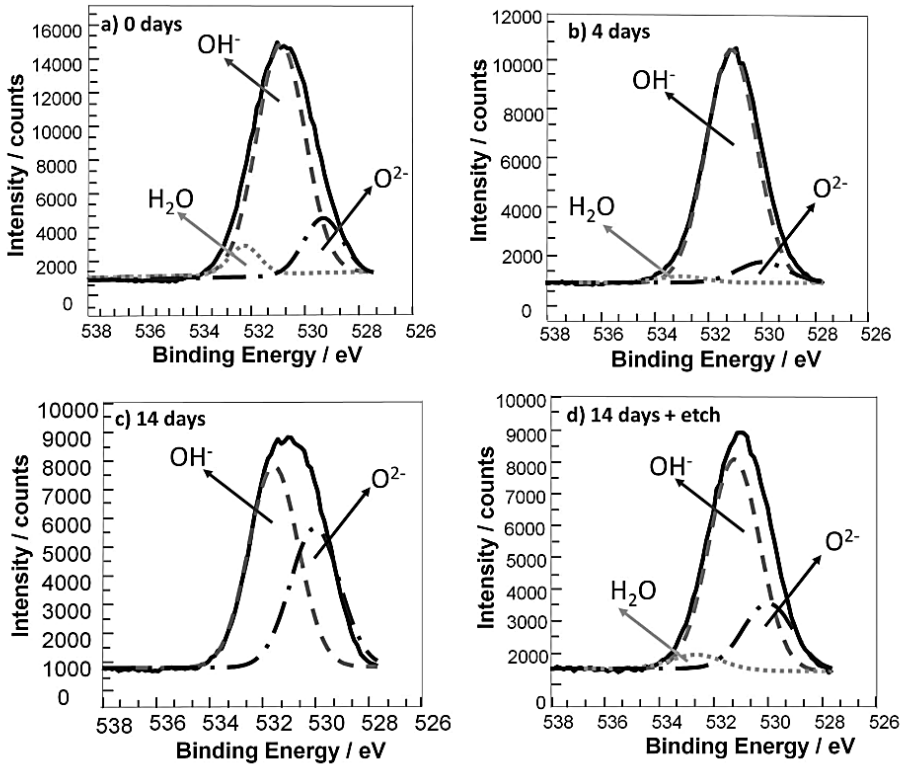


Figure 16. High resolution XPS O 1 s spectra recorded within a cross-shaped scribe on a GTS-Ce+GTS coating on AA7075-T6, before, and after 4 and 14 days immersion in 0.1 mol/L NaCl. After 14 days immersion the layer was etched using Ar^+ to reveal cerium deposits buried under aluminum oxide layer. Intensity of individual component peaks (expressed as %) is given in Table III. Solid curve denotes experimental data, and dashed and dotted curves are curve fitted component peaks.

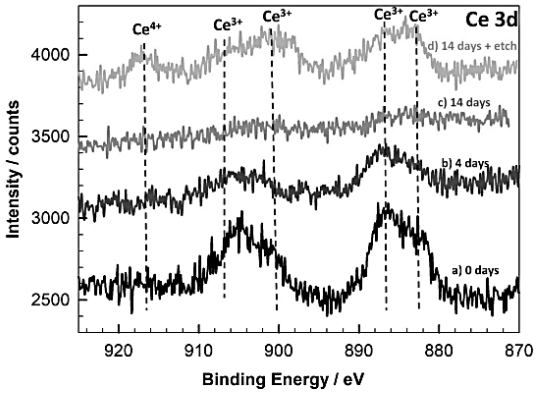


Figure 17. Non-normalized high resolution XPS Ce 3d spectra recorded within a cross-shaped scribe on a GTS-Ce+GTS coating on AA7075-T6, before, after 4 and 14 days of immersion in 0.1 mol/L NaCl. After 14 days immersion the layer was etched using Ar^+ to reveal cerium deposits buried under aluminum oxide layer.

area (label 3), while it was not detected out of the indents (label 2). Cerium had obviously migrated from the underlying coating and was deposited at damage sites after 4 days of immersion.

Therefore, in both cases – when scribed through the coating depth to reach the underlying substrate, or within the coating depth, the GTS-Ce+GTS coating was able to recover at damage site by the deposition of Ce-containing compound. However, the cracks induced by indentation propagate further during long-term immersion in NaCl (Fig. 13b) resulting in the observed cracking pattern. Therefore, indentation technique may be used as a complementary technique but that it may be more appropriate to use scribing procedure which does not induce damage (e.g. diamond blade).

In order to complement the EDS results and to study the oxidation state of Ce and elements of underlying substrate, XPS analysis was explored. The XPS spectra were recorded prior the immersion, and after 4 and 14 days of immersion in NaCl (Figs. 14–17). The diameter of XPS analysis is approximately 400 μm, i.e. similar to the diameter of the scribe. Therefore, the analysis identifies the elements coming from substrate (i.e. within the scribe) and the coating remnants (after being removed by diamond tip). The following elements were identified: Al and Zn originating from the substrate, O originating from the substrate and coating, and Si, C, and Ce related to the coating. Al 2p and O 1 s spectra were curve fitted, whilst Si 2p, Zn 2p, C 1 s and Ce 3d were described only qualitatively.

First, composition of surface prior immersion in NaCl will be discussed. Aluminum can originate from metal (71.0–71.5 eV) and aluminum oxide (74.6–74.8 eV) (Table III). A separate peak denoting the bonding between Al and Si, Al−O−Si, related to covalent silane-metal bonding[51] (73.2–73.6 eV) was not taken into account herein as we are concentrated on the processes within the scribe. Upon removal

Table II. Concentrations of elements obtained by EDS analysis at different locations on the cross shaped scribe on GTS-Ce+GTS coating deposited on AA7075-T6 after 4 days of immersion in 0.1 mol/L NaCl (locations 1–4) (SEM images in Fig. 11).

Location	Al [at.%]	O [at.%]	Si [at.%]	Zn [at.%]	Cu [at.%]	Ce [at.%]
1	70.9	23.8	7.9	1.9	/	0.1
2	60.3	34.8	3.0	4.2	1.7	0.1
3	70.4	21.7	1.7	5.2	1.0	0.3
4	62.4	25.6	2.8	6.7	2.2	0.2

Table III. Intensity of individual component peaks (expressed as %) obtained by curve fitting of XPS Al 2p (Al metal and Al_2O_3, Fig. 14) and O 1 s spectra (O^{2-}, OH^- and H_2O peaks, Fig. 16) recorded within scribe in GTS-Ce+GTS coating on AA7075-T6 before and after 4 and 14 days immersion in 0.1 mol/L NaCl. After 14 days, surface was etched to remove the oxide layer.

Immersion time	Al [%]	Al_2O_3 [%]	O^{2-} [%]	OH^- [%]	H_2O [%]
0	0	100.0	14.8	80.0	6.2
4 days	45.2	54.8	7.7	90.2	2.1
14 days	28.5	71.5	37.7	62.3	0
14 days and etching	78.4	21.6	21.0	75.2	3.8

of sol-gel coating within the scribe, Al oxide forms spontaneously. Therefore, prior immersion, only Al oxide is identified within the scribe (Fig. 14a, Table III). A small amount of zinc is also detected originating from the AA7075-T6 substrate (Fig. 15a). The center of the Zn $2p_{3/2}$ peak is located at 1022.5 eV. XPS Zn 2p spectrum cannot allow an exact differentiation between Zn metal and ZnO due to small chemical shift of only 0.9 eV.[60] Instead, Zn LMM spectra should be used for this purpose but due to a small amount of Zn such analysis would be ambiguous. Silicon originates from the coating. The Si 2p peak is centered at 103.7 eV (Fig. 15b). This peak could be comprised of several component peaks: Si−OH, Si−O−Si and Si−O−Al.[51] Carbon C1s peak is centered at 284.8 eV and relates to adventitious carbon and aliphatic carbon (C−C) present in the coating (Fig. 15c). However, the peak is quite broad which may be related to the presence of (C−O) bonds at 286.5 eV in the coating structure, as proposed also based on FTIR spectra.[43] More detailed analysis of Si 2p and C 1 s peaks is beyond the scope of this study and requires NMR analysis.

The O 1 s spectra can be separated into three component peaks: oxide, O^{2-}, at approx. 530 eV, hydroxide, OH^-, at approx. 531 eV, and water, H_2O, at approx. 533 eV (Fig. 16a).[50,61] Deconvolution of the peak shows that the native layer is composed mostly of hydroxide (Table III).

Prior immersion, four main peaks were observed in the Ce 3d spectrum, at 882.6, 886.6, 901.8 and 905.1 eV (Fig. 17). The XPS 3d spectra of cerium compounds show a complex satellite structures derived mainly from ligand to metal charge transfer transitions, i.e. O 2p → 4f transitions.[62] The Ce spectrum of Ce(III) compound is composed of four peaks corresponding to two spin-orbit features at 880.9, 885.5, 899.1 and 903.4 eV.[62] The spectrum of Ce(IV) compound is composed of six peaks corresponding to three spin-orbit features at 882.7, 886.6, 898.3, 901.3, 907.3 and 916.7 eV. It appears that prior immersion cerium is present primarily in the Ce(III) oxidation state, although some peaks may indicate the presence of small amount Ce(IV) state (i.e. at E_b higher than 905 eV). It should be noted that the concentration of Ce in sols GTS-Ce+GTS coating is very low (0.05 mol/L). Consequently, the concentration in the coating is also low, as evidenced by weak signal which is poorly defined. After 4 days of immersion the metal Al peak appears in the spectra (Fig. 14b), indicating that in the course of immersion Al oxide may be dissolved exposing Al metal. The intensities of Zn and C peaks decreased, and the Si peak disappeared, probably due to the coverage by deposited Ce-based layer. (Fig. 15). The O 1 s spectrum is still mainly composed of hydroxide contribution (Fig. 16b, Table III). The presence of tetravalent cerium may be indicated by the peak at 916.7 eV which distinguishes Ce(III) and Ce(IV) compounds (Fig. 17).[62] Taking into account that two types of oxide/hydroxide are formed (Al- and Ce-based), oxygen peak could be curve fitted by additional OH^- and/or O^{2-} component, as proposed previously.[50,63] Further study using well prepared standards would be required to corroborate further differentiation between two components.

After 14 days of immersion, however, cerium was not identified within the scribe (Fig. 17). This may be the consequence of progressive formation of an aluminum oxide film within the scribe in the course of prolonged immersion in 0.1 mol/L NaCl (Fig. 14c, Table III). At

the same time, Zn signal disappeared, and that of C 1 significantly increased which may be related to precipitation of coating remnants within the scribe (Fig. 15c). As the analysis diameter is similar to scribe diameter it is difficult to differentiate the origin of the signal (i.e. from scribe or surrounding coating remnants). It seems certain, however, that formation of Al oxide covered the underlying cerium oxide deposits. This was proved using Ar^+ etching which removed approximately 26 nm of Al oxide layer (Fig. 17). After etching, cerium was again detected within the scribe showing the characteristic peak of Ce(IV) at 916.7 eV thus proving that Ce(III) is oxidized to Ce(IV) species. The Al_2O_3 peak disappeared and that of Al and Zn metals increased (Figs. 14d, 15a).

Proposed mechanism of cerium inhibition and self-healing in GTS-Ce+GTS coatings.—The proposed self-healing mechanism and the role of Ce ions in the self-healing effect in the GTS-Ce+GTS coating can be summarized as follows. During immersion in aerated NaCl, Ce^{3+} ions from the underlying GTS-Ce coating can oxidize to Ce^{4+} through different pathways, assisted by O_2 or H_2O_2.[16,28] SEM/EDS and XPS analyses have confirmed that deposition of cerium within the cross-shaped scribe increased after 4 days' immersion. The oxidation state of cerium changes from mainly Ce(III) to Ce(IV). This process takes place at the substrate/electrolyte interface, i.e. within the coating. As the self-healing experiments were carried out at the scribe exposed to electrolyte, during the course of immersion the formation of aluminum oxide takes place as well which then covers the cerium oxide deposits underneath.

The self-healing ability may be achieved by the migration of $Ce(OH)_2^{2+}$ to local damaged regions where these ions precipitate as $Ce(OH)_4$ and CeO_2, which are highly insoluble.[16,28,36] According to thermodynamic calculations by Yasakau et al., $Ce(OH)_2^{2+}$ are stable only at pH below 3, thus their presence at neutral and slightly alkaline pH may be questionable.[36] However, results obtained in the present study show that the migration of Ce ions takes place as the healing of corrosion damage site is noticed. The exact speciation of migrating species could not be confirmed despite using different analytical techniques (XPS, EDS). In the literature the exact nature of migrating species has not been yet proven; this issue remains to be investigated further. The self-healing cycle can be repeated as long as Ce^{3+} are present in the coating.[33] It was proposed that the Ce^{3+}/Ce^{4+} redox reaction is dynamic, and proceeds readily in both directions.[59] According to results obtained using SEM/EDS, XPS and EIS, the self-healing effect of the GTS-Ce+GTS coating is operative, even after 14 days of immersion in NaCl solution, because of the presence of Ce^{3+} ions in the coating. Under these conditions the repetitive cycle of (i) Ce^{3+} to Ce^{4+} oxidation, (ii) $Ce(OH)_2^{2+}$ migration to damaged site, and (iii) transformation $Ce(OH)_2^{2+}$ to $Ce(OH)_4$ can continue.[50] The final step in the mechanism is the formation of insoluble CeO_2 at cathodic sites, providing additional hindering of the corrosion process.[35]

At a longer immersion time (21 days), the magnitude of impedance decreased, indicating diminished self-healing ability. However, the overall coating stability was still much higher than that of the coating without cerium (GTS), or in the case of GTS-Ce (Fig. 5).

Conclusions

1. Three types of sol-gel coatings prepared based on TEOS, GPTMS, SiO_2 and $Ce(NO_3)_3$ and applied on AA7075-T6 substrates. This was done in order to produce a coating which would exhibit a self-healing ability in chloride environment. Although all three coatings (GTS, GTS-Ce and GTS-Ce+GTS) improved the corrosion resistance of the substrate during 80 days immersion in NaCl, only the GTS-Ce+GTS coating containing cerium in the inner layer showed the self-healing properties. The GTS coating provides only barrier protection. GTS-Ce coating may be destabilized either due to the modified structure of the coatings due to incorporation of Ce, or due to progressive outward leaching of cerium which limits its role in the self-heling activity. Locking of Ce in the inner layer inhibits the destabilization of the coating and prolong its activity in the self-healing process.
2. Active role of cerium in the inhibition process was proved by long-term EIS measurements and immersion test on unscribed and scribed coatings. Self-healing of the GTS-Ce+GTS coating starts after 4 days of immersion in 0.1 mol/L NaCl. After an initial decrease, the impedance at low frequency increased by more than one order of magnitude proving the self-healing process. It is thus demonstrated that the migration of cerium ions occurred. Cerium is deposited on the alloy surface and within the cross-shaped scribe, in the form of hydroxide. The latter insoluble compound reduces the kinetics of the cathodic reaction and contributes to self-healing of the coating.
3. Although gradually transformed into Ce(IV) hydroxide, both oxidation states (Ce(III) and Ce(IV)) were identified, even after 14 days of immersion, indicating that the self-healing process was still operative.
4. All systems in the present work were found to have promising applications and could be regarded as potential replacements for hazardous chromate conversion coatings.
5. Future study will focus on the compatibility of these coatings with organic top coatings, e.g. adhesion and the corrosion performance of such full systems.

Acknowledgments

The authors acknowledge the financial support from the Slovenian Research Agency (research core funding No. P2-0393 and the project "Lightweight alloys based on aluminum as materials with increasing potential in the transportation industry", ID J1-6734). U. Tiringer acknowledges an Ad Futura scholarship for financing her stay at the CSIC. The authors thank dr. A. Drnovšek for SEM/EDS analysis, dr. J. Kovač for valuable discussion of XPS data, T. Filipič, MSc, for spectra acquisition, dr. P. Panjan for help in making Vicker´s indents at coated samples and Prof. R.H. Pain for proof reading the manuscript.

ORCID

Ingrid Milošev https://orcid.org/0000-0002-7633-9954

References

1. C. Vargel, *Corrosion of aluminum*, 1st. ed., Elsevier, Amsterdam, The Netherlands, (2004).
2. J. R. Davis, *Corrosion of aluminum and aluminum alloys*, ASM International, United States of America, (1999).
3. G. Kufman, *Introduction to aluminum alloys and tempers*, 1st. ed., ASM International, United States of America, (2000).
4. *CMCA(UK)* (2017) https://www.cmcauk.co.uk/reach-authorisation-list-update-imminent-sunset-dates/.
5. M. W. Kendig and R. G. Buchheit, *CORROSION*, **59**, 379 (2003).
6. J. W. Bibber, *Met. Finish.*, **99**, 15 (2001).
7. T. P. Chou, C. Chandrasekaran, and G. Z. Cao, *J. Sol-Gel Sci. Technol.*, **26**, 321 (2003).
8. R. B. Figueira, C. J. R. Silva, and E. V. Pereira, *J. Coat. Technol. Res.*, **12**, 1 (2014).
9. I. Milošev, B. Kapun, P. Rodič, and J. Iskra, *J. Sol-Gel Sci. Technol.*, **74**, 447 (2015).
10. R. L. Twite and G. P. Bierwagen, *Prog. Org. Coat.*, **33**, 91 (1998).
11. S. Zheng and J. Li, *J. Sol-Gel Sci. Technol.*, **54**, 174 (2010).
12. J. Wen and G. L. Wilkes, *Chem. Mater.*, **8**, 1667 (1996).
13. N. Pirhady Tavandashti, S. Sanjabi, and T. Shahrabi, *Mater. Corros.*, **62**, 411 (2011).
14. G. Schottner, *Chem. Mater.*, **13**, 3422 (2001).
15. M. L. Zheludkevich, I. M. Salvado, and M. G. S. Ferreira, *J. Mater. Chem.*, **15**, 5099 (2005).
16. I. Santana, A. Pepe, E. Jimenez-Pique, S. Pellice, I. Milošev, and S. Ceré, *Surf. Coat. Technol.*, **265**, 106 (2015).
17. A. J. Vreugdenhil, V. N. Balbyshev, and M. S. Donley, *J. Coat. Technol.*, **73**, 35.
18. R. N. Peres, E. S. F. Cardoso, M. F. Montemor, H. G. de Melo, A. V. Benedetti, and P. H. Suegama, *Surf. Coat. Technol.*, **303**, Part B, 372 (2016).
19. A. Durán, Y. Castro, M. Aparicio, A. Conde, and J. J. de Damborenea, *Int. Mater. Rev.*, **52**, 175 (2007).
20. N. N Voevodin, N. T Grebasch, W. S Soto, L. S Kasten, J. T Grant, F. E Arnold, and M. S Donley, *Prog. Org. Coat.*, **41**, 287 (2001).
21. N. C. Rosero-Navarro, S. A. Pellice, Y. Castro, M. Aparicio, and A. Durán, *Surf. Coat. Technol.*, **203**, 1897 (2009).

22. J. Ballarre, I. Manjubala, W. H. Schreiner, J. C. Orellano, P. Fratzl, and S. Ceré, *Acta Biomater.*, **6**, 1601 (2010).
23. N. N. Voevodin, J. W. Kurdziel, and R. Mantz, *Surf. Coat. Technol.*, **201**, 1080 (2006).
24. B. R. W. Hinton, *J. Alloys Compd.*, **180**, 15 (1992).
25. B. R. W. Hinton, D. R. Arnott, and N. E. Ryan, *Metals Forum*, **7**, 211 (1984).
26. L. Li, A. L. Desouza, and G. M. Swain, *The Analyst*, **138**, 4398 (2013).
27. A. J. Davenport, H. S. Isaacs, and M. W. Kendig, *Corros. Sci.*, **32**, 653 (1991).
28. A. J. Aldykiewicz, A. J. Davenport, and H. S. Isaacs, *J. Electrochem. Soc.*, **143**, 147 (1996).
29. W. Trabelsi, P. Cecilio, M. G. S. Ferreira, and M. F. Montemor, *Prog. Org. Coat.*, **54**, 276 (2005).
30. G. Yoganandan, K. Pradeep Premkumar, and J. N. Balaraju, *Surf. Coat. Technol.*, **270**, 249 (2015).
31. M. L. Zheludkevich, R. Serra, M. F. Montemor, K. A. Yasakau, I. M. Miranda Salvado, and M. G. S. Ferreira, *Electrochimica Acta*, **51**, 208 (2005).
32. N. C. Rosero-Navarro, L. Paussa, F. Andreatta, Y. Castro, A. Durán, M. Aparicio, and L. Fedrizzi, *Prog. Org. Coat.*, **69**, 167 (2010).
33. N. C. Rosero-Navarro, M. Curioni, Y. Castro, M. Aparicio, G. E. Thompson, and A. Durán, *Surf. Coat. Technol.*, **206**, 257 (2011).
34. X. Zhong, Q. Li, J. Hu, F. Luo, and Y. Dai, *Prog. Org. Coat.*, **69**, 52 (2010).
35. M. L. Zheludkevich, K. A. Yasakau, A. C. Bastos, O. V. Karavai, and M. G. S. Ferreira, *Electrochem. Commun.*, **9**, 2622 (2007).
36. K. A. Yasakau, M. L. Zheludkevich, S. V. Lamaka, and M. G. S. Ferreira, *J. Phys. Chem. B*, **110**, 5515 (2006).
37. K. Aramaki, *Corros. Sci.*, **44**, 1375 (2002).
38. M. Forsyth and B. Hinton, *Rare Earth-Based Corrosion Inhibitors*, p. 347, Elsevier, (2014).
39. L. Paussa, N. C. Rosero Navarro, D. Bravin, F. Andreatta, A. Lanzutti, M. Aparicio, A. Durán, and L. Fedrizzi, *Prog. Org. Coat.*, **74**, 311 (2012).
40. N. C. Rosero-Navarro, S. A. Pellice, A. Durán, S. Ceré, and M. Aparicio, *J. Sol-Gel Sci. Technol.*, **52**, 31 (2009).
41. N. C. Rosero-Navarro, S. A. Pellice, A. Durán, and M. Aparicio, *Corros. Sci.*, **50**, 1283 (2008).
42. H. Wang and R. Akid, *Corros. Sci.*, **50**, 1142 (2008).
43. U. Tiringer, A. Durán, Y. Castro, and I. Milošev, *J. Sol-Gel Coat. Technol.*, **85**, 546 (2018).
44. L. Paussa, N. C. Rosero-Navarro, F. Andreatta, Y. Castro, A. Duran, M. Aparicio, and L. Fedrizzi, *Surf. Interface Anal.*, **42**, 299 (2010).
45. N. C. Rosero-Navarro, S. A. Pellice, A. Durán, and M. Aparicio, *Corros. Sci.*, **50**, 1283 (2008).
46. J-B. Cambon, J. Esteban, F. Ansart, J-P. Bonino, V. Turq, S. H. Santagneli, C. V. Santilli, and S. H. Pulcinelli, *Mater. Res. Bull.*, **47**, 3170 (2012).
47. F. Mansfeld and Y. Wang, *Mater. Sci. Eng. A*, **198**, 51 (1995).
48. P. Chakraborty Banerjee and R. K. Singh Raman, *Electrochimica Acta*, **56**, 3790 (2011).
49. A. Zomorodian, F. Brusciotti, A. Fernandes, M. J. Carmezim, T. Moura e Silva, J. C. S. Fernandes, and M. F. Montemor, *Surf. Coat. Technol.*, **206**, 4368 (2012).
50. R. V. Lakshmi, S. T. Aruna, C. Anandan, P. Bera, and S. Sampath, *Surf. Coat. Technol.*, **309**, 363 (2017).
51. I. Milošev, Ž. Jovanović, J. B. Bajat, R. Jančić-Heinemann, and V. B. Mišković-Stanković, *J. Electrochem. Soc.*, **159**, C303 (2012).
52. S. Adhikari, K. A. Unocic, Y. Zhai, G. S. Frankel, J. Zimmerman, and W. Fristad, *Electrochimica Acta*, **56**, 1912 (2011).
53. J. A. Syed, S. Tang, and X. Meng, *Appl. Surf. Sci.*, **383**, 177 (2016).
54. S. P. Knight, M. Salagaras, A. M. Wythe, F. De Carlo, A. J. Davenport, and A. R. Trueman, *Corros. Sci.*, **52**, 3855 (2010).
55. P. Rodič and I. Milošev, *J. Electrochem. Soc.*, **163**, C85 (2016).
56. N. Birbilis and R. G. Buchheit, *J. Electrochem. Soc.*, **155**, C117 (2008).
57. R. G. Buchheit, *J. Electrochem. Soc.*, **142**, 3994 (1995).
58. O. Gharbi, N. Birbilis, and K. Ogle, *J. Electrochem. Soc.*, **163**, C240 (2016).
59. R. G. Buchheit, M. A. Martinez, and L. P. Montes, *J. Electrochem. Soc.*, **147**, 119 (2000).
60. I. Milošev and H.-H. Strehblow, *J. Electrochem. Soc.*, **150**, B517 (2003).
61. J. Beran, S. Hishita, K. Mašek, V. Matolín, and H. Haneda, *Ceram. Int.*, **40**, 323 (2014).
62. E. Bèche, P. Charvin, D. Perarnau, S. Abanades, and G. Flamant, *Surf. Interface Anal.*, **40**, 264 (2008).
63. E. Paparazzo, *Superlattices Microstruct.*, **105**, 216 (2017).

Chapter 5

Conclusions and Future Outlook

This chapter summarizes all the experimental results and thesis objectives. The effect of different pre-treatments on properties of aluminum alloys AA7075-T6 and AA2024-T3 were successfully studied and discussed. Moreover, hybrid sol-gel coatings for chromate conversion coatings replacement were developed.

The main conclusions are listed and discussed under each stated objective.

1) To gain a systematic approach of mechanical and chemical pre-treatment of aluminum alloys AA7075-T6 and AA2024-T3.

According to the results obtained in Chapter 2, both studied pre-treatments, mechanical and chemical pre-treatments, improve corrosion resistance of aluminum alloys AA7075-T6 and AA2024-T3. It was found out that the surface of AA7075-T6 after polished under non-aqueous liquid contains a higher amount of Mg compared to the surface of AA7075-T6 ground under water. Consequently, the corrosion potential of polished surface is more negative and corrosion behavior is improved. The effect of mechanical pre-treatment is less pronounced on the surface of AA2024-T3.

According to the XPS analysis, chemical treatment of AA7075-T6, based on NaOH solution and followed by desmutting in HNO_3, resulted in Cu enrichment and Mg dissolution. Cu deposits did not increase the current density in the cathodic range. Based on the literature, we concluded that Cu deposits are electrically isolated from the matrix and / or passivated due to the oxide formation, thus they do not affect the corrosion properties of AA7075-T6. On the other hand, chemical treatment, based on NaOH and HNO_3, of AA2024-T3 completely removed intermetallic particles from the surface and produced a rough layer at the surface.

After the treatment with a commercial cleaner, based on SurTec cleaning agent and followed by desmutting in HNO_3, the surface of AA7075-T6 was morphologically more similar to underwater ground surface of AA7075-T6. The effect of the commercial cleaner on the morphology of AA2024-T3 was lower compared to AA7075-T6. Furthermore, chemical treatments caused hydrophilicity of the surface of AA7075-T6 and AA2024-T3.

To conclude, pre-treatments are complex and specific for each alloy. A further *in situ* study, such as Scanning Vibrating Electrode Technique (SVET), is needed to completely understand all processes which take place on the surface during pre-treatments.

The objective was achieved in Chapter 2.

2) To gain a barrier and active corrosion protection of hybrid sol-gel coatings, based on GPTMS and TEOS.

According to the potentiodynamic and EIS results obtained in Chapter 3, hybrid sol-gel coating based on GPTMS, TEOS and SiO_2 nanoparticles expressed the barrier effect of coating. Addition of SiO_2 particles into the sol-gel coating has been reported to increase the barrier effect by increasing the coating thickness, density and reinforcement [66]–[72]. Furthermore, corrosion inhibitor $Ce(NO_3)_3$ was added to a hybrid sol-gel solution in order to provide an active corrosion protection of AA7075-T6 by the slow release of Ce inhibitor from the coating. The potentiodynamic polarization curves recorded in 0.1 M NaCl showed that coating containing cerium improved corrosion properties of sol-gel coating, evidenced by a decrease in current density. However, upon prolonged immersion a slow continuous current density increase was noticed which may be related to a progressive release of cerium from the coating leaving behind a porous structure, more susceptible to electrolyte ingress. Moreover, a long-term EIS measurements confirmed that the presence of cerium retards the degradation of coating. and increases its stability in 0.1 M NaCl. To conclude, hybrid sol-gel coatings, based on GPTMS and TEOS precursors and containing SiO_2 particles and $Ce(NO_3)_3$ provide a barrier and active corrosion protection of aluminum alloy AA7075.

The objective was achieved in Chapter 3.

3) To induce the in situ polymerization of the sol and to optimize the synthesis and curing of hybrid sol-gel coatings.

According to the results obtained from ATR-FTIR and UV-vis-NIR spectroscopy, the epoxy rings of GPTMS were opened and the reactions of hydrolysis and condensation were completed. Based on the acidic reactions, the epoxy ring of GPTMS in the present work was opened in accordance with the scheme in Figure 1.7B, leading to the product diol [64]. Consequently, the high degree of cross-linking of Si–O–Si network structure and high density was achieved *in situ*, during the synthesis of sol. Moreover, the effect of the curing procedure on coating properties was confirmed. Ramp-heated samples demonstrated a better corrosion behavior. The smaller current density and more positive corrosion potential of ramp-heated coating might be the result of denser coating, which was previously confirmed by the lower thickness and roughness and higher water angle as a result of more uniform evaporation of solvents during the ramp heating.

The objective was achieved in Chapter 3.

4) To obtain a self-healing effect of scribed hybrid sol-gel coating.

Three types of bi-layer coatings were prepared, based on TEOS, GPTMS, SiO_2 nanoparticles and $Ce(NO_3)_3$ and were applied on aluminum alloys AA7075-T6. Although all three coatings (in Chapter 4 denoted as GTS, GTS-Ce and GTS-Ce+GTS) improved the corrosion resistance of the substrate, only the GTS-Ce+GTS coating, containing cerium in the inner layer, showed the self-healing properties. The undoped GTS coating provides only barrier protection, whereas the GTS-Ce coating may be destabilized either due to the modified structure of the coating due to incorporation of Ce, or due to progressive outward leaching of cerium which limits its role in self-healing activity. Thus, locking of Ce in the inner layer decreases the destabilization of the coating and prolongs its activity in the self-healing process. The self-healing effect was confirmed by the long term EIS measurement, when after 4 days of immersion the impedance value after the initial decrease started to increase again confirming the self-healing. After 4 days of immersion, the scribe was partially healed. Although most of cerium was transformed into Ce(IV) hydroxide, Ce(III) was identified, even after 14 days of immersion, confirming that the self-healing process was still possible due to progressive deposition of Ce-based deposits.

The objective was achieved in Chapter 4.

5) To develop hybrid sol-gel coating as a replacement for chromate conversion coatings.

In accordance with the literature, developed coatings GTS, GTS-Ce and GTS-Ce+GTS, from Chapter 3 and 4, are a promising replacement for toxic chromate conversion coatings. Figure 1.11 represents potentiodynamic polarization measurements of uncoated AA7075-T6 and AA7075-T6 coated with GTS, GTS-Ce, GTS-Ce+GTS coatings, and with chromate conversion coating (CCC). It is noteworthy that the current density of coatings developed herein is smaller compared to CCC coating. In addition to the smaller current density, the advantage of herein developed coatings in comparison to CCC is in their color. CCC used in this work is yellow, whereas the developed coatings are transparent. However, the passivation range of CCC is greater compared to GTS, GTS-Ce and GTS-Ce+GTS coatings. Furthermore, due to their hydrophilicity, coatings developed herein could be used as primers for the deposition of water-based top coat/paints, which would additionally expand their passivation range. However, additional experiments, such as salt spray chamber testing and EIS measurements need to be carried out in order to provide all requirements [84]–[86].

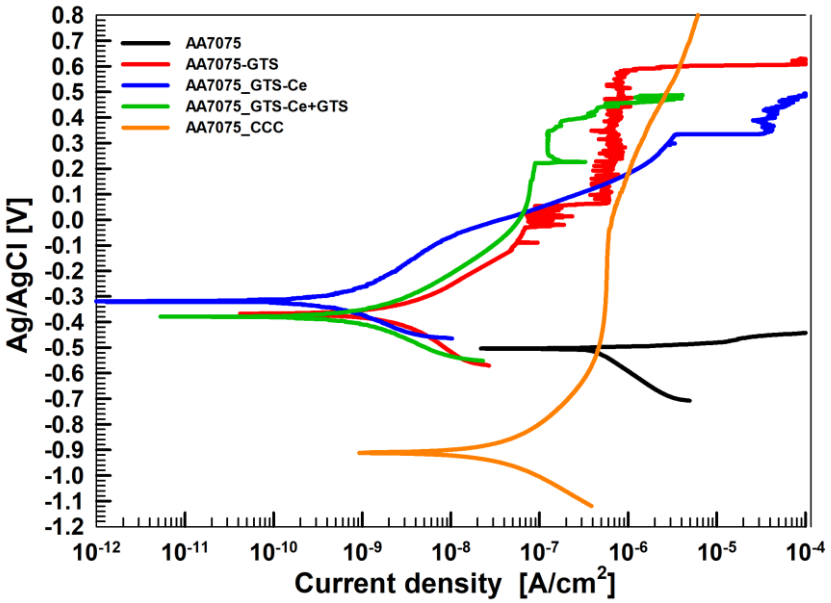


Figure 1.11: Potentiodynamic polarization curves recorded in 0.1 M NaCl, after 1 hour of stabilization for uncoated AA7075-T6 and coated by GTS, GTS-Ce and GTS-Ce+GTS and by green chromate primer-CCC.

The objective was achieved in Chapter 3 and Chapter 4.

Future work

In the present work, the exact reaction mechanism of the synthesis of hybrid sol-gel coatings in the present work is missing, thus our first future objective is to use proton (^{1}H NMR), carbon-13 (^{13}C NMR) and silicon-29 nuclear magnetic resonance spectroscopy (^{29}Si NMR), to facilitate the understanding of hybrid sol-gel coatings formation and the mechanism of the epoxy rings opening.

The effect of chemical pre-treatments of aluminum alloys on deposition and corrosion performance of conversion coatings has been extensively studied [25], [28], [31], [87]–[98], but there is still a lack in the literature about the effect of different chemical pre-treatments on deposition and on corrosion properties of deposited sol-gel coatings. Thus, one of our future objectives is to study the effect of different chemical pre-treatments of aluminum alloys on the deposition and corrosion performance of hybrid sol-gel coatings, to successfully transfer and implement the sol-gel process to the industry.

Hybrid sol-gel coatings based on GPTMS and TEOS are replacement for primers in industrial coating's applications, which require a top coat/paint on it. Top coat/paint is usually based on epoxy binders and can be applied to the primer with spray or dip coating technique. One of the most important requirements for industrial application is excellent adhesion between primer and top coat [99]. Thus, our future objective is to test the adhesion between hybrid sol-gel coatings and organic paints (based on epoxy binders), as well as the resistance of such a coating system against filiform corrosion, in salt chamber, in order to test how these coatings, satisfy the most demanding industrial requirements.

One of the promising corrosion inhibitors for aluminum alloys are also lithium based salts. They became of interest as potential corrosion inhibitors after reports of passivity of aluminum when it is exposed to alkaline lithium salt solution [100]–[102]. Moreover, it was found out that lithium-ions are able to leach from the organic coating and generate a protective layer in the damaged area, establishing a self-healing effect [103]–[105]. Thus, our future objective is to incorporate both, cerium and lithium inhibitors to the hybrid sol-gel coating, to improve barrier properties, active corrosion protection and self-healing of coating. We expect that such coatings will boost the performance of our hybrid sol-gel coatings to the level of CCCs or even better.

References

[1] Anonymous, "EU climate action," *Climate Action - European Commission*, 23-Nov-2016. [Online]. Available: https://ec.europa.eu/clima/citizens/eu_en. [Accessed: 09-Apr-2018].

[2] *Directive 2002/95/EC of the European Parliament and of the Council of 27 January 2003 on the restriction of the use of certain hazardous substances in electrical and electronic equipment*, vol. OJ L. 2003.

[3] J. W. Bibber, "An overview of nonhexavalent chromium conversion coatings—Part I: aluminum and its alloys," *Metal Finishing*, vol. 99, no. 12, pp. 15–22, Dec. 2001.

[4] R. B. Figueira, C. J. R. Silva, and E. V. Pereira, "Organic–inorganic hybrid sol–gel coatings for metal corrosion protection: a review of recent progress," *J Coat Technol Res*, vol. 12, no. 1, pp. 1–35, Aug. 2014.

[5] Rita B. Figueira, Isabel R. Fontinha, Carlos J. R. Silva, and Elsa V. Pereira, "Hybrid Sol-Gel Coatings: Smart and Green Materials for Corrosion Mitigation," *Coatings*, vol. 6, no. 1, p. 12, Mar. 2016.

[6] J. R. Davis, *Corrosion of aluminum and aluminum alloys*, vol. 1999. United States of America: ASM International, 1999.

[7] C. Vargel, *Corrosion of aluminum*, 1.st. ed. Amsterdam, The Netherlands: Elsevier, 2004.

[8] M. Pourbaix, *Atlas of electrochemical equilibria in aqueous solutions*. Houston, Tex.: National Association of Corrosion Engineers, 1974.

[9] "PlasmaPure-UC - Ultra-Pure Alumina for Extreme Duty Semiconductor Applications by CoorsTek," *AZoM.com*, 05-Feb-2010. [Online]. Available: https://www.azom.com/article.aspx?ArticleID=5098. [Accessed: 09-Apr-2018].

[10] G. Kufman, *Introduction to aluminum alloys and tempers*, 1 st. ed. United States of America: ASM International, 2000.

[11] "GENERAL ALUMINUM INFORMATION from Aircraft Spruce." [Online]. Available: http://www.aircraftspruce.com/catalog/mepages/aluminfo.php. [Accessed: 24-Feb-2018].

[12] N. Birbilis and R. G. Buchheit, "Investigation and Discussion of Characteristics for Intermetallic Phases Common to Aluminum Alloys as a Function of Solution pH," *J. Electrochem. Soc.*, vol. 155, no. 3, pp. C117–C126, Jan. 2008.

[13] R. G. Buchheit, M. A. Martinez, and L. P. Montes, "Evidence for Cu Ion Formation by Dissolution and Dealloying the Al2CuMg Intermetallic Compound in

Rotating Ring-Disk Collection Experiments," *J. Electrochem. Soc.*, vol. 147, no. 1, pp. 119–124, Jan. 2000.

[14] I. Milošev and P. Rodič, "Cerium Chloride and Acetate Salts as Corrosion Inhibitors for Aluminum Alloy AA7075-T6 in Sodium Chloride Solution," *CORROSION*, vol. 72, no. 8, pp. 1021–1034, Apr. 2016.

[15] P. Rodič and I. Milošev, "Corrosion Inhibition of Pure Aluminium and Alloys AA2024-T3 and AA7075-T6 by Cerium(III) and Cerium(IV) Salts," *J. Electrochem. Soc.*, vol. 163, no. 3, pp. C85–C93, Jan. 2016.

[16] M. W. Kendig and R. G. Buchheit, "Corrosion Inhibition of Aluminum and Aluminum Alloys by Soluble Chromates, Chromate Coatings, and Chromate-Free Coatings," *CORROSION*, vol. 59, no. 5, pp. 379–400, May 2003.

[17] G. W. Critchlow and D. M. Brewis, "Review of surface pretreatments for aluminium alloys," *International Journal of Adhesion and Adhesives*, vol. 16, no. 4, pp. 255–275, 1996.

[18] P. G. Sheasby and R. Pinner, *The Surface Treatment and Finishing of Aluminium and Its Alloys(Volumes 1 & 2)*, 6 Har/Cdr edition. Materials Park, Ohio; finishing publications: ASM International, 2001.

[19] Guang-Ling Song, *Corrosion Prevention of Magnesium Alloys*. Elsevier, 2013.

[20] Q. Meng and G. S. Frankel, "Effect of Cu Content on Corrosion Behavior of 7xxx Series Aluminum Alloys," *J. Electrochem. Soc.*, vol. 151, no. 5, pp. B271–B283, Jan. 2004.

[21] A. L. Y. Liu, "Corrosion behaviour of mechanically polished AA7075-T6 aluminium alloy," *Surface and Interface Analysis - SURF INTERFACE ANAL*, vol. 42, no. 4, pp. 185–188, 2010.

[22] W. Zhang and G. S. Frankel, "Transitions between pitting and intergranular corrosion in AA2024," *Electrochimica Acta*, vol. 48, no. 9, pp. 1193–1210, Apr. 2003.

[23] G. S. Frankel and N. Sridhar, "Understanding localized corrosion," *Materials Today*, vol. 11, no. 10, pp. 38–44, Oct. 2008.

[24] Z. Zhao and G. S. Frankel, "On the first breakdown in AA7075-T6," *Corrosion Science*, vol. 49, no. 7, pp. 3064–3088, Jul. 2007.

[25] S. Joshi, W. G. Fahrenholtz, and M. J. O'Keefe, "Effect of alkaline cleaning and activation on aluminum alloy 7075-T6," *Applied Surface Science*, vol. 257, no. 6, pp. 1859–1863, Jan. 2011.

[26] Y. Liu *et al.*, "Influence of nitric acid pre-treatment on Al–Cu alloys," *Electrochimica Acta*, vol. 53, no. 13, pp. 4454–4460, May 2008.

[27] Y. Liu *et al.*, "Corrosion behaviour of mechanically polished AA7075-T6 aluminium alloy," *Surf. Interface Anal.*, vol. 42, no. 4, pp. 185–188, Apr. 2010.

[28] P. Campestrini, H. Terryn, A. Hovestad, and J. H. W. de Wit, "Formation of a cerium-based conversion coating on AA2024: relationship with the microstructure," *Surface and Coatings Technology*, vol. 176, no. 3, pp. 365–381, Jan. 2004.

[29] D. Wang and G. P. Bierwagen, "Sol–gel coatings on metals for corrosion protection," *Progress in Organic Coatings*, vol. 64, no. 4, pp. 327–338, Mar. 2009.

[30] T. P. Chou, C. Chandrasekaran, and G. Z. Cao, "Sol-Gel-Derived Hybrid Coatings for Corrosion Protection," *Journal of Sol-Gel Science and Technology*, vol. 26, no. 1–3, pp. 321–327, Jan. 2003.

[31] S. Joshi, W. G. Fahrenholtz, and M. J. O'Keefe, "Alkaline activation of Al 7075-T6 for deposition of cerium-based conversion coatings," *Surface and Coatings Technology*, vol. 205, no. 17–18, pp. 4312–4319, May 2011.

[32] R. L. Twite and G. P. Bierwagen, "Review of alternatives to chromate for corrosion protection of aluminum aerospace alloys," *Progress in Organic Coatings*, vol. 33, no. 2, pp. 91–100, Feb. 1998.

[33] I. Milošev, B. Kapun, P. Rodič, and J. Iskra, "Hybrid sol–gel coating agents based on zirconium(IV) propoxide and epoxysilane," *J Sol-Gel Sci Technol*, vol. 74, no. 2, pp. 447–459, May 2015.

[34] S. Zheng and J. Li, "Inorganic–organic sol gel hybrid coatings for corrosion protection of metals," *J Sol-Gel Sci Technol*, vol. 54, no. 2, pp. 174–187, May 2010.

[35] J. Wen and G. L. Wilkes, "Organic/Inorganic Hybrid Network Materials by the Sol−Gel Approach," *Chem. Mater.*, vol. 8, no. 8, pp. 1667–1681, Jan. 1996.

[36] H. Wang and R. Akid, "Encapsulated cerium nitrate inhibitors to provide high-performance anti-corrosion sol–gel coatings on mild steel," *Corrosion Science*, vol. 50, no. 4, pp. 1142–1148, Apr. 2008.

[37] A. C. Pierre, *Introduction to Sol-Gel Processing*. Springer US, 1998.

[38] C. J. Brinker, A. J. Hurd, P. R. Schunk, G. C. Frye, and C. S. Ashley, "Review of sol-gel thin film formation," *Journal of Non-Crystalline Solids*, vol. 147, pp. 424–436, Jan. 1992.

[39] N. Pirhady Tavandashti, S. Sanjabi, and T. Shahrabi, "Evolution of corrosion protection performance of hybrid silica based sol–gel nanocoatings by doping inorganic inhibitor," *Materials and Corrosion*, vol. 62, no. 5, pp. 411–415, May 2011.

[40] G. Schottner, "Hybrid Sol−Gel-Derived Polymers: Applications of Multifunctional Materials," *Chemistry of Materials*, vol. 13, no. 10, pp. 3422–3435, Oct. 2001.

[41] M. L. Zheludkevich, I. M. Salvado, and M. G. S. Ferreira, "Sol–gel coatings for corrosion protection of metals," *J. Mater. Chem.*, vol. 15, no. 48, pp. 5099–5111, Dec. 2005.

[42] F. Andreatta *et al.*, "Development and industrial scale-up of ZrO2 coatings and hybrid organic–inorganic coatings used as pre-treatments before painting aluminium alloys," *Progress in Organic Coatings*, vol. 72, no. 1, pp. 3–14, Sep. 2011.

[43] M. Fedel, E. Callone, S. Diré, F. Deflorian, M.-G. Olivier, and M. Poelman, "Effect of Na-Montmorillonite sonication on the protective properties of hybrid silica coatings," *Electrochimica Acta*, vol. 124, pp. 90–99, Apr. 2014.

[44] P. Rodič, J. Iskra, and I. Milošev, "A hybrid organic–inorganic sol–gel coating for protecting aluminium alloy 7075-T6 against corrosion in Harrison's solution," *J Sol-Gel Sci Technol*, vol. 70, no. 1, pp. 90–103, Apr. 2014.

[45] P. C. R. Varma, J. Colreavy, J. Cassidy, M. Oubaha, C. McDonagh, and B. Duffy, "Corrosion protection of AA 2024-T3 aluminium alloys using 3, 4-diaminobenzoic acid chelated zirconium–silane hybrid sol–gels," *Thin Solid Films*, vol. 518, no. 20, pp. 5753–5761, Aug. 2010.

[46] D. Álvarez, A. Collazo, M. Hernández, X. R. Nóvoa, and C. Pérez, "Characterization of hybrid sol–gel coatings doped with hydrotalcite-like compounds to improve corrosion resistance of AA2024-T3 alloys," *Progress in Organic Coatings*, vol. 67, no. 2, pp. 152–160, Feb. 2010.

[47] S. Bera, T. K. Rout, G. Udayabhanu, and R. Narayan, "Comparative Study of Corrosion Protection of Sol–Gel Coatings with Different Organic Functionality on Al-2024 substrate," *Progress in Organic Coatings*, vol. 88, pp. 293–303, Nov. 2015.

[48] V. R. Capelossi, M. Poelman, I. Recloux, R. P. B. Hernandez, H. G. de Melo, and M. G. Olivier, "Corrosion protection of clad 2024 aluminum alloy anodized in tartaric-sulfuric acid bath and protected with hybrid sol–gel coating," *Electrochimica Acta*, vol. 124, no. Supplement C, pp. 69–79, Apr. 2014.

[49] Z. Feng, Y. Liu, G. E. Thompson, and P. Skeldon, "Sol–gel coatings for corrosion protection of 1050 aluminium alloy," *Electrochimica Acta*, vol. 55, no. 10, pp. 3518–3527, Apr. 2010.

[50] M. Gobara, H. Kamel, R. Akid, and A. Baraka, "Corrosion behaviour of AA2024 coated with an acid-soluble collagen/hybrid silica sol–gel matrix," *Progress in Organic Coatings*, vol. 89, pp. 57–66, Dec. 2015.

[51] A. N. Khramov, V. N. Balbyshev, N. N. Voevodin, and M. S. Donley, "Nanostructured sol–gel derived conversion coatings based on epoxy- and amino-silanes," *Progress in Organic Coatings*, vol. 47, no. 3–4, pp. 207–213, Sep. 2003.

[52] T. L. Metroke, O. Kachurina, and E. T. Knobbe, "Spectroscopic and corrosion resistance characterization of GLYMO–TEOS Ormosil coatings for aluminum alloy corrosion inhibition," *Progress in Organic Coatings*, vol. 44, no. 4, pp. 295–305, Aug. 2002.

[53] K. A. Yasakau, M. L. Zheludkevich, S. V. Lamaka, and M. G. S. Ferreira, "Mechanism of Corrosion Inhibition of AA2024 by Rare-Earth Compounds," *J. Phys. Chem. B*, vol. 110, no. 11, pp. 5515–5528, Mar. 2006.

[54] A. Zomorodian *et al.*, "Anti-corrosion performance of a new silane coating for corrosion protection of AZ31 magnesium alloy in Hank's solution," *Surface and Coatings Technology*, vol. 206, no. 21, pp. 4368–4375, Jun. 2012.

[55] H. Wang and R. Akid, "A room temperature cured sol–gel anticorrosion pre-treatment for Al 2024-T3 alloys," *Corrosion Science*, vol. 49, no. 12, pp. 4491–4503, Dec. 2007.

[56] M. L. Zheludkevich, R. Serra, M. F. Montemor, I. M. Miranda Salvado, and M. G. S. Ferreira, "Corrosion protective properties of nanostructured sol–gel hybrid coatings to AA2024-T3," *Surface and Coatings Technology*, vol. 200, no. 9, pp. 3084–3094, Feb. 2006.

[57] M. L. Zheludkevich, R. Serra, M. F. Montemor, K. A. Yasakau, I. M. Miranda Salvado, and M. G. S. Ferreira, "Nanostructured sol–gel coatings doped

with cerium nitrate as pre-treatments for AA2024-T3: Corrosion protection performance," *Electrochimica Acta*, vol. 51, no. 2, pp. 208–217, Oct. 2005.

[58] E. Roussi, A. Tsetsekou, D. Tsiourvas, and A. Karantonis, "Novel hybrid organo-silicate corrosion resistant coatings based on hyperbranched polymers," *Surface and Coatings Technology*, vol. 205, no. 10, pp. 3235–3244, Feb. 2011.

[59] M. Schem *et al.*, "CeO2-filled sol–gel coatings for corrosion protection of AA2024-T3 aluminium alloy," *Corrosion Science*, vol. 51, no. 10, pp. 2304–2315, Oct. 2009.

[60] H. Wang, R. Akid, and M. Gobara, "Scratch-resistant anticorrosion sol–gel coating for the protection of AZ31 magnesium alloy via a low temperature sol–gel route," *Corrosion Science*, vol. 52, no. 8, pp. 2565–2570, Aug. 2010.

[61] S. R. Davis, A. R. Brough, and A. Atkinson, "Formation of silica/epoxy hybrid network polymers," *Journal of Non-Crystalline Solids*, vol. 315, no. 1–2, pp. 197–205, Jan. 2003.

[62] I. Milošev, B. Kapun, P. Rodič, and J. Iskra, "Hybrid sol–gel coating agents based on zirconium(IV) propoxide and epoxysilane," *J Sol-Gel Sci Technol*, vol. 74, no. 2, pp. 447–459, Jan. 2015.

[63] P. Innocenzi, G. Brusatin, and F. Babonneau, "Competitive Polymerization between Organic and Inorganic Networks in Hybrid Materials," *Chem. Mater.*, vol. 12, no. 12, pp. 3726–3732, Dec. 2000.

[64] J.-B. Cambon *et al.*, "Effect of cerium on structure modifications of a hybrid sol–gel coating, its mechanical properties and anti-corrosion behavior," *Materials Research Bulletin*, vol. 47, no. 11, pp. 3170–3176, Nov. 2012.

[65] N. N. Voevodin, J. W. Kurdziel, and R. Mantz, "Corrosion protection for aerospace aluminum alloys by Modified Self-assembled NAnophase Particle (MSNAP) sol–gel," *Surface and Coatings Technology*, vol. 201, no. 3–4, pp. 1080–1084, Oct. 2006.

[66] Ianina Santana, Andrés Pepe, Emilio Jimenez-Pique, Sergio Pellice, Ingrid Milošev, and Silvia Ceré, "Corrosion protection of carbon steel by silica-based hybrid coatings containing cerium salts: Effect of silica nanoparticle content," *Surface and Coatings Technology*, vol. 265, pp. 106–116, Mar. 2015.

[67] Josefina Ballarre, Inderchand Manjubala, Wido H. Schreiner, Juan Carlos Orellano, Peter Fratzl, and Silvia Ceré, "Improving the osteointegration and bone-implant interface by incorporation of bioactive particles in sol-gel coatings of stainless steel implants," *Acta Biomater*, vol. 6, no. 4, pp. 1601–1609, Apr. 2010.

[68] A. J. Vreugdenhil, V. N. Balbyshev, and M. S. Donley, "Nanostructured silicon sol-gel surface treatments for Al 2024-T3 protection," *Journal of Coatings Technology*, vol. 73, no. 915, pp. 35–43.

[69] R. N. Peres, E. S. F. Cardoso, M. F. Montemor, H. G. de Melo, A. V. Benedetti, and P. H. Suegama, "Influence of the addition of SiO2 nanoparticles to a hybrid coating applied on an AZ31 alloy for early corrosion protection," *Surface and Coatings Technology*, vol. 303, Part B, pp. 372–384, Oct. 2016.

[70] A. Durán, Y. Castro, M. Aparicio, A. Conde, and J. J. de Damborenea, "Protection and surface modification of metals with sol–gel coatings," *International Materials Reviews*, vol. 52, no. 3, pp. 175–192, May 2007.

[71] N. N Voevodin *et al.*, "An organically modified zirconate film as a corrosion-resistant treatment for aluminum 2024-T3," *Progress in Organic Coatings*, vol. 41, no. 4, pp. 287–293, May 2001.

[72] N. C. Rosero-Navarro, S. A. Pellice, Y. Castro, M. Aparicio, and A. Durán, "Improved corrosion resistance of AA2024 alloys through hybrid organic–inorganic sol–gel coatings produced from sols with controlled polymerisation," *Surface and Coatings Technology*, vol. 203, no. 13, pp. 1897–1903, Mar. 2009.

[73] B. R. W. Hinton, "Corrosion inhibition with rare earth metal salts," *Journal of Alloys and Compounds*, vol. 180, no. 1, pp. 15–25, Mar. 1992.

[74] B. R. W. Hinton, D. R. Arnott, and N. E. Ryan, "INHIBITION OF ALUMINUM ALLOY CORROSION BY CEROUS CATIONS.," *ResearchGate*, vol. 7, no. 4, pp. 211–217, Mar. 1984.

[75] A. J. Aldykiewicz, A. J. Davenport, and H. S. Isaacs, "Studies of the Formation of Cerium-Rich Protective Films Using X-Ray Absorption Near-Edge Spectroscopy and Rotating Disk Electrode Methods," *J. Electrochem. Soc.*, vol. 143, no. 1, pp. 147–154, Jan. 1996.

[76] A. J. Davenport, H. S. Isaacs, and M. W. Kendig, "XANES investigation of the role of cerium compounds as corrosion inhibitors for aluminum," *Corrosion Science*, vol. 32, no. 5, pp. 653–663, Jan. 1991.

[77] L. Li, A. L. Desouza, and G. M. Swain, "In situ pH measurement during the formation of conversion coatings on an aluminum alloy (AA2024)," *Analyst*, vol. 138, no. 15, pp. 4398–4402, Aug. 2013.

[78] W. Trabelsi, P. Cecilio, M. G. S. Ferreira, and M. F. Montemor, "Electrochemical assessment of the self-healing properties of Ce-doped silane solutions for the pre-treatment of galvanised steel substrates," *Progress in Organic Coatings*, vol. 54, no. 4, pp. 276–284, Dec. 2005.

[79] G. Yoganandan, K. Pradeep Premkumar, and J. N. Balaraju, "Evaluation of corrosion resistance and self-healing behavior of zirconium–cerium conversion coating developed on AA2024 alloy," *Surface and Coatings Technology*, vol. 270, pp. 249–258, May 2015.

[80] N. C. Rosero-Navarro *et al.*, "Optimization of hybrid sol–gel coatings by combination of layers with complementary properties for corrosion protection of AA2024," *Progress in Organic Coatings*, vol. 69, no. 2, pp. 167–174, Oct. 2010.

[81] N. C. Rosero-Navarro, M. Curioni, Y. Castro, M. Aparicio, G. E. Thompson, and A. Durán, "Glass-like CexOy sol–gel coatings for corrosion protection of aluminium and magnesium alloys," *Surface and Coatings Technology*, vol. 206, no. 2–3, pp. 257–264, Oct. 2011.

[82] Xiankang Zhong, Qing Li, Junying Hu, Fei Luo, and Yan Dai, "Effect of cerium concentration on microstructure, morphology and corrosion resistance of cerium–silica hybrid coatings on magnesium alloy AZ91D," *Progress in Organic Coatings*, vol. 69, no. 1, pp. 52–56, Sep. 2010.

[83] M. L. Zheludkevich, K. A. Yasakau, A. C. Bastos, O. V. Karavai, and M. G. S. Ferreira, "On the application of electrochemical impedance spectroscopy to study the self-healing properties of protective coatings," *Electrochemistry Communications*, vol. 9, no. 10, pp. 2622–2628, Oct. 2007.

[84] "Advanced Surface Technologies - Metal Finishings, Denver," *Advanced Surface Technologies / AST Finishing, Inc.* [Online]. Available: https://www.astfinishing.com/. [Accessed: 09-Apr-2018].

[85] "MIL-STD-202 G ELECTRONIC ELECTRICAL COMPONENT PARTS." [Online]. Available: http://everyspec.com/MIL-STD/MIL-STD-0100-0299/MIL-STD-202G_2397/. [Accessed: 09-Apr-2018].

[86] "Military Testing," *Assured Testing Services*. [Online]. Available: https://www.assuredtestingservices.com/militaryaerospace. [Accessed: 09-Apr-2018].

[87] R. Grilli, "Conversion coatings for aluminium alloys: a surface investigation for corrosion mechanisms," University of Surrey, United Kingdom, Doctor Degree, 2010.

[88] C. E. Moffitt, D. M. Wieliczka, and H. K. Yasuda, "An XPS study of the elemental enrichment on aluminum alloy surfaces from chemical cleaning," *Surface and Coatings Technology*, vol. 137, no. 2–3, pp. 188–196, Mar. 2001.

[89] Y. Liu *et al.*, "Behaviour of copper during alkaline corrosion of Al–Cu alloys," *Corrosion Science*, vol. 50, no. 5, pp. 1475–1480, May 2008.

[90] A. de Frutos *et al.*, "Influence of pre-treatments in cerium conversion treatment of AA2024-T3 and 7075-T6 alloys," *Surface and Coatings Technology*, vol. 202, no. 16, pp. 3797–3807, May 2008.

[91] S. S. Golru, M. M. Attar, and B. Ramezanzadeh, "Effects of different surface cleaning procedures on the superficial morphology and the adhesive strength of epoxy coating on aluminium alloy 1050," *Progress in Organic Coatings*, vol. 87, pp. 52–60, Oct. 2015.

[92] N. J. Cherepy, T. H. Shen, A. P. Esposito, and T. M. Tillotson, "Characterization of an effective cleaning procedure for aluminum alloys: surface enhanced Raman spectroscopy and zeta potential analysis," *Journal of Colloid and Interface Science*, vol. 282, no. 1, pp. 80–86, Feb. 2005.

[93] L. Fedrizzi, A. Bianchi, F. Deflorian, S. Rossi, and P. L. Bonora, "Effect of chemical cleaning on the corrosion behaviour of painted aluminium alloys," *Electrochimica Acta*, vol. 47, no. 13–14, pp. 2159–2168, May 2002.

[94] B. L. Treu, S. Joshi, W. R. Pinc, M. J. O'Keefe, and W. G. Fahrenholtz, "Characterization of localized surface states of Al 7075-T6 during deposition of cerium-based conversion coatings," *Journal of The Electrochemical Society*, vol. 157, no. 8, pp. C282–C287, 2010.

[95] W. G. Fahrenholtz, M. J. O'Keefe, H. Zhou, and J. T. Grant, "Characterization of cerium-based conversion coatings for corrosion protection of aluminum alloys," *Surface and Coatings Technology*, vol. 155, no. 2–3, pp. 208–213, Jun. 2002.

[96] A. E. Hughes, J. D. Gorman, P. R. Miller, B. A. Sexton, P. J. K. Paterson, and R. J. Taylor, "Development of cerium-based conversion coatings on 2024-T3 Al alloy after rare-earth desmutting," *Surf. Interface Anal.*, vol. 36, no. 4, pp. 290–303, Apr. 2004.

[97] W. Pinc, S. Geng, M. O'Keefe, W. Fahrenholtz, and T. O'Keefe, "Effects of acid and alkaline based surface preparations on spray deposited cerium based conversion coatings on Al 2024-T3," *Applied Surface Science*, vol. 255, no. 7, pp. 4061–4065, Jan. 2009.

[98] F. J. Monteiro, M. A. Barbosa, D. R. Gabe, and D. H. Ross, "Surface pretreatments of aluminium for electroplating," *Surface and Coatings Technology*, vol. 35, no. 3, pp. 321–331, Nov. 1988.

[99] H. Jiang, R. Browning, P. Liu, T. A. Chang, and H.-J. Sue, "Determination of epoxy coating wet-adhesive strength using a standardized ASTM/ISO scratch test," *J Coat Technol Res*, vol. 8, no. 2, pp. 255–263, Mar. 2011.

[100] J. Gui and T. M. Devine, "Influence of lithium on the corrosion of aluminum," *Scripta Metallurgica*, vol. 21, no. 6, pp. 853–857, Jun. 1987.

[101] R. G. Buchheit, M. D. Bode, and G. E. Stoner, "Corrosion-Resistant, Chromate-Free Talc Coatings for Aluminum," *CORROSION*, vol. 50, no. 3, pp. 205–214, Mar. 1994.

[102] M. R. S. Castro, J. C. Nogueira, G. P. Thim, and M. A. S. Oliveira, "Adhesion and corrosion studies of a lithium based conversion coating film on the 2024 aluminum alloy," *Thin Solid Films*, vol. 457, no. 2, pp. 307–312, Jun. 2004.

[103] P. Visser, Y. Liu, H. Terryn, and J. M. C. Mol, "Lithium salts as leachable corrosion inhibitors and potential replacement for hexavalent chromium in organic coatings for the protection of aluminum alloys," *J Coat Technol Res*, vol. 13, no. 4, pp. 557–566, Jul. 2016.

[104] P. Visser *et al.*, "The corrosion protection of AA2024-T3 aluminium alloy by leaching of lithium-containing salts from organic coatings," *Faraday Discuss.*, vol. 180, no. 0, pp. 511–526, Jul. 2015.

[105] P. Visser, M. Meeusen, Y. Gonzalez-Garcia, H. Terryn, and J. M. C. Mol, "Electrochemical Evaluation of Corrosion Inhibiting Layers Formed in a Defect from Lithium-Leaching Organic Coatings," *J. Electrochem. Soc.*, vol. 164, no. 7, pp. C396–C406, Jan. 2017.

Bibliography

Publications Related to the Thesis

All publications related to the thesis should be referenced in the text.

Journal Articles

1. U. Tiringer, J. Kovač, I. Milošev, "Effect of mechanical and chemical pre-treatments on the morphology and composition of surfaces of aluminium alloys 7075-T6 and 2024-T3. *Corros. Sci.*, vol. 119, pp. 46–59, 2017.

2. U. Tiringer, I. Milošev, A. Durán, Y. Castro, " Hybrid sol–gel coatings based on GPTMS/TEOS containing colloidal SiO2 and cerium nitrate for increasing corrosion protection of aluminium alloy 7075-T6. *J.Sol-Gel Sci.Technol.* Vol. 85, pp. 546–557, 2017.

.

3. U. Tiringer, Y. Castro, A Durán, I. Milošev, "Self-healing effect of $Ce(NO_3)_3$ in hybrid sol-gel coatings based on GPTMS, TEOS and SiO_2 nanoparticles applied on aluminium alloy 7075-T6." *J. Electrochem. Soc.,* Vol. 165, pp. C213-C225, 2018.

Conference Paper

1. U. Tiringer, I. Milošev, " The optimization of cleaning pre-treatment of aluminium alloy AA 7075, " *7th Jožef Stefan International Postgraduate School Students' Conference,* Ljubljana, Slovenia, 2015.

2. U. Tiringer, I. Milošev, A. Durán," Inhibition and self-healing effect of $Ce(NO_3)_3$ in hybrid sol-gel coating applied on aluminium alloy 7075-T6," *7th ISE Satellite Student Regional Symposium on Electrochemistry*, Zagreb, Croatia, 2017.

3. U. Tiringer, I. Milošev, A. Durán, "Self-healing effect of $Ce(NO_3)_3$ in coating based on GPTMS, TEOS and SiO_2 nanoparticles applied on aluminium alloy 7075-T6," *6th Regional Symposium on Electrochemistry South-East Europe*, Balatonkenese, Hungary, 2018.

4. U. Tiringer, I. Milošev, "Self-healing effect of multi-layer sol-gel coatings doped with cerium, " *20th European Corrosion Congress et Process Safety Congress*, Prague, Czech Republic, 2017.

5. U. Tiringer, J. Kovač, I. Milošev, " The effect of AA7075 and AA2024 substrate pre-treatment and alkaline cleaning procedures on the surface morphology and composition, " *16th Joint Vacuum Conference*, Portorož, Slovenia, 2016.

6. U. Tiringer, I. Milošev, " The optimization of cleaning pre-treatment of aluminum alloy AA7075, " *9th Young researchers' day*, Ljubljana, Slovenia, 2015.

7. U. Tiringer, J. Kovač, I. Milošev, " The optimization of cleaning pre-treatment of aluminium alloy AA 7075 and testing of commercial conversion coating, "*5th Regional Symposium on Electrochemistry South-East Europe*, Pravets, Bulgaria, 2015.

Biography

The author Urša Tiringer was born on April 22, 1989 in Postojna, Slovenia. She finished primary and secondary education in 2008 at the School Center Postojna.

She proceeded with her university study programme in Chemistry at the Faculty of Chemistry and Chemical Technology at the University of Ljubljana. She obtained the 1st cycle diploma degree in Analytical Chemistry in July 2012 under the supervision of Dr. Nataša Gros, associate professor, and the 2nd-cycle master's degree in Physical Chemistry in September 2014 under the supervision of Asst. Prof. Črtomir Podlipnik.

In October 2014, she continued with her PhD studies at the Jožef Stefan International Postgraduate School in the field of Nanosciences and Nanotechnologies and in November 2014 she was enrolled as a young researcher under the supervision of Prof. Dr. Ingrid Milošev at the Jožef Stefan Institute. Her PhD study is financed by the Slovenian Research Agency (ARRS).

In 2015, she was awarded the Ad Futura scholarship for a PhD student exchange and spent a period of four months at the Institute of Ceramics and Glass at the Department of Glasses, Madrid, Spain. There she studied under the supervision of Prof. Dr. Alicia Durán.

During her time as a PhD student, her research has been focused on finding the replacement of hazardous and toxic chromate conversion coatings for corrosion protection of aluminum alloys. Developed coatings for corrosion protection were synthesized by the sol-gel route and showed to be a promising replacement for chromate conversion coatings.